UNIVERSITÉ DU QUÉBEC À MONTRÉAL

PROCESSES DRIVING NEAR-0°C CONDITIONS IN COLD REGIONS

THESIS

PRESENTED

IN PARTIAL REQUREMENT FOR

DOCTORATE IN EARTH AND ATMOSPHERIC SCIENCES

BY

SUJAN BASNET

JUNE 2026

UNIVERSITÉ DU QUÉBEC À MONTRÉAL

PROCESSUS À L'ORIGINE DES CONDITIONS PROCHES DE 0°C DANS LES RÉGIONS FROIDES

THÈSE

PRÉSENTÉ(E)

COMME EXIGENCE PARTIELLE

DU DOCTORAT EN SCIENCES DE LA TERRE ET DE L'ATMOSPHÈRE

PAR

SUJAN BASNET

JUIN 2026

ACKNOWLEDGEMENT

This Ph.D. has been a long and difficult journey, and I could never have reached this point without the patience, kindness, and encouragement of so many people who walked beside me.

First and foremost, I want to thank Julie Mireille Thériault, my supervisor, for believing in me and for giving me the freedom to explore my own path. Her support, whether in pursuing research ideas or in taking part in conferences, workshops, and other experiences, has been a gift. Those opportunities not only shaped my scientific career but also helped me grow as a person. I am deeply grateful for her generosity and guidance, which made all the difference.

To my family and loved ones: thank you for being my anchor. To my wife, Anuja Thapa, your love and unwavering support carried me through the most exhausting moments. I truly could not have done this without you by my side. Even during the times, we were apart, you gave me the strength to persevere. To my late parents, Dhurba and Renuka Basnet, I have always felt your presence and encouragement, and your belief in me continues to give me strength even in your absence. To my sister, Sanju Basnet, and my brother-in-law, Asim Ghimire, thank you for always cheering me on and being a source of comfort and strength. I am also indebted to my in-laws, Janak Thapa and Anju Karki, whose encouragement continually pushed me forward, even when the road seemed endless.

Finally, to all my friends and colleagues in the Département des sciences de la Terre et de l'atmosphère, thank you for walking this journey with me. I am especially grateful to my friends, Bastien Gratia, Margaux Girouard, and Madeleine Fol, whose encouragement, laughter, and unwavering support made the challenges of graduate life easier to bear. Sharing both successes and struggles alsongside you sustained my motivation and gave me strength when I needed it most. I would also like to thank Mathieu Lachapelle for the lively discussions and thoughtful feedback during my studies. Those conversations not only shaped my research but also deepened my appreciation for the science. My sincere thanks also go to Katja Winger, Hadleigh Thompson, and François Roberge for their technical assistance.

This thesis is as much a reflection of your support as it is of my own work, and I will be forever grateful.

DÉDICACE

"What did I know, what did I know
of love’s austere
and lonely offices? "
Robert Hayden

TABLE DES MATIÈRES

LISTE DES FIGURES

LISTE DES TABLEAUX

LISTE DES ABRÉVIATIONS, DES SIGLES ET DES ACRONYMES

SN	Snow
FR	Freezing rain
RN	Rain
PL	Ice pellets
DZ	Drizzle
FZDZ	Freezing drizzle
CTRL	Control
PGW	Pseudo-global warming
P1	Pathway 1
P2	Pathway 2
P3	Pathway 3
P4	Pathway 4

RÉSUMÉ

Les températures de l'air proches de 0°C représentent un point d'inflexion critique dans les processus atmosphériques, influençant les transitions de phase des précipitations, les cycles gel–dégel ainsi qu'un large éventail de processus environnementaux et infrastructurels. Dans le contexte du réchauffement climatique, comprendre l'évolution spatiale et temporelle de ces phénomènes est essentiel pour améliorer la prévision des aléas, renforcer la résilience des infrastructures et élaborer des stratégies d'adaptation au climat. Cette thèse étudie le comportement des épisodes proches de 0°C, y compris les précipitations, sur l'est du Canada et des États-Unis, dans des scénarios climatiques actuel (CTRL) et de pseudo-réchauffement global (PGW), en utilisant des simulations climatiques régionales à haute résolution.

La première partie de cette recherche porte sur la caractérisation des trajectoires de température proches de 0°C à partir de 11 années de simulations à 2,5 km de résolution. Quatre trajectoires distinctes ont été identifiées, les plus fréquentes étant la trajectoire 3 (refroidissement suivi d'un réchauffement) et la trajectoire 4 (réchauffement suivi d'un refroidissement). Ces trajectoires présentent des patrons spatiaux marqués, la trajectoire 3 dominant dans les régions méridionales et la trajectoire 4 dans le nord. Sous conditions PGW, la frontière entre ces régimes se déplace vers le nord. Le nombre d'heures proches de 0°C augmente dans le nord et diminue dans le sud, tandis que le calendrier des événements se décale plus tard en automne et plus tôt au printemps. La distribution des températures montre que des maxima peuvent se produire à des températures proches de 0°C, tant dans le climat actuel que dans un climat plus chaud. Ces maxima proches de 0°C se réorganisent sous réchauffement: dans l'est du Canada, les maxima secondaires deviennent primaires, tandis qu'ils diminuent dans l'est des États-Unis.

La deuxième partie examine le rôle du dégagement de chaleur latente lors des épisodes de pluie verglaçante, en particulier son impact sur la température de surface et la phase des précipitations. Une étude de cas d'une importante tempête de pluie verglaçante en avril 2023 sur l'est du Canada a été simulée à l'aide du modèle GEM avec le schéma de microphysique P3 (Predicted Particle Properties) modifié. Les résultats montrent que le dégagement de chaleur latente issu du gel des gouttelettes surfondue accroît significativement les températures de l'air à 2 m, les poussant

souvent au-dessus du seuil de congélation et entraînant ainsi de la pluie plutôt que de la pluie verglaçante. La médiane des cumuls de pluie verglaçante a diminué de 34,4 %, et le temps nécessaire pour atteindre 0°C à la surface diminué de 2,5 heures. Ces résultats soulignent l'importance des processus liés à la chaleur latente dans la modulation de la phase des précipitations et mettent en évidence la nécessité d'une représentation précise des rétroactions microphysiques dans les modèles climatiques.

La troisième partie étudie l'évolution des épisodes de pluie verglaçante de longue durée (≥6 heures) sous les scénarios CTRL et PGW dans le sud-est des États-Unis, le sud du Québec et le Nouveau-Brunswick. Les simulations révèlent une diminution de la fréquence de ces événements sous PGW, accompagnée d'une transition accrue vers la pluie pendant et après les épisodes. Les températures de surface au début des événements sont plus élevées dans le climat PGW, le sud du Québec présentant l'augmentation la plus forte (+4,18°C). Dans cette région, des conditions de surface plus sèches favorisent un refroidissement par évaporation, contribuant au maintien de températures sous le point de congélation. Par ailleurs, l'épaisseur et la température maximale de la couche de fonte en altitude diminuent sous PGW, indiquant une couche de fonte plus froide malgré un réchauffement de surface. Le dégagement de chaleur latente demeure un facteur dominant limitant la durée des événements, supprimant la pluie verglaçante dans 84 % des cas dans le sud-est des États-Unis sous climat actuel et dans 90 % des cas au sud du Québec sous PGW.

Dans l'ensemble, cette thèse propose une évaluation complète des conditions proches de 0°C et de l'évolution des types de précipitations hivernales dans un contexte de réchauffement climatique. Les résultats mettent en évidence l'interaction complexe entre transitions de température, rétroactions liées à la chaleur latente et dynamiques de phase des précipitations. Ils offrent des pistes essentielles pour le développement de modèles climatiques, la réduction des risques et la planification des infrastructures dans les régions vulnérables aux extrêmes météorologiques hivernaux. De plus, cette thèse contribue à l'avancement des connaissances sur les impacts des changements climatiques dans les régions froides et souligne l'importance de la modélisation à haute résolution pour saisir les processus localisés qui gouvernent la variabilité météorologique et climatique.

ABSTRACT

Air temperatures close to 0°C represent a critical inflection point in the atmospheric processes, influencing precipitation phase transitions, freeze–thaw cycles, and a wide range of environmental and infrastructural processes. In the context of a warming climate, understanding how these phenomena evolve spatially and temporally is essential for improving hazard forecasting, infrastructure resilience, and climate adaptation strategies. This thesis investigates the behavior of near-0°C episodes, including precipitation, across Eastern Canada and the United States under both current (CTRL) and pseudo-global warming (PGW) climate scenarios using high-resolution regional climate simulations.

The first component of this research focuses on the characterization of near-0°C temperature pathways using 11 years of 2.5-km resolution simulations. Four distinct temperature transition pathways were identified, with Pathway 3 (cooling followed by warming) and Pathway 4 (warming followed by cooling) being the most prevalent. These pathways exhibit strong spatial patterns, with Pathway 3 dominating in southern regions and Pathway 4 in the north. Under PGW conditions, the boundary between these regimes shifts northward. Near-0°C temperature hours increase in northern areas and decrease in the south, while the timing of events shifts later in the fall and earlier in the spring. The temperature distribution shows that peaks can occur at temperatures close to 0°C in both the current and warmer climate. These near-0°C peaks in temperature distributions reorganize under warming: secondary near-0°C peaks in Eastern Canada become primary, whereas those in the Eastern U.S. diminish.

The second component examines the role of latent heat release during freezing rain events, particularly its impact on surface temperature and precipitation phase. A case study of a major freezing rainstorm in April 2023 over Eastern Canada was simulated using the GEM model with the modified Predicted Particle Properties (P3) microphysics scheme. Results show that the release of latent heat from freezing supercooled droplets increases 2-m air temperatures, often pushing them above the freezing threshold and resulting in rain instead of freezing rain. The median cumulative freezing rain decreased by 34.4%, and the time required for surface temperatures to reach 0°C was reduced by 2.5 hours. These findings underscore the importance of latent heat

processes in modulating precipitation phase and highlight the need for accurate representation of microphysical feedbacks in climate models.

The third component investigates the evolution of long-duration freezing rain events (≥6 hours) under CTRL and PGW scenarios across southeastern U.S., southern Quebec, and New Brunswick. Simulations reveal a decrease in the frequency of such events under PGW, accompanied by a shift toward rain during and after the events. Onset surface temperatures are warmer in PGW, with southern Quebec experiencing the largest increase (4.18°C). In southern Quebec, drier onset surface conditions in PGW enhance evaporative cooling, helping to maintain subfreezing temperatures. Additionally, the depth and maximum temperature of the melting layer aloft decrease under PGW, indicating a cooler melting layer despite surface warming. Latent heat release remains a dominant factor in limiting event duration, suppressing freezing rain in 84% of events in the southeastern U.S. under current climate and in 90% of events in southern Quebec under PGW.

Together, this thesis provides a comprehensive assessment of near-0°C conditions and winter precipitation types of evolution in a changing climate. The results highlight the complex interplay between temperature transitions, latent heat feedbacks, and precipitation phase dynamics. They offer critical insights for climate model development, hazard mitigation, and infrastructure planning in regions vulnerable to winter weather extremes. Furthermore, this thesis contributes to the growing body of knowledge on climate change impacts in cold regions and underscores the importance of high-resolution modeling in capturing localized processes that govern weather and climate variability.

Introduction

In cold regions, near-0°C air temperatures, whether accompanied by precipitation or not, can have devastating social, environmental, and economic impacts (Jahn et al., 2015). These conditions can lead to power outages, traffic accidents, and disruptions to daily life. When air temperature rises above 0°C, they can accelerate the melting of snow and ice, potentially causing damaging floods within a few days. Precipitation during these periods can further intensify the impacts. Depending on the vertical temperature profile, winter precipitation can occur in various forms, including ice pellets, snow, snow pellets, and freezing rain (Thériault et al., 2012). The type of precipitation that reaches the surface can influence regional hydrology, affecting snowpack variability (Sospedra-Alfonso et al., 2015), water quality and quantity (Trenouth et al., 2015), and increasing the risk of spring flooding (Stewart et al., 2015).

Many regions of Canada have experienced the consequences of near-0°C events (Mekis et al., 2020; Stewart et al., 2023). The 1998 ice storm in southern Quebec and eastern Ontario resulted in 28 deaths and nearly one billion dollars in damages from repairing transmission lines alone (Lecomte et al., 1998). In 2017, a prolonged freezing event caused significant damage to utility infrastructure, leading to power outages that affected 133,000 homes in New Brunswick (Thériault et al., 2022). The impacts of winter precipitation have been well documented (Martner et al., 1992; Rauber et al., 2001). At a U.S. workshop on quantitative precipitation forecasting (Ralph et al., 2005), the data assimilation and modelling group identified the main challenge in forecasting winter precipitation as determining the type of precipitation when surface temperatures are near freezing. Therefore, understanding the processes and types of precipitation associated with near-0°C conditions is essential for early risk planning, mitigation, and management.

1.1 Literature review

1.1.1 Climatology of near-0°C conditions

Mekis et al. (2020) conducted a 31-year climatological study across Canada to examine near-0°C atmospheric conditions from 1981 to 2011. The findings revealed that the leeward side of the western Cordillera experienced the highest frequency of near-0°C atmospheric conditions. Atlantic Canada had the second highest occurrence during the cold season, influenced by maritime effects.

Northern Canada averaged approximately one occurrence per week, while southern Ontario also showed higher frequencies due to the influence of warm air masses from the south. Although the number of near-0°C occurrences remained relatively stable over the study period, the average annual temperature showed an increasing trend. Figure 1.1 illustrates the average annual number of days with near-0°C conditions across Environment and Climate Change Canada (ECCC) weather stations from 1981 to 2011.

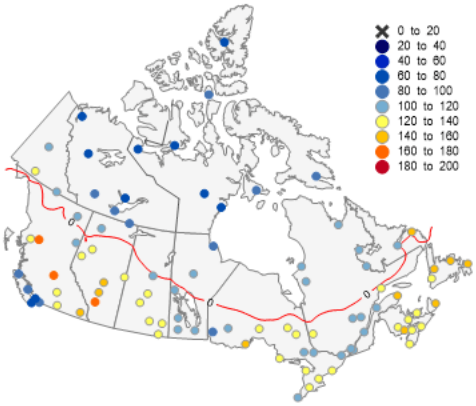

Figure 1.1: Average annual number of days with near-0°C conditions from 1981-2011 across Canada (adapted from Mekis et al., 2020). The red line indicates the 0°C isotherm.

Surface air temperature can transition through near-0°C conditions via four distinct pathways (Mekis et al., 2020), as illustrated in Figure 1.2. Depending on the location, these temperature fluctuations can be influenced by factors such as sky conditions (e.g., cloud cover or clear skies), the diurnal cycle (daily temperature variation), precipitation (including latent heat released during freezing rain), or the presence of large-scale weather systems. Freezing rain typically occurs when temperatures shift from below to above 0°C. According to Stewart et al. (1995), this temperature evolution is often associated with the passage of a warm front. In their study, Mekis et al. (2020) found that Pathway 3 was the most frequently observed among the selected weather stations.

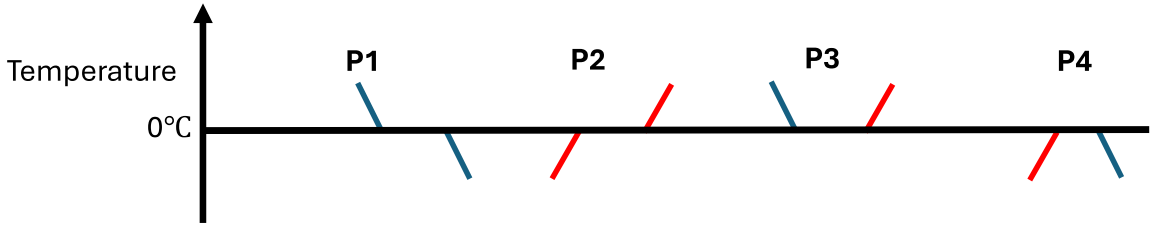

Figure 1.2: Four temperature pathways (P1, P2, P3 and P4) that enter and exit near-0°C conditions. The blue color represents cooling, and the red color represents warming.

Stewart et al. (2023) examined near-0°C surface temperatures using both retrospective and pseudo-global warming simulations. Their findings suggest that the annual occurrence of near-0°C conditions over southern Canada could increase from 985 hours to 1,035 hours under warmer climate scenarios. In terms of temperature distribution, 45% of southern Canada currently exhibits a temperature peak near 0°C. These peaks are most observed along the eastern and western coasts of Canada and are expected to persist under warmer conditions. The fraction of near-0°C occurrences accompanied by precipitation varies spatially between the two simulations, ranging from approximately 15 to 25% over Quebec and Atlantic Canada to more than 50% in certain areas of the Pacific Coast.

Several studies have investigated the types of precipitation that occur near 0°C. Precipitation types within this temperature range include freezing rain, freezing drizzle, ice pellets, snow pellets, snow, and rain. Research has explored the relationship between rain and snow, noting an increased probability of rain as temperatures rise from near-0°C. Transitions between rain and snow also commonly occur in this temperature range. Stewart et al. (1992) summarized literature indicating that near-0°C conditions are optimal for producing large snowflakes (greater than 20 mm in diameter) through collision processes. Additionally, the release of latent heat from freezing rain can warm the surface to near-0°C (Stewart, 1985; Lackmann et al., 2002). The formation of various precipitation types near 0°C is possible due to partial and complete phase changes occurring within this temperature range.

1.1.2 Winter precipitation type formation

A wide variety of precipitation types can occur during winter, especially under near-0°C conditions. These types can be categorized based on the physical state of the particles: ice, liquid, and mixed phase. Further classification is possible by examining particle characteristics such as size, shape, density, and terminal velocity (Stewart et al., 2015). Occasionally, a mixture of precipitation types may be observed at the surface, including combinations of rain, snow, ice pellets, and freezing rain (Stewart and King, 1987; Stewart and Crawford, 1995; Zerr, 1997). This variability arises from the diverse range of hydrometeors present in the atmosphere, each of which can evolve differently. The mechanisms behind the formation of various winter precipitation types have been extensively studied (Zerr, 1997; Isaac et al., 1996; Stewart and King, 1987; Stewart, 1985). These processes

involve both mass and phase changes, making them complex and difficult to quantify (Knight, 1979). However, significant progress has been made in recent decades (Kumjian et al., 2013; Zhang et al., 2011; Lachapelle et al., 2022).

Winter precipitation types can form through either ice-phase processes or warm-rain processes (Stewart et al., 2015). In the warm-rain process, supercooled water can exist well below freezing temperatures in the absence of ice nuclei. This allows precipitation to reach the surface as liquid and freeze upon contact with a sub-freezing surface. In contrast, ice-phase processes involve phase changes as precipitation falls through the atmosphere. These typically occur when there is a melting layer aloft and a refreezing layer below (Figure 1.3a). Solid precipitation particles, sometimes with varying degrees of riming, enter the melting layer and melt either partially or completely. If a particle melts partially, the remaining ice within it can initiate refreezing, resulting in ice pellets or liquid-core pellets reaching the surface. If the particle melts completely, it may fall as freezing rain, unless locally formed ice crystals near the surface trigger collisional freezing. In cases where no refreezing layer is present (Figure 1.3b), the melting region is close to the surface, and precipitation can reach the ground in a completely or partially melted state.

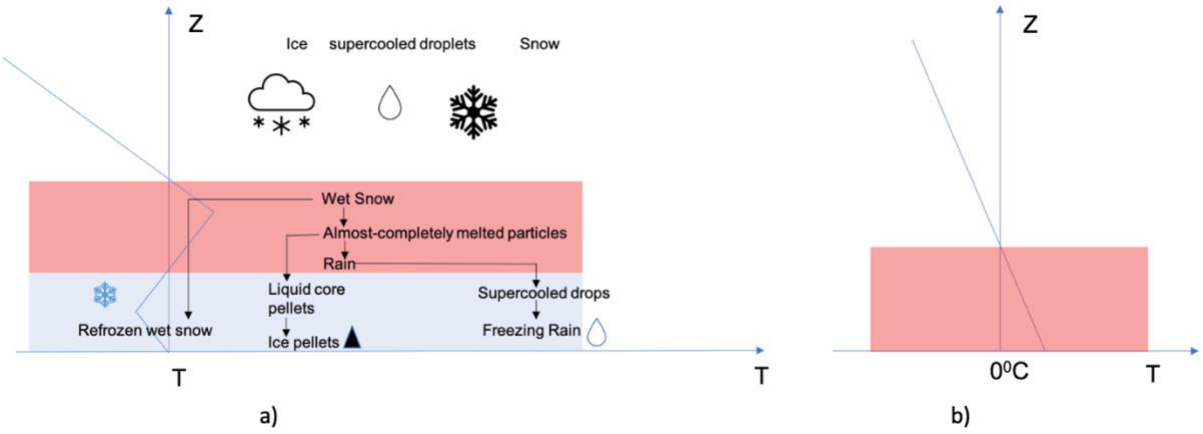

Figure 1.3: Schematic diagram of the evolution of the precipitation type when falling through a) The melting layer (red block) above the freezing layer (blue block) b) the melting layer (red block) close to the surface.

Ice pellets and freezing rain can form under similar atmospheric conditions (Hanesiak and Stewart, 1995; Zerr, 1997). The depth and temperature of the transition region play a critical role in determining whether snowflakes melt sufficiently, which in turn affects the resulting precipitation type. To distinguish the environmental conditions that lead to freezing rain or ice pellets, it is

important to understand how hydrometeors behave within the melting and freezing layers (Czys et al., 1996). Based on sounding observations, Zerr (1997) identified that a maximum temperature of 4.9°C and a melting layer depth of 1,360 m serve as thresholds separating freezing rain from ice pellets.

1.1.3 Thermodynamic feedbacks

The formation of various types of winter precipitation is closely linked to phase changes, which alter environmental conditions. Melting of solid precipitation absorbs latent heat, which cools the environmental air. In contrast, freezing of liquid water releases latent heat, warming the environmental air and often contributing to temperatures near 0°C (McCray et al., 2019). One consequence is the self-limiting diabatic effect of freezing rain, where latent heat release can raise surface air temperatures and erode the freezing layer. As precipitation falls into a melting layer, it cools the air, allowing subsequent particles to descend further before melting (Findeisen, 1940). If ambient temperatures reach 0°C, the melting layer may be eliminated. Observations show that freezing rain can increase surface temperatures by up to 3°C (Lackmann et al., 2002), and only 11% of such events last longer than four hours due to this self-limiting nature (Cortinas et al., 2004). These processes can lead to the formation of an isothermal layer at 0°C, effectively ending freezing rain.

Neglecting the effects of latent heat in weather models can result in a cold bias and significantly affect the accuracy of predicted precipitation types. Atlas et al. (1969) developed an equation (Equation 1.1) to estimate the amount of snow required to erode a temperature inversion and the corresponding heat needed to form an isothermal layer.

$$Lm = \int_0^{H_x} \rho c_p \gamma_x z \, dz \tag{1.1}$$

where L is the latent heat of fusion, m is the mass of melted snow in the column, H_x is the depth of the isothermal layer x, γ_x is the unperturbed lapse rate of layer a or b and ρ is the air density.
The cooling due to melting can cause supersaturation which can lead to the formation of cloud droplets (Thériault et al., 2006). Formation of cloud droplets warms the environmental air and decreases the impact of cooling caused by melting. If neither condensation nor evaporation is considered, the rate at which melting occurs in an atmospheric column can be calculated.

Quantitative estimates for the time required (δt) to eliminate an inversion with an initial temperature greater than 0℃ layer can be shown by the Equation 1.2.

$$\delta t = \frac{1}{\rho_l R_m} m_{total} \tag{1.2}$$

where ρ_l is the density of water, and R_m is the rainfall rate, m_{total} is the total mass of melted snow. Using the first law of thermodynamics, Lackmann et al. (2002) provided a quantitative estimate of the latent heat released by freezing rain. The net latent heat release or absorption (ΔQ) is given by Equation 1.3.

$$\Delta Q = L_f \rho_l R_m \tag{1.3}$$

The latent heat released during freezing is partitioned between the lowest levels of the atmosphere and the ground surface. Ground cover can vary such as snow, bare soil, forest, or road and accurately quantifying how latent heat is distributed between these land types and the atmosphere remains challenging. For example, the partitioning over frozen soil differs significantly from that over unfrozen soil, as more energy is required to warm frozen soil. Similarly, when the ground is covered with snow, the partitioning of latent heat changes because snow acts as an insulator, affecting the heat flux into or out of the ground.

1.1.4 Other factors leading to temperature change

Mekis et al. (2020) and Stewart et al. (2023) justified the temperature range of -2°C to +2°C as a reasonable window for studying near-0°C conditions due to its strong association with phase changes in precipitation. Notably, up to 75% of freezing rain events in Northern Canada and the prairies occur within this range, which is commonly referred to as the “mixed precipitation regime”. Additionally, according to CEATI (2017), snow becomes too wet to adhere to structures above 2°C, while -2°C marks the threshold below which snow begins to stick and accumulate (Furukawa et al., 1987). This section outlines various factors that contribute to crossing the 0°C threshold, as well as those that help maintain temperatures near 0°C.

Surface orography plays a significant role in temperature transitions during the cold season. Air moving horizontally cannot pass through large obstacles like mountains and must rise over them. Orographic lifting on the windward side leads to cloud formation and moisture loss, creating warm and dry conditions on the leeward slope. Chinook winds in the Rockies are a well-known example,

capable of causing dramatic temperature increases. Gough (2008) reported a 30°C rise in Calgary due to chinooks in 1883. Topographic features also channel regional winds, especially through narrow mountain passes, which can shift local temperatures. Additionally, north-facing slopes in the Northern Hemisphere receive less sunlight than south-facing slopes (Nie et al., 1992), resulting in prolonged shading and limited ground warming. Higher elevations are naturally cooler due to the environmental lapse rate.

Air masses can bring both sub-zero and above-zero temperatures, along with associated precipitation. In winter, coastal regions of Canada are influenced by cold continental polar air masses (dry and clear-skies) and maritime polar air masses (cool and moist), often resulting in rain or snow (Spiridonov et al., 2021). During summer, the Arctic front retreats, and coastal areas experience warmer, drier continental tropical air masses. The Ontario and Quebec regions are similarly affected, with added moisture from the Great Lakes contributing to higher humidity in summer and increased snowfall in winter (Notaro et al., 2021; Shi & Xue, 2019). The Prairies, in contrast, are dominated by dry and stable continental Arctic and polar air masses, as maritime air masses lose moisture crossing the west coast and mountain ranges (McGinn, 2010).

Cloud cover influences temperature fluctuations. Mekis et al. (2020) found that cloudy conditions reduce daytime heating and nighttime cooling, contributing to long-duration near-0°C events. Clouds interact with both longwave and shortwave radiation, affecting surface heating. On clear days, solar radiation reaches the surface more effectively, warming it. On cloudy days, cloud droplets reflect incoming radiation, leading to cooler temperatures. At night, clouds act as absorbers and emitters of infrared radiation, keeping temperatures warmer than on clear nights. Hanson (1961) showed that radiation over the Arctic was twice as strong on clear days compared to overcast ones. Zhang et al. (1996) also demonstrated that cloud base temperature and height influence surface radiative fluxes.

Large bodies of water such as lakes, seas, and oceans help maintain near-0°C conditions in many Canadian regions. During colder seasons, ocean temperatures often hover near-0°C (Phillips, 1990; Larouche and Galbraith, 2016). Sea ice in northern regions also contributes to temperature regulation. Similarly, the Great Lakes maintain near-0°C water temperatures during winter. Land

has a low specific heat capacity, leading to rapid temperature changes, whereas water's higher specific heat capacity moderates temperature fluctuations. As a result, coastal areas experience more stable climates, with proximity to water bodies playing a key role in maintaining near-0°C conditions.

Snow cover influences air temperature through melting and freezing processes. Melting snow releases liquid water, which can then freeze, both processes driving air temperature toward 0°C (Takeuchi et al., 2002). Snow also depresses daytime temperatures due to its high albedo. Namias (1963) found that increasing surface albedo from 0.2 to 0.8 warmed a 1 km boundary layer by 7.5°C. Strack et al. (2003) identified two main reasons for snow's cooling effect: reduced incoming radiation due to high albedo and the temperature limit of snow, which cannot exceed 0°C. Any additional energy is used for melting rather than warming.

Seasonally frozen soil, widespread across Canada, affects surface temperatures through its freezing and thawing behavior. Boone et al. (2000) noted that frozen soil helps maintain near-0°C conditions. Soil characteristics also influence atmospheric boundary conditions. The partitioning of solar energy into latent, sensible, and ground heat fluxes depends on factors such as soil moisture (Pielke, 2001; Sutton et al., 2006) and texture (Ek and Cuenca, 1994). Fan (2009) showed that soil temperature and moisture impact air temperature through surface energy exchanges and evaporation.

1.2 Research gaps and Objectives

Despite the wide implications of near-0°C conditions, several key gaps remain. First, although near-0°C temperature pathways are critical for determining precipitation phase, freeze–thaw cycles, and associated environmental impacts, existing research has largely focused on isolated weather stations. This leaves a lack of large-scale, high-resolution analysis under both current and future climate scenarios. Second, while the role of latent heat in phase transitions is acknowledged, no studies have directly implemented and quantified its impact within weather prediction models, particularly regarding near-surface warming during freezing rain events. Third, the thermodynamic

conditions of long-duration freezing rain events in a warming climate are not fully understood. In particular, the latent heat released at the surface during freezing rain plays a key role in modulating event persistence and transitions yet has not been thoroughly examined in a climatological context across current and future climates. These gaps limit our ability to accurately model, forecast, and mitigate the impacts of freezing rain and near-0°C temperature variability. Thus, the overall goal is to improve our understanding of episodes of near-0°C conditions and their changes in warmer climate conditions. In particular,

1. To characterize near-0°C temperature pathways across Eastern Canada and the Eastern United States under current and future climate scenarios using high-resolution regional climate simulations.
2. To quantify the impact of latent heat release from freezing rain on near-surface air temperature and precipitation phase transitions through implementation in numerical weather models.
3. To examine the climatological thermodynamic conditions of long-duration freezing rain events in both current and warmer climates, with a particular focus on the role of latent heat release at the surface in modulating event persistence and transitions.

To attain the objectives, we use Canadian Regional Climate Model (CRCM6-GEM5) model (Roberge et al. 2024) and observational datasets from Environment and Climate Change Canada (ECCC) and Integrated Surface Database (ISD; Smith et al., 2011). A freezing rain event was simulated using CRCM6-GEM5 to quantify the impact of latent heat release on near-surface air temperature and precipitation phase transitions, with the latent heat parameterization implemented directly within the model.

The CRCM6-GEM5 simulations (Roberge et al. 2025) were used to understand the near-0°C temperature pathways and thermodynamic freezing rain processes across Eastern Canada and the Eastern United States. To understand how these processes evolve in a future warmer climate, we use the the pseudo-global-warming (PGW) approach. In the regional climate modeling community, the PGW approach (Schär et al., 1996) has been widely used as an alternative to the traditional GCM-based dynamical downscaling strategy. Rather than driving a regional climate model (RCM)

with direct output from a global climate model (GCM), the PGW strategy imposes climate change signals (Δ) derived from the difference between future and historical GCM time slices. These signals are applied to historical events by modifying the initial and lateral boundary conditions, producing a PGW simulation that represents how the current climate would appear under future warming conditions (Brogli et al., 2023).

The PGW approach offers key advantages over conventional downscaling. Because the same lateral boundary conditions are used in both historical and PGW simulations, differences are not obscured by internal variability. Only one additional simulation is needed, making PGW considerably less computationally expensive than traditional downscaling (Brogli et al., 2023). With Δ applied as a monthly mean perturbation without interannual variability, a simulation period shorter than the typical 30 years suffices to assess future warming. PGW is well suited to the storyline approach for climate vulnerability assessment, allowing researchers to examine how historical extreme events might unfold under warmer conditions (Hazeleger et al., 2015; Shepherd, 2019; Brogli et al., 2023). It has also been used to investigate changes in precipitation (Rasmussen and Liu, 2017), local temperature (Expósito et al., 2015), and snow cover (Hara et al., 2008; Kawase et al., 2013; Ikeda et al., 2021)

These objectives are addressed in the following chapters of this thesis. The structure of these chapters are as follows:

Chapter 2 presents the climatology of temperature pathways entering and exiting near-0°C conditions from 2012 to 2022, based on data from model simulations and surface station observations. The analysis identifies six key regions across Eastern Canada and the United States where near-0°C temperature pathways are most prominent. For each region, the seasonality, frequency, and dominant modes of these pathways are characterized. Changes in the pathways under a warmer climate are then examined using the pseudo-global warming (PGW) scenario.

In Chapter 3, the influence of latent heat released during the freezing of supercooled drops is examined for the 5-6 April 2023 ice storm in southeastern Canada. High-resolution simulation

incorporating the latent heat from freezing rain are used to quantify investigate the impact of the latent heat release associated with freezing rain on the air temperature and the type of precipitation. In Chapter 4, the climatological characteristics of long-duration ($\geqslant$6 hours) freezing rain events are analyzed under both current and warmer future climates using CRCM6-GEM5 simulations. The study examines events across the southeastern United States, southern Quebec, and New Brunswick to identify the thermodynamic conditions that favor prolonged freezing rain in the CTRL and PGW scenarios. The chapter further explores the climatological role of latent heat in modulating and potentially suppressing freezing rain occurrence under both current and warmer climate conditions.

CHAPTER 2

Near-0°C temperature pathways from high-resolution simulation in current and pseudo-global warming future over Eastern Canada and United States

This chapter is presented in the format of a scientific article published in the Journal of Geophysical Research: Atmospheres.

Basnet, S., & Thériault, J. M. (2026). Near-0°C temperature pathways from high-resolution simulation in current and pseudo-global warming future over Eastern Canada and United States. Journal of Geophysical Research: Atmospheres. https://doi.org/10.1029/2025JD045714

Abstract

Near-0°C (−2°C to +2°C) air temperatures are critical for determining the phase of precipitation, the onset of freeze–thaw cycles, and associated impacts on the environment and infrastructure. Change is expected in a warming climate, yet large-scale, high-resolution understanding of near-0°C transitions remain limited, particularly under future conditions. Here we use 11-year high-resolution (2.5-km) regional climate simulations for current and future warmer scenarios to assess near-0°C temperature pathways across eastern Canada and the United States. We show that the annual 0°C isotherm shifts northward in a warmer climate, with near-0°C hours increasing in northern regions and decreasing in the south. We studied how temperatures move in and out of the near-0°C range and found that events staying entirely above 0°C (P3) are more common in southern areas, while those staying entirely below 0°C (P4) are more frequent in the north. In the warmer climate, the dividing line between these two patterns shifts farther north. Except for P4, most pathways that occur in the spring in the current climate occur in the winter in warmer climate, especially in the northern part of the domain. As the climate warms, temperature distributions in northern regions show a more pronounced peak near 0°C, while in southern regions the peak near 0°C occurs less often. These findings demonstrate that near-0°C pathways and peaks will undergo spatial and temporal reorganization under climate warming. The results offer key insights for planners and engineers aiming to adapt to increased variability around freezing and thawing affecting snow removal, infrastructure resilience, and seasonal flood risk.

2.1 Introduction

The occurrence of air temperatures near 0°C can have various severe social, economic, and environmental consequences, influencing processes like growing season, flooding season, snow melt/accumulation, permafrost thaw, unseasonal frosts, and animal hibernation (Stewart et al., 2015). In regions like Finmark, Norway, where reindeer forage lichen through snow, air temperatures hovering around 0°C can trap fodder beneath the ice layers (Turunen et al., 2016; Eira et al., 2018). The damage associated with these events can be catastrophic. Thus, understanding and monitoring near-0°C events is vital as changes in their duration and frequency can have wide-reaching consequences across various sectors, with longer events posing an even greater concern.

Several studies have been carried out to understand the different aspects of near-0°C conditions. Fujibe et al. (2001) found a higher frequency of surface temperature hovering around 0°C compared to other temperature ranges. Boone et al. (2000) found that frozen or thawing soil can help maintain temperatures near freezing. Mekis et al. (2020) used data from 92 climatic stations across Canada to characterize near-0°C conditions in Canada. Stewart et al. (2019) showed a northward movement of the 0°C isotherm with climate change. Kerguillec (2015) studied the seasonal and annual trends and variability of temperatures crossing the 0°C threshold in 20 weather stations in Norway. Based upon an ensemble of climatic models, Kjellström et al. (2016) presented projected changes in these crossings towards the end of century over Fennoscandia. Leduc et al. (2025) concluded that the annual number of freeze–thaw days is expected to be the same in Canada and the northern part of the U.S. based on a set of bias-adjusted CMIP6 global climate projections.

Weather systems and climatic variability can both impact near-0°C occurrences, as can topography, particularly high terrain (e.g., Cardinal et al., 2024). The flow field in mountainous regions allow temperatures to pass through 0°C in the winter season. The moderating effect of oceans and other water bodies in contributing to near-0°C occurrences during winter can be seen in Atlantic Canada, areas surrounding the Great Lakes, and the Arctic (Mekis et al., 2020). This occurs because water bodies that have temperatures close to 0°C help bring the air temperatures above them to similar values. Mekis et al. (2020) also showed that for all stations, the longest duration near-0°C events were dominated by cloudy conditions that reduced the temperature swings between day and night.

Phase changes such as melting and freezing can drive temperatures towards 0°C (e.g., Stewart, 1985; Takeuchi et al., 2002; Basnet et al., 2025). For example, during a freezing rain event, when solid precipitation falls through the melting layer, the melting process extracts latent heat of fusion from the surrounding air, driving its temperature to 0°C. This process can produce a deep 0°C isothermal layer and enhance snow aggregation. Conversely, when supercooled droplets freeze upon contact with a surface, the release of latent heat can warm the near-surface cold layer to 0°C, potentially causing a transition from freezing rain to rain. However, cold-air advection or cold onset temperature can offset the effects of latent heat, with the result that the temperature can take a long time to reach 0°C. Both precipitation and snow cover act in a similar way to tip temperatures towards 0°C.

Brief studies have been carried out to understand temperature pathways, defined as the way temperature enters and exits near-0°C conditions, at various locations in Canada. Mekis et al. (2020) looked at temperature pathways at nine weather stations across Canada, while Cardinal et al. (2024) conducted a temperature pathway study at three weather stations in western Canada: Smithers, Prince Rupert and Terrace. While the climatological occurrence of near-0°C pathways may change in the future with warmer and moister conditions, Stewart et al. (2019) contend that near-0°C temperatures in southern Canada will continue to occur in a warmer climate. However, to our knowledge, a large-scale detailed domain analysis of temperature pathways, particularly in a future warmer climate, has not yet been conducted. Given the importance of near-0°C occurrences our study will begin to address some of the knowledge gaps in our understanding of temperature pathways that enter and exit near-0°C conditions in the current and future climate. Hence the goal of this study is to characterize near-0°C temperature pathways in the current climate and in a future warmer climate over eastern Canada and the United States. Two 11-year simulations will be used to address this issue: one representing historical conditions and the other based on the Pseudo-Global Warming (PGW) approach using the CRCM6-GEM5 model. The PGW framework provides a way to isolate the effects of a warmer climate by imposing large-scale thermodynamic changes on the current climate, allowing us to examine how warming influences temperature pathways through both atmospheric feedbacks and microphysical processes.

The paper is organized as follows: Section 2.2 describes the configurations of the control CTRL and PGW experiments, along with the study domain, datasets, and variables used in the analysis. Section 2.3 compares the CTRL outputs with observations. Section 2.4 presents the characteristics of near-0°C temperatures in a warmer climate. Section 2.5 details the near-0°C events and their corresponding pathways. Section 2.6 discusses the physical mechanism for near-0°C conditions, and Section 2.7 presents our concluding remarks.

2.2 Data sets and methods

2.2.1 Regional climate simulations

The Canadian Regional Climate Model version six, based on the Global Environmental Multiscale GEM model, version 5.1.1 (CRCM6-GEM5), was used to conduct the simulations (Roberge et al., 2024). The domain size of the simulations is 1330 x 1060 grid points with a 2.5-km grid-spacing across the eastern United States and Canada, as shown in Figure 2.1. There were 66 vertical levels. CRCM6-GEM5 uses a fully implicit semi-Lagrangian scheme (Tanguay et al., 1992), hence larger time step can be used than other integration schemes. The timestep used was 60 s. The simulation outputs for all fields were hourly. Land surface processes were represented by Canadian Land surface scheme (CLASS, Verseghy, 2000), and clouds and precipitation were represented by the Predicted Particle Properties (P3; Morrison and Milbrandt, 2015) bulk microphysics scheme. Other physical parametrizations include Kuo-transient shallow convection parameterization (Kuo, 1965; Bélair et al., 2005), turbulent kinetic energy closure planetary boundary layer and vertical diffusion (Benoit et al., 1989; Delage and Girard, 1992; Delage, 1997) and correlated-k terrestrial and solar radiation scheme (Li and Barker, 2005).

The CTRL simulation was driven using the CRCM6-GEM5 with a grid spacing of 12 km for the period 2012-2022 which itself is driven by ERA5 reanalysis data (Hersbach et al., 2020). The PGW simulation was configured identically to the CTRL simulation, except that its initial and lateral boundary conditions were modified to account for climate perturbations (Schär et al., 1996; Liu et al., 2017). An 11-year period was selected mainly to limit the computational cost. Nevertheless, because the perturbation applied follows a fixed monthly cycle representing only the mean climate change signal, this relatively short period can capture the long-term average response to warming (Brogli et al., 2023).

The climate change perturbation was taken from monthly mean fields averaged across an ensemble of 30 General Circulation Models (GCMs) from the CMIP6. The climate change signal was calculated between the periods 1990–2014 and 2076–2100 using the scenario Shared Socio-economic Pathway (SSP) 5-8.5. The list of CMIP6 GCMs used, the variables included, and the details of interpolation onto the ERA5 grid are documented in Roberge et al. (2025). The perturbed physical fields include horizontal wind, geopotential, temperature, specific humidity, sea surface temperature and sea ice fraction. CRCM6-GEM5 reads the ocean temperature and sea ice fraction directly from the input files as lower boundary condition. Perturbations from the PGW forcing are applied to these lower-boundary fields as well. Soil temperature was initialized with the perturbed values and was allowed to evolve during the simulation. The data used are available at Roberge et al. (2025).

The main assumption in the PGW approach is that the atmospheric circulation at the lateral boundaries is similar to CTRL but perturbed by the warmer and moister perturbations. Hence, the same weather systems are simulated but in warmer and moister conditions. It is then possible to study the thermodynamic feedbacks from the climate change signal on the historical climate. Given the uncertainty in the future changes in the large-scale circulation (Shepherd, 2014), the PGW approach is an acceptable assumption to study phenomena driven by thermodynamics processes (Rasmussen et al., 2020). The PGW approach has been successfully applied in numerous studies to investigate changes in near-0°C conditions (e.g. Stewart et al., 2023), changes in freezing rain occurrences (e.g. Marinier et al. 2023; Chartrand et al. 2023) and changes in snow cover (e.g. Kawase et al., 2013; Ikeda et al., 2021) under warmer climate conditions.

The meteorological outputs used in the study were 2-m air temperature, amount and type of precipitation, and snow depth. Precipitation analysis was based on hourly data, using a minimum threshold of 0.2 mm liquid water equivalent to define model precipitation occurrence (e.g. Chartrand et al., 2023; Marinier et al., 2023). Freezing rain was determined by the presence of rain when 2-m air temperature is < 0°C. The presence of snow was defined as snow depth greater than 1 cm (Stewart et al., 2023).

2.2.2 Observation and data set

Hourly 2-m observations of temperature were obtained from the Integrated Surface Database (ISD; Smith et al., 2011) dataset through the National Oceanic and Atmospheric Administration National Centers for Environmental Information (NCEI). We excluded stations that had less than 80% of the annual hours for the 11 years we studied, following a similar criterion to Cortinas et al. (2004) and McCray et al. (2019). This yielded 83 stations, whose data were used for analysis and model evaluation (Figure 2.1).

The 2-m air temperature was extracted from the closest grid points to each station. The total number of near-0°C hours and mean 2-m air temperature were computed for the same period using the simulation output data. The correlation between the station data and the CTRL simulation near-0°C temperatures was calculated to assess whether the simulation could be used to investigate the near-0°C events. We selected regions to further study near-0°C conditions and compare differences within the domain (Figure 2.1) based on the spatial variability of their climatological characteristics.

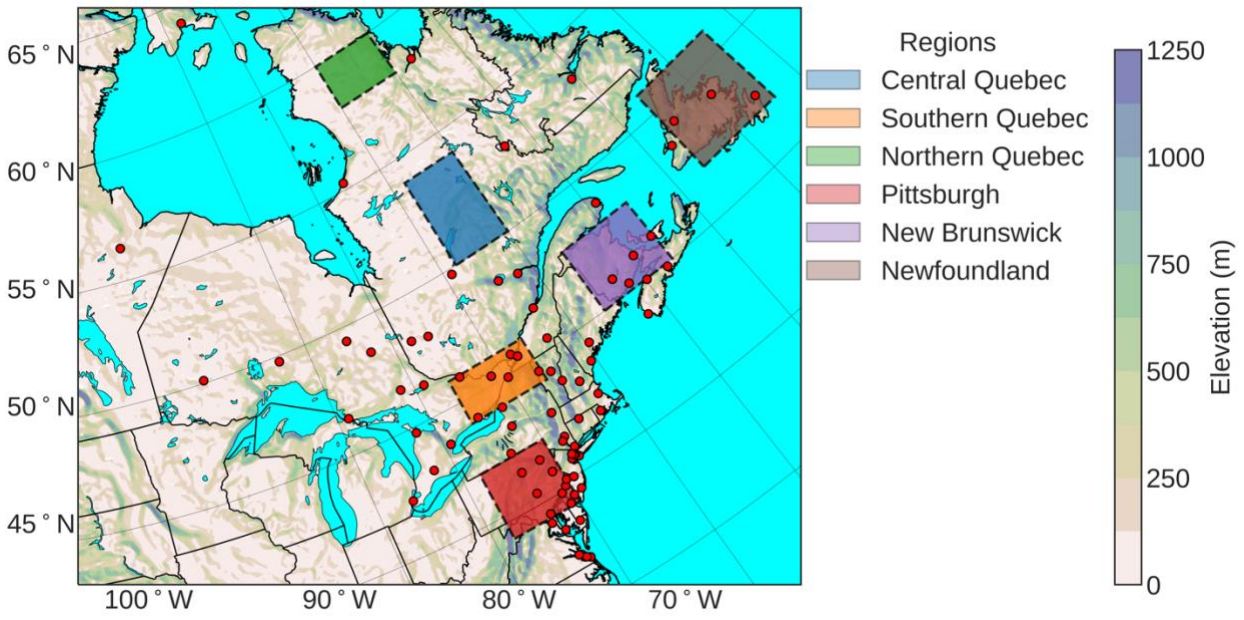

Figure 2.1: The domain of the simulations across the United States and Canada with the 83 weather stations used to validate the CTRL and PGW simulations (red circles). Colored rectangles highlight the six sub-regions that were the focus of analysis, Central Quebec (blue), Southern Quebec (orange), Northern Quebec (green), New Brunswick (purple), Newfoundland (brown), and Pittsburgh (red).

2.2.3 Defintion

2.2.3.1 Temperature pathways

Near-0℃ 2-m air temperatures are defined as temperatures between -2℃ and +2℃ (e.g., Mekis et al., 2020; Stewart et al., 2023). This temperature range captures a critical transition zone where multiple forms of precipitation occur, often simultaneously. Up to 75% of freezing rain events in Canada happen within this range, which is commonly referred to as the "mixed precipitation regime." According to CEATI (2017), the high liquid content of snow above 2°C prevents it from adhering to structures. Conversely, -2°C is considered the upper limit at which snow can stick to surfaces and begin accreting (Furukawa et al., 1987).

Several methods have been used to calculate the duration of near-0℃ and precipitation events (Cortinas, 2000; Ressler et al., 2012; Mekis et al., 2020). We define the duration of a near-0℃ event as the number of consecutive hourly observations during which air temperatures between -2℃ and +2℃ were observed. We classify these events as short-duration if they last less than six hours, and as long-duration if they persist for six hours or more. The temperatures at the start and end of the event can be above or below 0℃. The entry and exit temperature of an event is described as a pathway. There are four possible temperature pathways (P) and they are shown in Figure 2.2.

- Pathway 1 (P1) occurs when the temperature decreases from above to below near-0℃ conditions;
- Pathway 2 (P2) occurs when the temperature increases from below to above near-0℃ conditions;
- Pathway 3 (P3) occurs when the temperature remains above near-0℃ conditions throughout; and
- Pathway 4 (P4) occurs when the temperature remains below near-0℃ conditions throughout.

We analyzed various characteristics of temperature pathways, including the number of different pathways with and without precipitation, their seasonal distribution, and the most frequently occurring pathway in both the current and warmer climate conditions. Near-0°C events with

precipitation are defined as any near-0°C events that include at least one hour with precipitation exceeding 0.2 mm. This ensures that any precipitation occurrences are captured. When multiple near-0 °C events with precipitation occur within the same synoptic-scale event but are separated by more than one hour, they are treated as distinct events, following the approach of Cardinal et al. (2024). While this captures precipitation during near-0°C periods, precipitation events occurring outside the range are not included in our analysis, as our focus is on the air temperature rather than the precipitation itself.

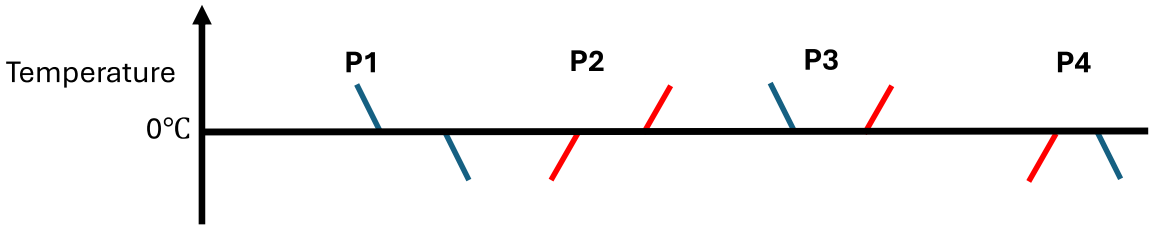

Figure 2.2: Four temperature pathways (P1, P2, P3 and P4) that enter and exit near-0°C conditions. The blue color represents cooling, and the red color represents warming. Adapted from Mekis et al. (2020)

2.2.3.2 Temperature distribution

Hourly 2-m air temperatures were grouped into bins of 4°C intervals, allowing near-0°C conditions to be analyzed in comparison with other temperature ranges. We used a peak detection algorithm from a Python library (Scipy) to find the most prominent peaks in this distribution (Virtanen et al., 2020). The types of temperature peaks studied are shown in Figure 2.3.

These are

- Primary Peak: If the highest peak falls within the temperature range of -2°C to +2°C, it is considered the primary peak.
- Secondary Peak: If the highest peak is not within the -2°C to +2°C range, but there is still a local maximum within this range, it is considered a secondary peak. For this secondary peak to be recognized, its frequency must be higher than the peaks in the adjacent ranges (i.e., +2°C to +6°C and -2°C to -6°C).
- No Peak: Neither the primary nor secondary peak criteria are met.

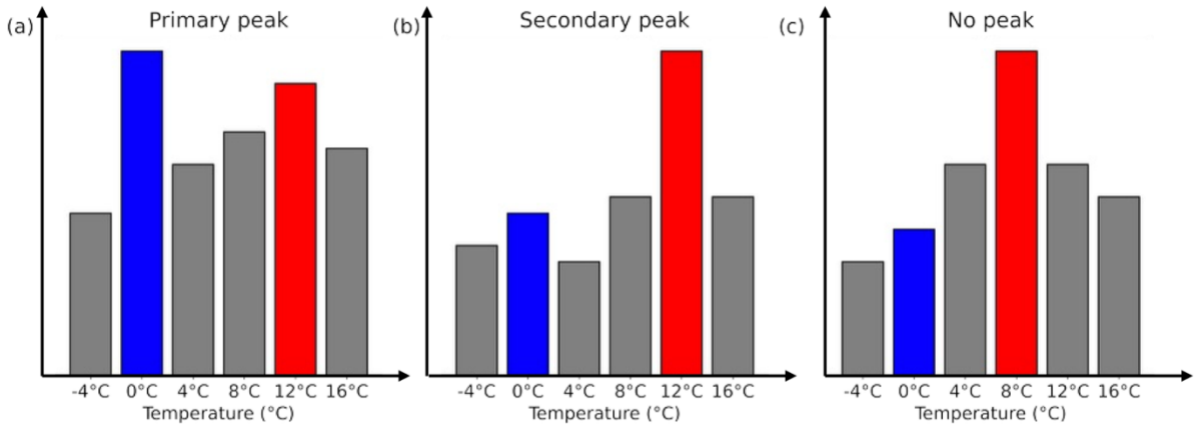

Figure 2.3: Schematic diagram showing plots of temperature distribution and types of peaks: (a) Primary peak, (b) Secondary peak, and (c) No peak. In each plot, the x axis is the temperature, and the y axis is the occurrence.

Using the classified arrays from both simulations, we constructed a transition matrix to summarize how each grid cell's near-0°C peak classification transitioned between CTRL and PGW, capturing all combinations of the three possible categories. Grid points over oceans and lakes were excluded from the analysis. Table 1 outlines the nine possible transitions considered.

Table 2.1: Near-0°C peak categories in a transition matrix used to determine the peak transition between CTRL and PGW. Each element denotes a transition class.

CTRL → PGW	Primary peak	Secondary peak	No peak
Primary peak	Stays primary	Becomes secondary	Becomes no peak
Secondary peak	Becomes primary	Stays secondary	Becomes no peak
No peak	Becomes primary	Becomes secondary	Stays no peak

2.3 Model evaluation

We evaluated the ability of the CRCM6-GEM5 to simulate the 2-m air temperature. The 2-m air temperature was generally relatively well simulated, with a very high R-squared value (0.98) (Figure 2.4). The simulated annual occurrences of near-0°C air temperature also closely matched the station observations (R-squared value 0.84). In western Ontario, the simulated annual average 0°C air temperature isotherm was slightly farther north than the observed one. However, from central Quebec to the east coast, the simulated 0°C isotherm line matched the observed values more closely. Finally, the Atlantic region of Canada has the highest number of near-0°C occurrences, which is well reproduced in the simulations.

Among the stations selected for the study, St. John's, Newfoundland, recorded the highest average annual occurrences of near-0°C temperatures, with approximately 1965 h. St. John's has strong maritime influences and less cold continental airflows, even compared to the rest of the Newfoundland region (Banfield and Jacobs, 1998). During winter, the western and northern regions of Newfoundland are impacted by late-winter sea ice and a higher frequency of cold continental air masses. The J.A. Douglas McCurdy Sydney Airport in Nova Scotia also recorded a significant number of annual near-0°C hours, totaling 1672 h. These high numbers may be attributed to the relatively cooler air in the North Atlantic Ocean, which limits the air temperature near the coast. Furthermore, the dominant westerly winds blowing from the interior of Eastern Canada also bring cold air to the region (Bonsal and Prowse, 2003). However, the model underestimated the annual near-0°C hourly occurrences at both stations. Southern Ontario also produces a high number of near-0°C hourly occurrences, which may be because of the warm air from the south during the cold season (Mekis et al., 2020). Finally, southeastern United States stations produced the fewest number of observed near-0°C hours.

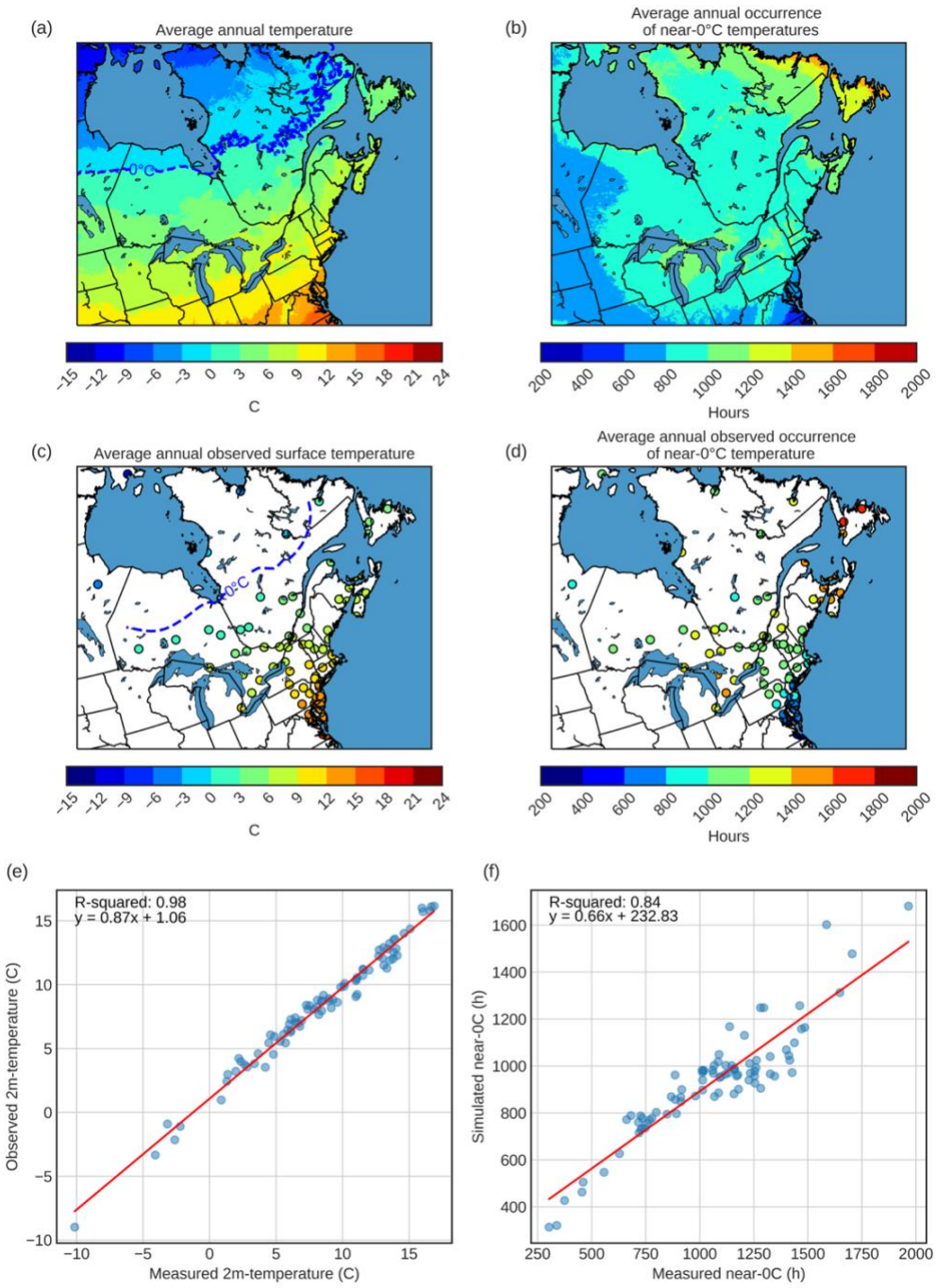

Figure 2.4: Comparison of the simulations (CTRL) and observations over the January 2012–December 2022 period for the 83 locations. (a) CTRL average annual temperatures; (b) CTRL average annual occurrences of near-0°C conditions; (c) observed average annual 2-m temperature (d) observed annual occurrences of near-0°C conditions; (e) scatter plot of observed and simulated 2-m temperatures; (f) scatter plot of observed and simulated near-0°C hours.

We examined the distribution of near-0°C temperature occurrences, with specific focus on the shape of the probability distribution and occurrence of a primary, secondary, or no peak (Figure 2.5). Primary peaks were observed over 42.2% of the domain, secondary peaks over 39.2%, and

no peak over 18.6% in the CTRL simulations. The simulations revealed that primary and secondary peaks are common in eastern Canada, while most of the southeastern part of the United States shows no peak of near-0°C temperatures. Newfoundland and Labrador, the eastern part of Ontario and the western part of Quebec are predominantly associated with primary peaks. Primary peaks are common in the eastern part of New Brunswick, close to the ocean, whereas secondary peaks are dominant in the western part of New Brunswick. Most of the land surrounding Hudson Bay shows secondary peaks. The region of Quebec just north of New Brunswick had a combination of primary, secondary and no peak. In this region, the simulation was able to replicate the primary peak observed at Gaspé Airport. We compared our temperature distribution simulation against Stewart et al. (2023) for both Rouyn-Noranda and Sault Ste. Marie, the only sites in Eastern Canada for which their study showed the temperature distributions. Our results were consistent with theirs, with both sites displaying a peak of near-0°C temperatures (Figure 2.5).

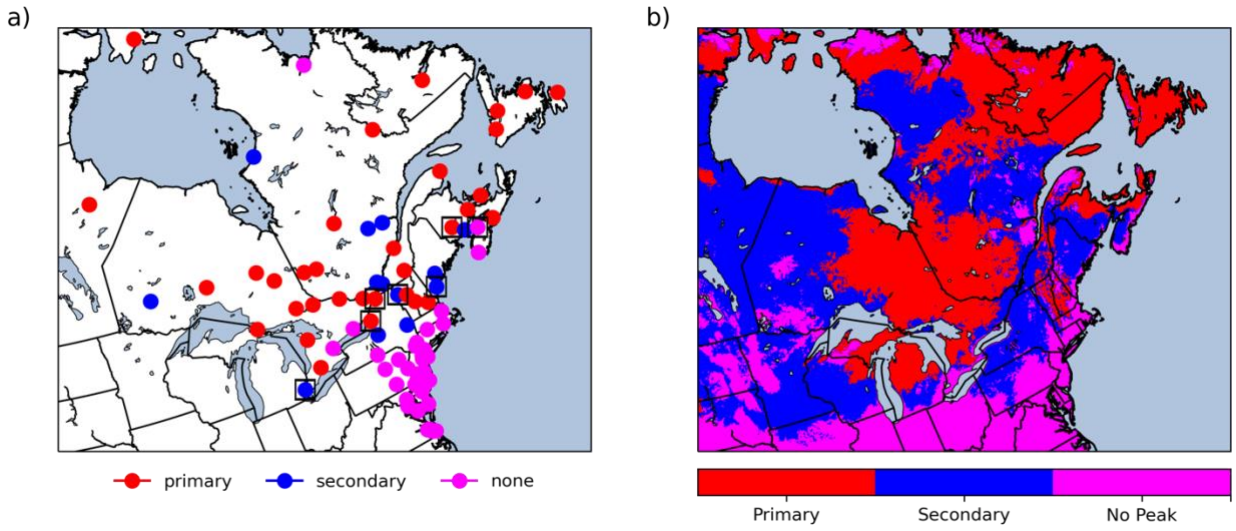

Figure 2.5: Spatial distribution of near-0°C peaks in the temperature distribution over the January 2012–December 2022 period. (a) Observed. (b) Simulated. Open squares indicate sites where observations did not match the CTRL peaks.

Among the stations shown in Figure 2.5, there were 33 with primary peaks, 13 with secondary peaks, and 37 stations with no peaks. Most of the stations without peaks are in Eastern United States and some regions of Ontario, Nova Scotia and northern Quebec. The peak types are well simulated when compared with observations, as the corresponding simulation results showed 31 primary peaks, 14 secondary peaks, and 38 stations with no peaks. The simulations successfully replicated the peak type in 76 out of 83 stations. Of the 7 stations that did not replicate the peak type, 3 stations had an observed primary peak (CYFC (Fredericton, NB), KART (Syracuse, NY), and KMSS (Massena, NY)), while the simulation indicated a secondary peak. Three stations had an observed secondary peak (CYQG (Windsor, ON), KBTV (Burlington, VT), and KPWM (Portland, ME)), of which 2 (CYQG and KPWM) were simulated as having no peak, while KBTV

was simulated as a primary peak. Finally, no peak was observed at CYZX (Greenwood, NS), but the simulation indicated a secondary peak. More information on the model evaluation is provided in the Appendix B

2.4 Characteristics of near-0°C temperatures in warmer climate

2.4.1 Mean annual near-0°C air temperatures

Under PGW, the 2-m temperature shows annual increases of ~4°C in the south and ~9°C in the northeastern domain (Figure 2.6). The 0°C isotherm moves from Central Quebec to the northern tip of Quebec in PGW. A comparison between PGW-CTRL shows that the highest increase in near-0°C hours occurs in Central (68.9%) and Northern Quebec (114.2%). In contrast, there is a decrease of 32% in near-0°C hours in Pittsburgh. Other regions show only a slight reduction in the number of near-0°C hours. The eastern part of Newfoundland and Nova Scotia, which experience the highest occurrences of near-0°C hours in CTRL, see a decrease of at least 400 hours in the PGW, while low occurrences of near-0°C hours occur along the eastern coast, south of Nova Scotia. The highest value in PGW, approximately 2,340 hours, occurs in the Northern Quebec region..

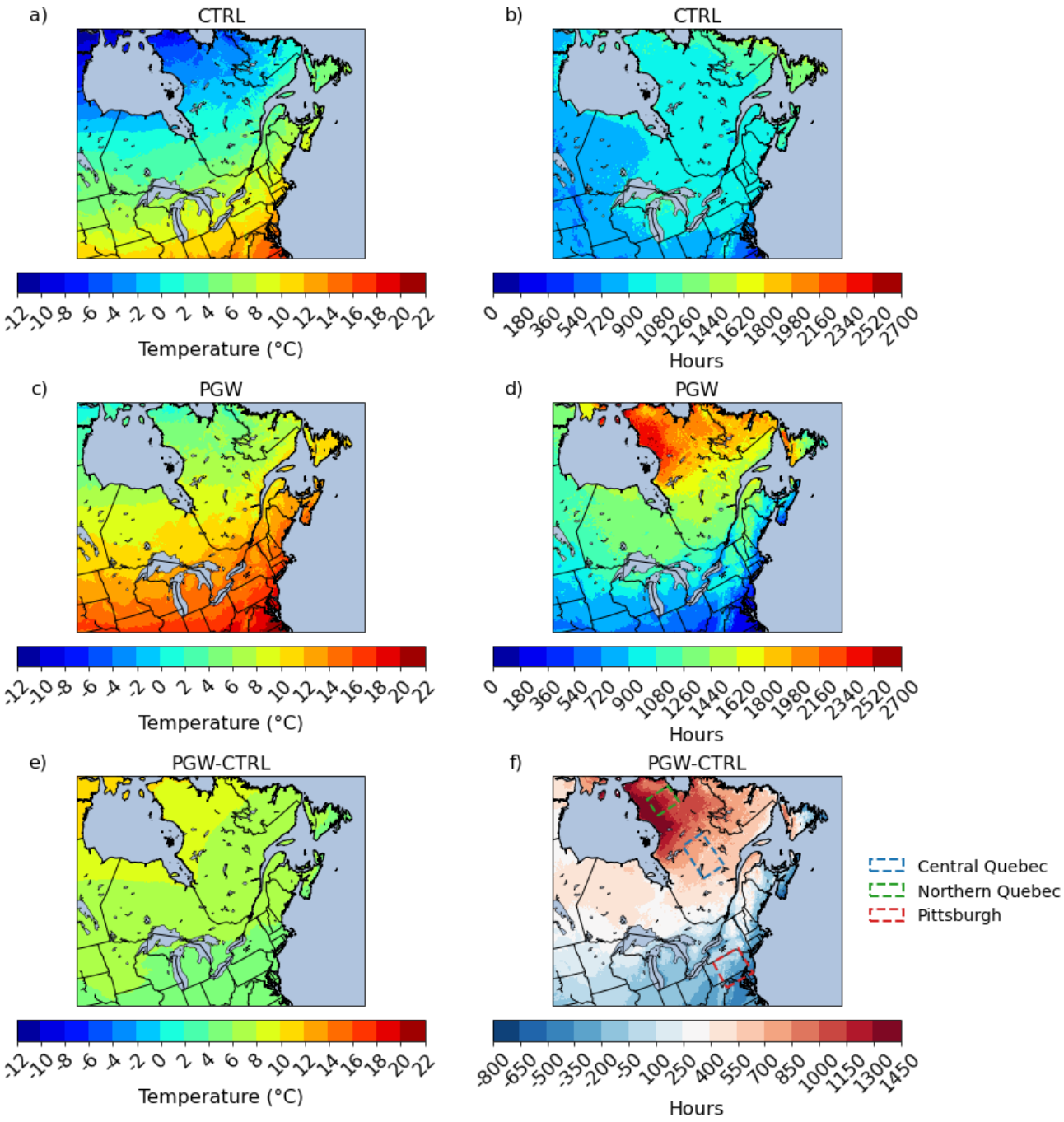

Figure 2.6:Average temperatures for (a) CTRL, (c) PGW, and (e) PGW-CTRL. Average annual near-0°C occurrences for (b) CTRL (d) PGW (f) PGW-CTRL over the January 2012–December 2022 period across eastern Canada and the United States.

The PGW shows that there will be declines of 30–50% in annual near-0°C hours with precipitation in most regions, except Central Quebec (+62.3%) and Northern Quebec (+140.0%) (Figure 2.7). Among the regions in the study, the highest number of near-0°C hours with precipitation in the

PGW is around 335 h (Northern Quebec). In CTRL, the maximum near-0°C hours with precipitation was around 257 h along the coast of Newfoundland. In PGW, the eastern Canada and United States shows a decrease in near-0°C hours with precipitation. The pattern of near-0°C occurrences with precipitation mirrored the results for near-0°C occurrences alone, with increases and decreases occurring in similar regions.

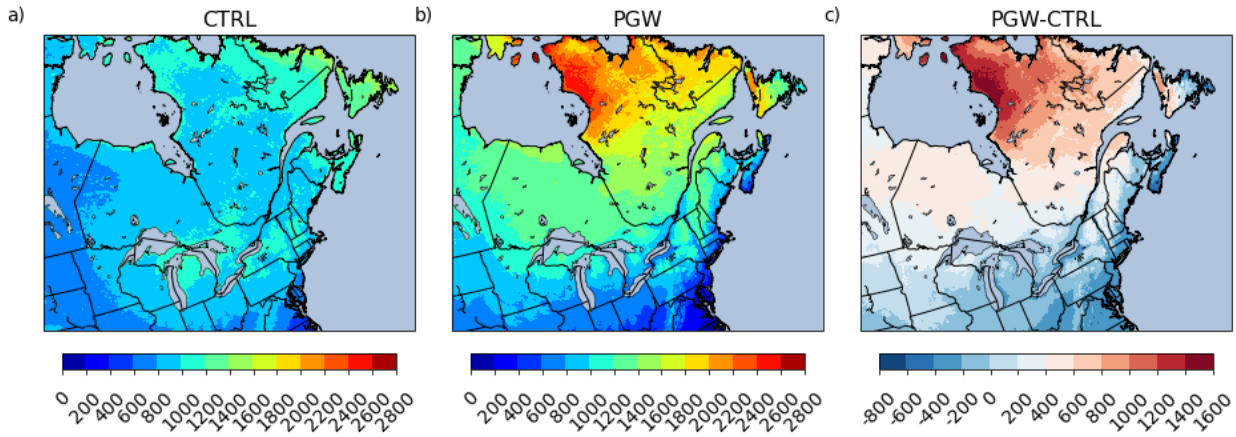

Figure 2.7: Average annual near-0°C occurrences with precipitation (a) CTRL, (b) PGW, (c) PGW-CTRL, over the January 2012–December 2022 period across eastern Canada and United States.

2.4.2 Air temperature distribution

We further analyzed the occurrence of peaks in near-0°C temperatures in the simulation by comparing these temperature peaks in the CTRL and PGW (Figure 2.8). Primary peaks increase from 42.2% of the domain in the CTRL simulation to 58.6% in the PGW simulation. Secondary peaks decrease substantially, from 39.2% in CTRL to 0.03% in PGW. The proportion of the domain with no observed peaks increases from 18.6% in CTRL to 41.4% in PGW. The notable differences in peak occurrences between the PGW and CTRL simulations reflect changes in temperature patterns. Most of the peaks in western Ontario and parts of Central Quebec change from secondary peaks to primary peaks. The southern region of the domain and parts of the east coast show a high increase in occurrences of no peak. There are almost no secondary peaks in the PGW, a decrease which corresponds to an increase of no peak in the southern part of domain and an increase of primary peaks in the northern part.

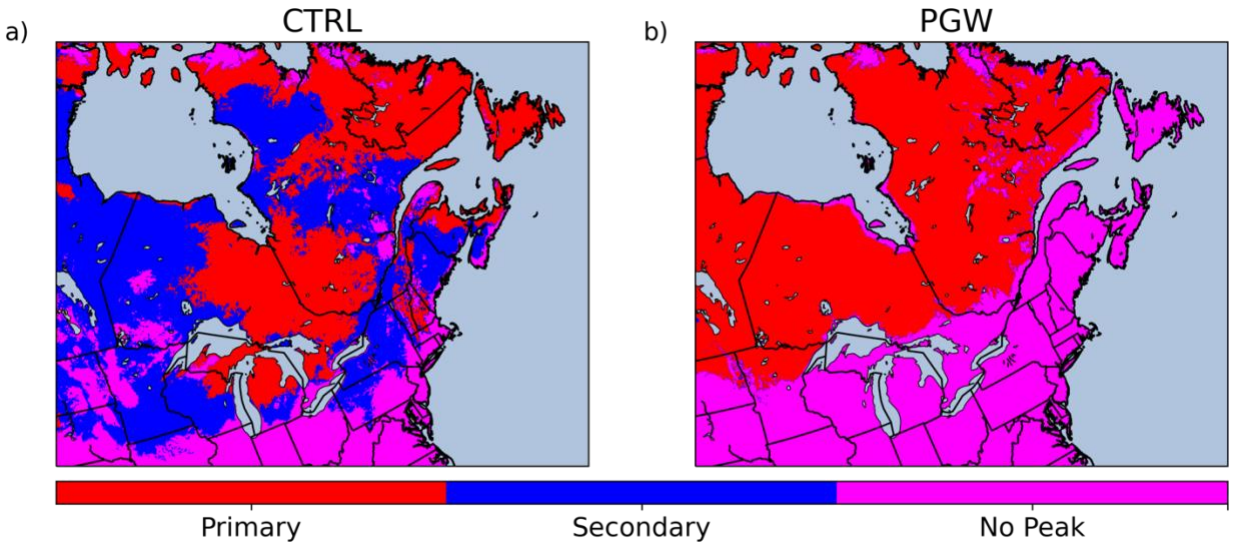

Figure 2.8: Spatial distribution of near-0°C primary (red), secondary (blue), and no peak (pink) in (a) CTRL and (b) PGW simulations

We performed a spatial analysis of the transitions in near-0°C peak classifications from the CTRL to the PGW (Figure 2.9). In CTRL, a large portion of the domain originally classified as primary peaks shifted under PGW; ~23.3% of all grid cells transitioned from primary peaks to no peak, while 18.7% of grid cells had a primary peak in CTRL and remained unchanged in PGW. No grid cells in this category shifted to secondary peak. Grid cells initially classified as secondary peaks exhibited more varied transitions. For example, 15.8% of all grid cells started as secondary peaks and became primary peaks, 10.0% shifted from secondary peaks to no peak, and only a negligible fraction (~0.015%) began and remained secondary peaks. This suggests a substantial weakening of secondary peaks under warmer climate conditions. Finally, 30.2% of grid cells initially exhibited no peak in CTRL and remained unchanged in PGW, and 2.0% began as no peak and transitioned to primary peaks. These results highlight a general decline in secondary peaks, under warmer climate conditions, with a notable shift toward primary peak in the north and no peaks in the south.

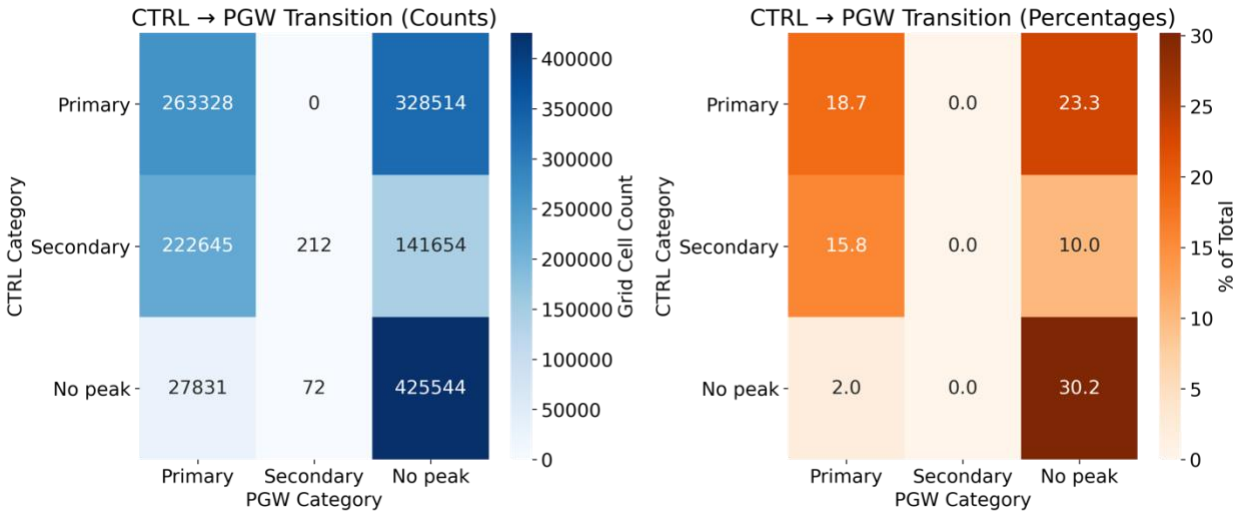

Figure 2.9: Transition matrix heatmaps showing the changes in peak events from the CTRL to the PGW scenario. (a) Absolute counts of grid cells transitioning between peak classifications: primary, secondary, and no peak. (b) Corresponding percentages of total grid cells, illustrating the relative frequency of each transition.

2.4.3 Number of events and their distribution

The average number of near-0°C events per year is different from the number of hours with near-0°C conditions. Pittsburgh and Newfoundland experience the highest annual number of events (~140 events). Most of the events in the Pittsburgh are short duration events (~60%), while Newfoundland not only has a high number of events, but 50–60% of these are long-duration events. Mekis et al. (2020) found a similar high occurrence of near-0°C events that were longer in duration in the Atlantic region. In the PGW scenario, the number of events increases in Central Quebec and Northern Quebec and decreases in all other regions. In fact, the greatest decrease is in Pittsburgh (36.1%). The lowest percentage of short duration events is in Northern Quebec in CTRL, and changes to Central Quebec in PGW. The highest percentage of events > 24 hours is in Northern Quebec in CTRL, which changes to Newfoundland in the PGW simulation.

2.5 Temperature pathways

2.5.1 Occurrence of precipitation pathways

The 2-m air temperature can transition into and out of near-0°C conditions through various pathways. Figure 2.10 illustrates that Pittsburgh exhibits the highest frequency of P1 (40 yr^{-1}) and P2 (30 yr^{-1}) among the regions analyzed in the CTRL simulation. In contrast, in the PGW

simulation, the New Brunswick region shows the highest occurrence of P1 (29 yr^{-1}) and P2 (24 yr^{-1}). Notably, the frequency of P2 decreases in most regions, except for Northern Quebec. In terms of percentage change, P1 and P2 show the greatest decreases in Pittsburgh, with reductions of 45.9% and 49.3%, respectively. Under CTRL conditions, the highest frequency P3 occurs in Pittsburgh (44 yr^{-1}) and the highest frequency of P4 occurs in Newfoundland (41 yr^{-1}). Under PGW conditions, the highest occurrence of P3 is observed in Newfoundland (71 yr^{-1}) and the highest occurrence of P4 is observed in Northern Quebec (96 yr^{-1}). Notably, the frequency of P3 consistently increases across all PGW regions. The most significant increases observed are a 64.9% increase in P3 in Newfoundland and a 200% increase in P4 in Northern Quebec.

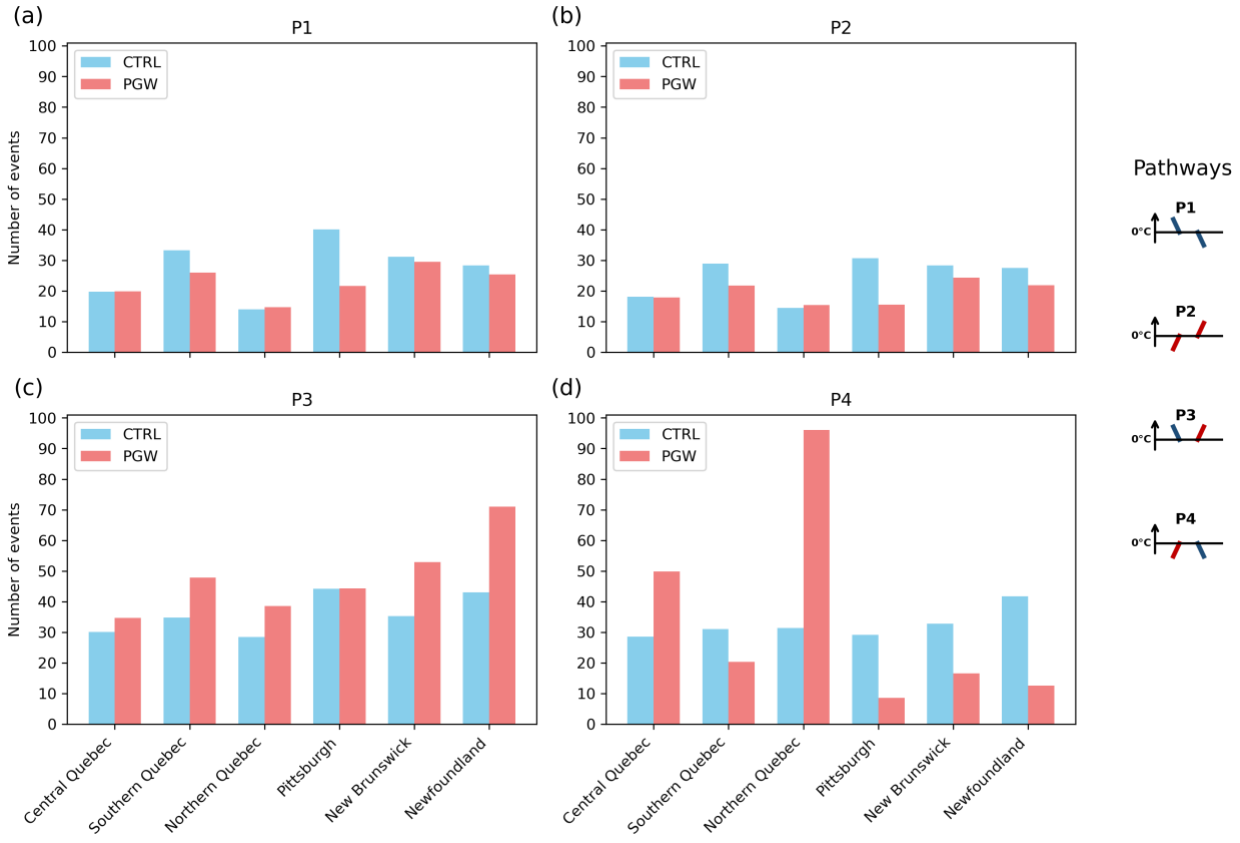

Figure 2.10: Average annual number of near-0°C events following temperature pathways (a) pathway 1, (b) pathway 2, (c) pathway 3, and (d) pathway 4 for the selected regions in the CTRL and PGW simulations.

The dominant near-0°C temperature pathways were determined at each grid point by identifying which of the four pathways (P1–P4) occurred most frequently. Based on this approach, we produced a spatial map of dominant pathways (mode) for both CTRL and PGW simulations (Figure 2.11). In CTRL, P3 accounts for 49.24% of the area and P4 for 46.96%, indicating that they are

dominant pathways across the domain. P1 is the most prevalent in 3.81% of the region. In contrast, the PGW shows an increase in P3, which accounts for 65% of the domain, followed by P4 at 34.87%. P1 is negligible in PGW. Both simulations suggest that P2 is not a dominant pathway throughout the year, but it still occurs, as in Mekis et al. (2020). For example, P2 occurs predominantly in southern Canada during winter and shifts to northern Canada during spring (not shown). P2 may mainly require warm frontal passages, often associated with freezing rain in the cold season, to allow the air temperature to increase to >2°C (e.g. Stewart et al., 1985). These are episodic events, which could partly explain why it never emerged as the dominant pathway. Additionally, the diurnal cycle can also impact P2 (section 6.1).

The CTRL simulation shows that northern regions are more dominated by P4 whereas southern regions are dominated by P3. The warmer air temperature in PGW causes the line separating the P3 and P4 regions to shift northward into the southern part of Canada. Additionally, certain northern regions, particularly areas close to water bodies including Atlantic Canada and the southern tip of Hudson Bay, show a greater dominance of P3 in the warmer climate simulation.

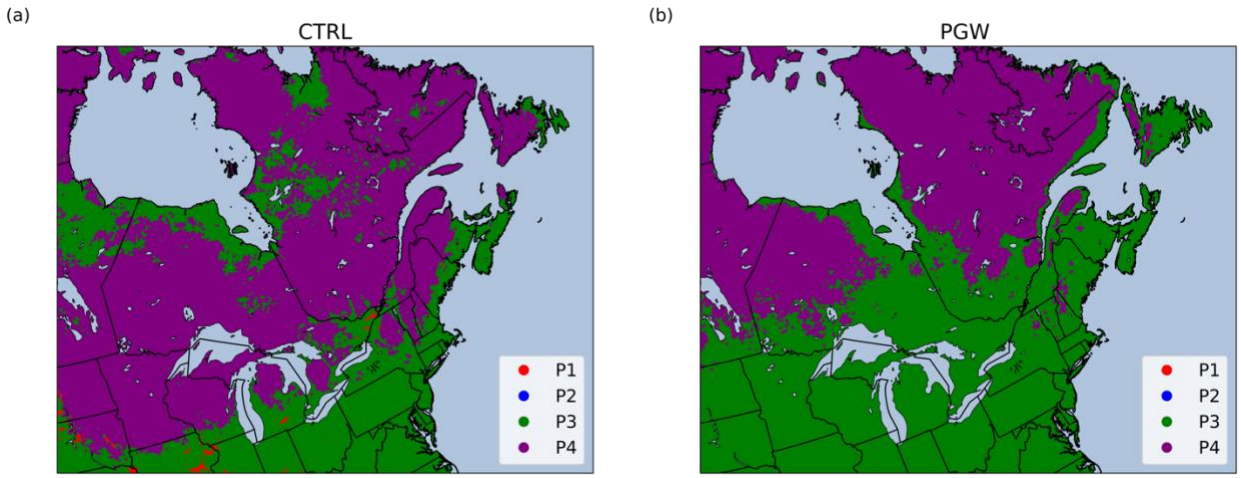

Figure 2.11: Most commonly occurring temperature pathways in the (a) CTRL and b) PGW simulations.

2.5.2 Seasonal variation of temperature pathways

Next, we investigated the seasonal variation of the occurrence of near-0°C events over the year. The timing of near-0°C events changes drastically between the CTRL and PGW scenarios. Under PGW, the onset of near-0°C events consistently occurs later in the fall, while their cessation occurs earlier in the spring across all regions. In Northern Quebec, the median delay in the fall onset of near-0°C events is 45 days. In Newfoundland, the median advance in the spring cessation of these

events is 32 days earlier, while their onset in fall is delayed by up to 40 days. These shifts collectively result in a shorter period during which temperatures hover around 0°C.

Figure 2.12 illustrates the seasonal percentages of near-0°C pathway occurrences in both CTRL and PGW. The standard climatological seasons i.e., September to November for fall, December to February for winter, March to May for spring, were used in analyzing seasonal values (no near-0°C pathways were observed in summer). In CTRL, P1, P2, and P3 predominantly occur during the spring season across all regions. Conversely, P4 is primarily observed during the winter season, except in Northern and Central Quebec. Most of the pathways for Northern Quebec and Central Quebec occur in the fall and spring. The comparatively warmer air temperatures in Pittsburgh restrict the occurrence of P4 almost exclusively to the winter. This pattern is replicated in the PGW simulation, in which many pathways that previously occurred during the spring in more northern regions shift to the winter. Notably, P4 demonstrates the least seasonal shift, as it predominantly occurs in winter in both simulations.

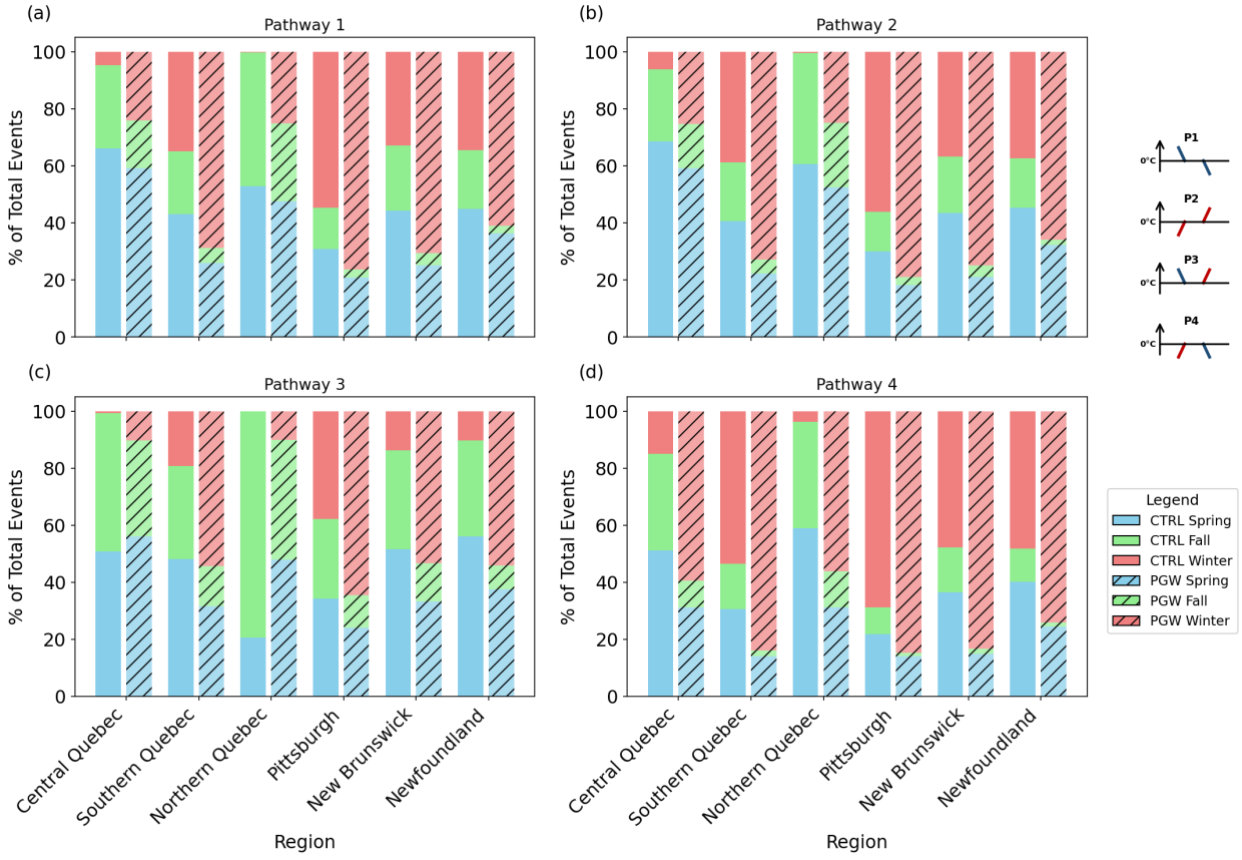

Figure 2.12: Seasonal distribution of temperature pathways in spring, fall and winter for (a) pathway 1, (b) pathway 2, (c) pathway 3, (d) pathway 4.

2.5.3 Temperature pathways and associated precipitation

The event duration and pathways across various locations with and without precipitation were investigated. Precipitation patterns across all regions indicate that the mean duration of near-0°C events with precipitation is longer. In section 2.4.3, we showed that the Newfoundland region has a high percentage of long-duration events. Figure 2.7 shows that this region also experiences a high amount of precipitation under near-0°C conditions. During the cold season, relatively warm sea-surface temperatures can raise surface air temperatures (Banfield and Jacobs, 1998), and precipitation phase changes may bring air temperatures to near-0°C, likely explaining the higher prevalence of long-duration events in the region.

Among the types of precipitation, freezing rain exhibits the longest duration, followed by snow, and then rain (Figure 2.13a). In the case of freezing rain, a lower onset air temperature or cold-air advection can compensate for warming from latent heat release of freezing rain, resulting in a longer time before the 2-m temperature reaches 0°C. Comparing mean duration between pathways shows that P1 typically has the longest duration. Northern Quebec had the longest mean near-0°C event duration (~11.1 h), and Pittsburgh had the shortest (~6.3 h). Figure 2.13b shows the dominant precipitation type associated with each pathway. Specifically, freezing rain is most common during P2 (46.4%), rain predominantly occurs during P3 (37.7%), and snow is most common during P4 (39.9%). Stewart et al. (1985) mentioned that freezing rain mostly occurs during the passage of a warm front, which is consistent with P2 temperature evolution, where the temperature rises from below to above 0°C. In PGW, the dominant precipitation types by pathway remain the same for snow and rain, while the most frequent freezing rain pathway shifts from P2 to P4.

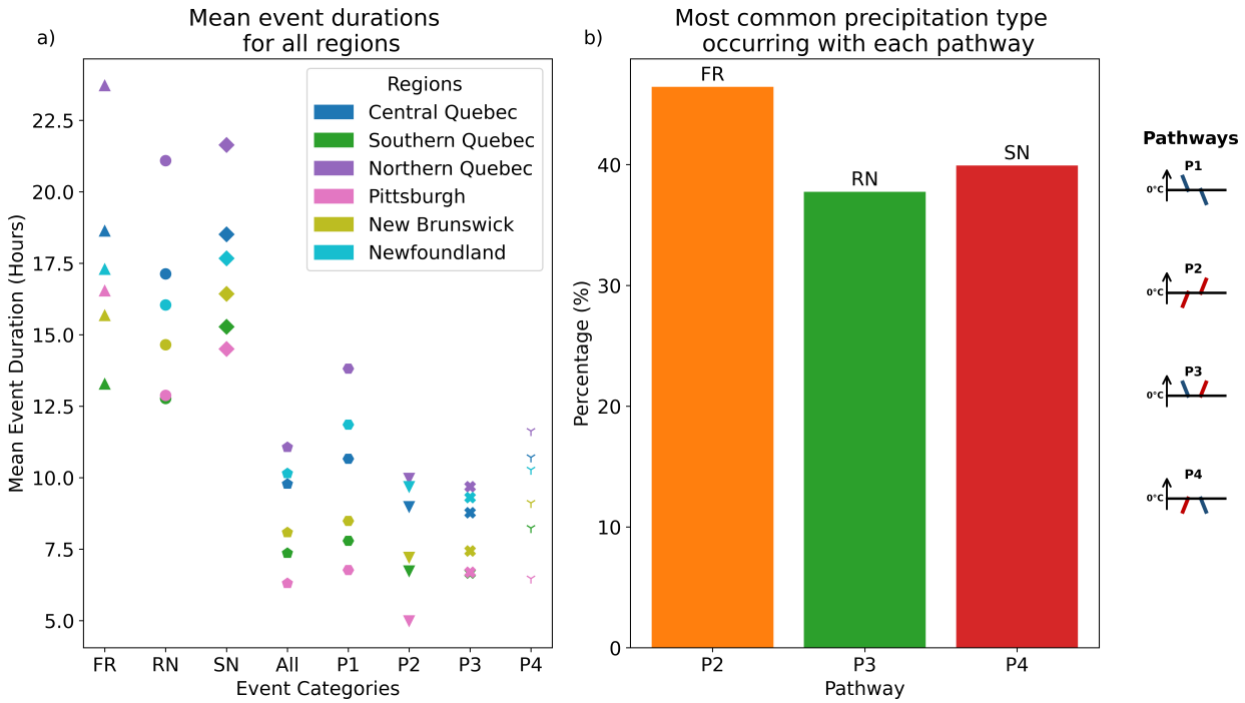

Figure 2.13: a) Mean event duration (in hours) of near-0°C events with different temperature pathways and precipitation. All refers to the mean across all pathways. RN = rain, SN = snow, FR = freezing rain. (b) Most common pathway associated with each precipitation type (rain, snow and freezing rain), shown as the percentage of events occurring in that pathway in the CTRL run.

2.6 Physical mechanism

2.6.1 Influence of radiative heating and snow cover on near-0°C temperature pathways

We investigated the role of radiative heating during near-0°C events by studying differences in the event onset and event cessation at sunrise and sunset (Figure 2.14). Previous studies have performed similar analyses on the role of radiative heating during freezing rain and freezing drizzle events (Cortinas et al., 2004; McCray et al., 2019) and thunderstorms (Kelly et al., 1985). Since there were no interregional differences in the diurnal cycle, all the regions were aggregated (Figure 2.14).

Figure 2.14 shows events that are explicitly separated by the presence or absence of precipitation. The onset and cessation of P1 events occur predominantly post-sunset, consistent with nocturnal cooling, though this signal weakens considerably in the presence of precipitation. Similarly, P2 events under dry conditions show a pronounced post-sunrise peak at both onset and end, reflecting

solar-driven warming that is suppressed under precipitating conditions. The most pronounced decrease in peaks for P3 events occurs at cessation, where temperatures rise. For P4 events, where cooling is expected at event end, the peaks in dry conditions are flatter with precipitation. Precipitation introduces processes like cloud–radiative feedbacks, evaporative cooling, and latent heat release, that can obscure or dampen the underlying diurnal signature. These results suggest that the effect of the diurnal cycle on near-0°C temperature pathways under dry conditions is more pronounced than with precipitation. However, some near-0°C events may only have precipitation during the event itself and not close to the onset or cessation, meaning a diurnal signature may still be present in those cases.

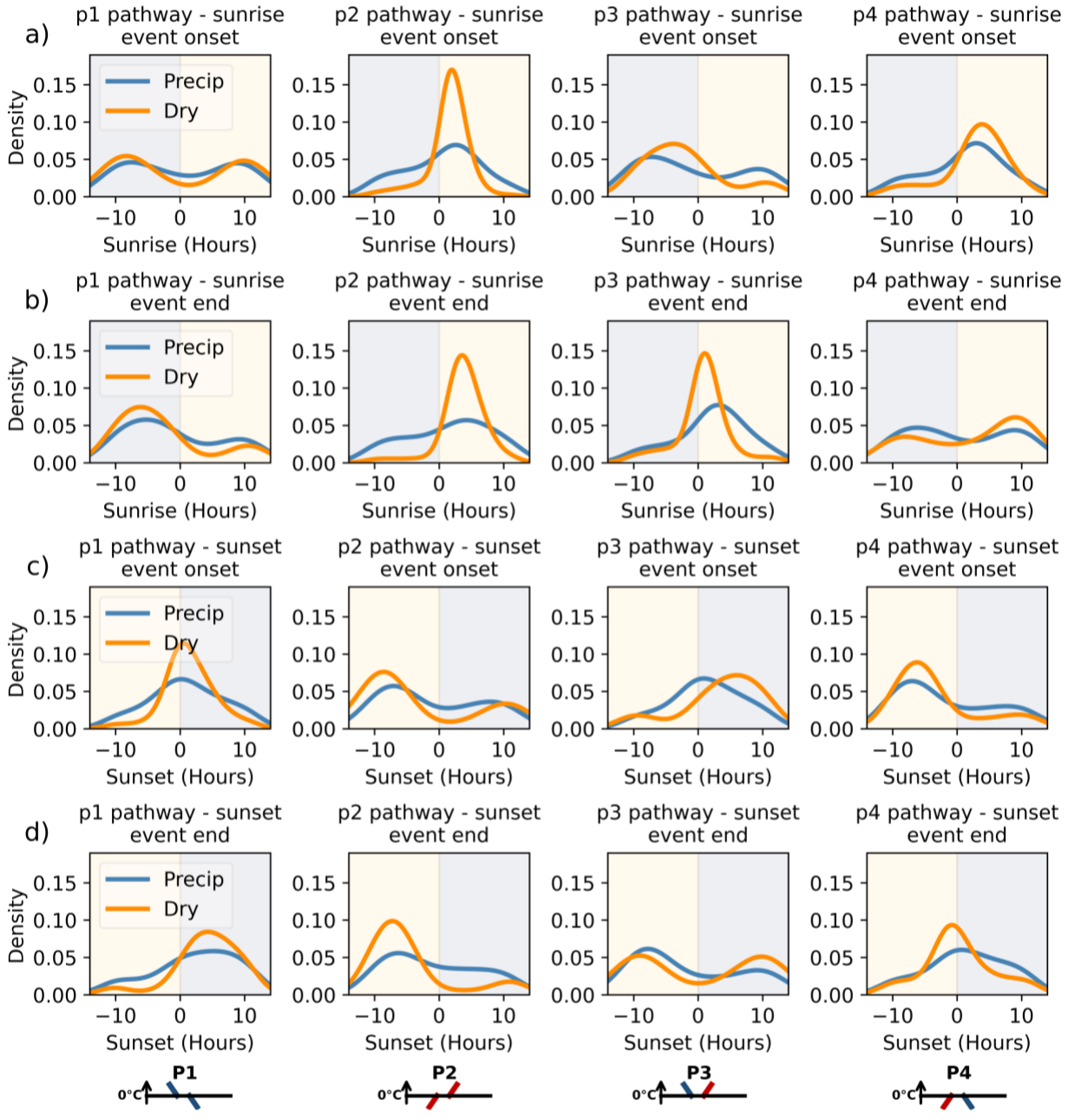

Figure 2.14: Normalized frequency distribution of near-0°C temperature pathway events for the four temperature pathways (P1, P2, P3 and P4), aggregated for all regions, comparing precipitating (blue) and without precipitation (dry, orange) events. (a) Event onset relative to sunrise in hours. (b) Event end relative to sunrise in hours. (c) Event onset relative to sunset in hours. (d) Event end relative to sunset in hours. Curves are derived using kernel density estimation (KDE). The events are relative to sunrise and sunset hours, which is the 0 hours on the x axis. The yellow shading is prior to (a, b) sunrise and (c, d) sunset. Similarly, the grey shading is after (a, b) sunrise and (c, d) sunset.

We examined the impact of snow cover on near-0°C temperatures. Takeuchi et al. (2002) stated that snow cover can melt, and liquid pooling can freeze, both of which drive temperatures close to

0°C. Under CTRL, the annual median near-0°C hours with snow on the ground are 952 h (Newfoundland), 690 h (Central Quebec), 688 h (New Brunswick), 663 h (Northern Quebec), and 569 h (Southern Quebec). This suggests that melting and freezing could influence those near-0°C hours. In Central and Northern Quebec, these hours increase under PGW simulations. In contrast, in Newfoundland, New Brunswick, and Southern Quebec, they decrease. In CTRL, around 70% of near-0°C hours with snow occurred during spring in Central and Northern Quebec. Under PGW, this becomes almost equally split between winter and spring, while New Brunswick shifts from spring to winter dominance.

A possible relationship between snow cover and the temperature pathways was also examined. Figure 2.15 shows that P3 is associated with snow-free ground, whereas P4 events typically occur when snow is present on the ground. This is consistent with the air temperature prior to and following the near-0°C events: warmer conditions for P3 and colder conditions for P4. In the case of P4, the incoming solar radiation could have melted the snowpack, allowing the near-0°C conditions to persist instead of increasing to warmer air temperatures. This prolonged phase change dominates the energy budget over air warming, enabling P4 to persist while limiting sensible heating. In contrast, snow-free ground could warm more readily to higher air temperatures that allow air temperature to rise above the near-0°C threshold, as seen in the P2 case. In northern regions where snow is present in winter and early spring, it may lead to less occurrence of P2 and P4.

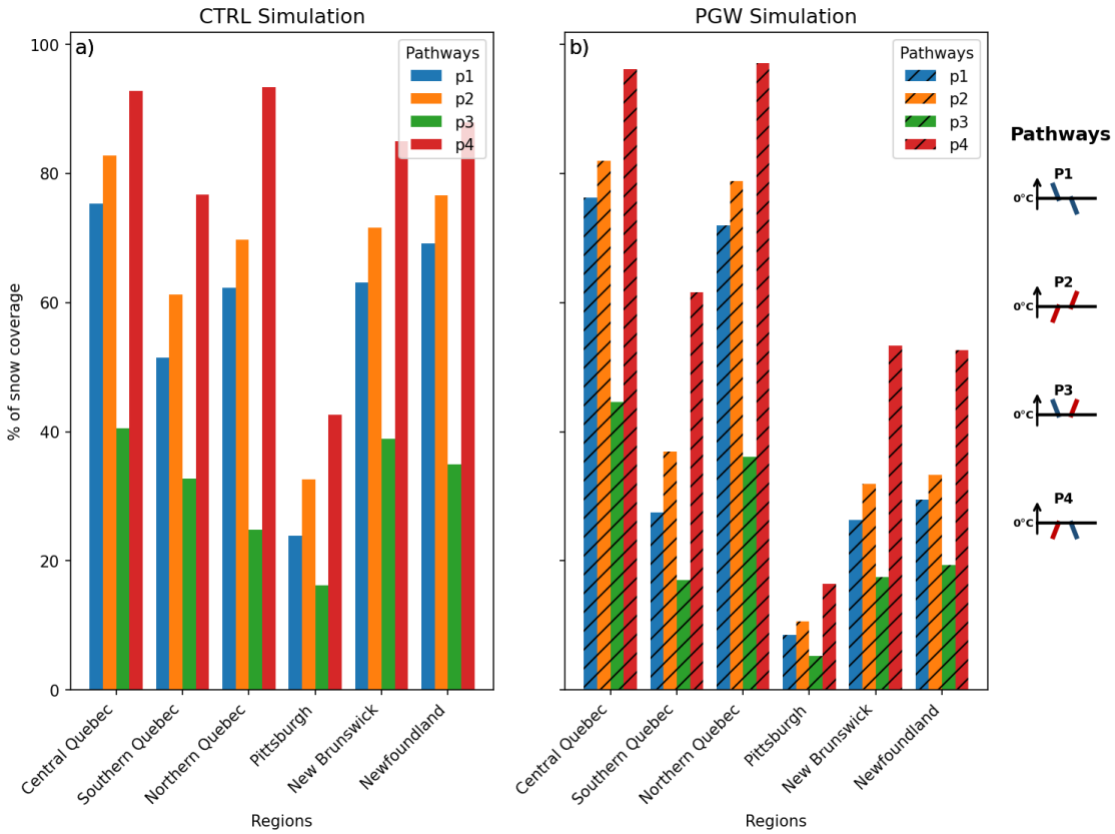

Figure 2.15: (a) % of events that have snow greater > 1 cm during different temperature pathways in the CTRL run, (b) % of events that have snow greater > 1 cm during different temperature pathways in the PGW run.

2.6.2 Movement of peaks

Latent heat exchanges from the freezing and melting processes bring air temperatures toward 0°C. To understand the decreased number of near-0°C temperature peaks under warmer climate conditions, we examined the roles of snowfall and snow cover. Although the total number of precipitation hours remains largely unchanged between the CTRL and PGW scenarios, both snowfall hours and the number of days with snow on the ground decrease substantially in PGW. This reduction coincides with an increase in the frequency of no near-0°C peaks, particularly in Southern Quebec, Pittsburgh, New Brunswick, and Newfoundland. This suggests that diminishing snow presence could lead to less occurrence of near-0°C peaks.

The near complete loss of secondary peaks could possibly be associated with reduced snow cover, which limits the melting process that would otherwise maintain temperature near 0°C (Stewart et

al., 2023). Besides, decreased amount of snowfall impacting the snowpack at the surface, cooling due to melting snowfall can cool the air temperature towards 0°C (Wexler, 1954). The shift towards more grid cells with no peaks from secondary peaks is consistent with seasonal feedbacks linked to snow cover. In regions where spring temperatures rise gradually, a modest baseline warming would cause the 0°C threshold to be reached earlier along the slow warming (Rawlins et al., 2016). In contrast, regions that warm rapidly in spring would experience little change in thaw timing, as air temperatures cross 0°C quickly regardless. Northern regions that retain snow longer show weaker feedbacks and maintain a higher frequency of near-0 °C events under warming scenarios.

During the cold season, ocean waters and the Great Lakes remain close to 0°C, helping to maintain air temperatures near 0°C and prolonging near-0°C conditions along adjacent coastlines (Larouche and Galbraith, 2016). These water bodies can moderate air temperature along the coastlines. Previous studies (Larouche and Galbraith, 2016; Galbraith et al., 2012) have shown sea surface and air temperature trends are closely linked in the Gulf of St. Lawrence and Hudson Bay regions. In PGW, slightly warmer water reduced this stabilizing influence. Hence, changes in water temperatures under warmer climate conditions altered the frequency of near 0°C occurrence in coastal areas.

2.7 Conclusions

2.7.1 Summary and conclusions

Our study investigating changes in near-0°C conditions over eastern Canada and the United states using 11-year simulations conducted with the CRCM6-GEM5 in both CTRL and PGW at 2.5-km grid-spacing. The model was able to capture the near-0°C conditions. Our results show contrasting changes of near-0°C conditions under warmer climate conditions, with an overall increasing duration in northern regions as cold winters warm toward 0°C and decreasing duration in southern Canada and the United States due to reduced snow cover and earlier spring warming. Despite the warming, near-0°C conditions remained in some regions due to the different variation of the air temperature distribution and the conditions entering, maintaining and leaving the near-0°C conditions. The analysis of the simulations allows us to draw the following conclusions:

- The temperature pathways associated with freezing rain changed from P2 to P4 suggesting that it would occur in relatively warmer conditions in warmer climate conditions.

- The P3 and P4 are the most dominant pathways in the CTRL, with similar magnitudes. The dominant pathway in the south is P3, while in the north it is P4. However, in the PGW simulation, the boundary separating these pathways appears to move further north within the study domain, and P3 becomes the clearly dominant pathway.
- Near-0°C events with precipitation last longer than non-precipitation events. Freezing rain, rain, and snow tend to occur during the P2, P3, and P4 pathways, respectively. P1 and P2 events appear to be influenced by diurnal heating effects, and P4 is the pathways associated with the highest occurrence of snow cover.
- Under the PGW, the onset of near-0°C events consistently occurs later in the fall, while their cessation occurs earlier in the spring across all regions. The greatest interval between onset and cessation is observed in Northern Quebec. Except for P4, most pathways that occur in the spring in the CTRL occur in the winter in PGW, especially in the northern part of the domain. P4 continues to occur in winter in both simulations, even in warmer conditions.
- Near-0°C temperature peaks continue to occur in the warmer climate conditions. There is an increased area with primary or no peaks. Most of the secondary peaks in Canada transition into primary peaks, while those in the United States transition into no peaks.

2.7.2 Limitations

Some limitations are associated with the findings from this study. These are given below.

First, the PGW approach has some limitations. While the PGW approach has difficulties capturing changes in the general circulation, which influence weather conditions and precipitation, it captures the thermodynamic effects well (e.g., Hall et al., 2024). Both historical and PGW runs have identical boundaries except for the monthly mean perturbations. This assumption limits the simulation of general circulation changes, but it can reduce internal variability relative to conventional downscaling of GCMs (e.g., Giorgi, 2019). This reduction in internal variability is even stronger when multi-model GCM ensembles are used (Hall et al., 2024). A northward shift of the jet stream could lead to an earlier spring sooner and more near-0 °C events north of our domain. Nevertheless, new insights on changes in near-0 °C occurrence in the future can be gained using

PGW, because it can generate climate projections that are broadly similar to those from direct downscaling of Global Circulation Models (GCMs) (Hall et al. 2024).

Second, direct downscaling could have been used in this study but would have required more computational resources. The PGW approach requires less computational expense because it only needs one historical simulation and uses a time-slice approach. Direct dynamical downscaling requires multiple baseline simulations and a continuous full time series downscale (Gutowski et al., 2021). Furthermore, the PGW approach requires less computational resources than direct dynamical downscaling because it only needs one historical simulation and uses a time-slice approach. Moreover, the computational cost is reduced because a shorter period is sufficient. The perturbation applied follows a fixed monthly cycle representing only the mean climate change signal. Thus, results are not influenced by interannual variability, so a shorter simulation period can capture the long-term average response to warming (Brogli et al., 2023).

Third, a challenge in modeling near-0°C conditions in high latitudes is that some land surface models can unrealistically constrain 2-m air temperatures to 0°C during snowmelt, causing delayed melt and biased surface energy exchanges (Guan et al., 2020). To evaluate whether this affects our simulations, we examined 2-m air temperature and snowpack evolution at three northern Quebec sites: Kuujjuaq, Kuujjuarapik, and Rivière aux Feuilles over a four-month spring period. Although minor biases exist, the modeled temperatures rise naturally during snowpack ablation and closely track the observed seasonal increase, showing no artificial stagnation at 0°C commonly seen in other models.

Fourth, there was a near-complete loss of secondary peaks in PGW. A fixed bandwidth of 4°C bins in our calculation of the near-0°C peak may have accentuated this apparent drop. A more robust kernel density estimation method would likely smooth and better resolve peaks across the full distribution range without showing such a dramatic drop.

Finally, our findings show both agreements and differences with previous studies. Stewart et al. (2023) examined the distribution of peaks in southern Canada and found that, in the CTRL simulation, the distribution consisted of both primary and secondary peaks, which is consistent

with our findings, although the locations vary slightly in some regions. In PGW, primary peaks were dominant, with a small proportion of no-peak events, again in agreement with our results. These differences could be due to the use of CMIP6 in our simulation, whereas Stewart et al. (2023) used CMIP5 to perturb the CTRL. In addition, the simulation periods differ: ours covers 2012–2022, while theirs spans 2000–2013. Furthermore, Leduc et al. (2025), by contrast, investigated freeze–thaw days (FTDs) and reported that, under a projected warming scenario, FTDs are expected to become substantially more frequent in winter and less frequent in fall and spring. Except for pathway P4, our results similarly indicate a shift in pathways from spring toward the winter season. It is worth noting, however, that the definitions of near-0°C conditions differ between studies: both Stewart's study and ours define them as the number of hours with temperatures between −2°C and +2°C, whereas Leduc et al. (2025), following Hershfield (1974), defines FTDs as days when the daily minimum is below 0°C and the daily maximum is above 0°C, thereby emphasizing the occurrence of a freezing-point crossing within a single day.

2.7.3 Implications

Overall, this study showed that although climate warming generally shifts temperature distributions northward, this shift is not uniform, and some temperature occurrences persist near 0°C rather than continuing to increase (Stewart et al., 2023). Air temperatures persisting at near-0°C can lead to an increase in atmospheric conditions favorable for freezing rain and wet snow, resulting in icing on structures such as during the ice storm in April 2023 (Thériault et al. 2026). In addition, near-0°C cycles regulate activities such as maple syrup production in southeastern Canada and the northeastern United States (Legault et al., 2019). On longer term, persistence near 0°C can accelerate permafrost thaw in cold regions. This highlights the need to better understand these temperature pathways under warmer climate conditions.

CHAPTER 3

Quantification of the impact of latent heat associated with the freezing of supercooled drops at the surface during freezing rain over eastern Canada

This chapter is presented in the format of a scientific article published in the journal Atmospheric research.

Basnet, S., & Thériault, J. M. (2025). Quantification of the impact of latent heat associated with the freezing of supercooled drops at the surface during freezing rain over Eastern Canada. Atmospheric Research, 323, 108120.

Abstract

The formation of winter precipitation is driven by ice-phase and liquid-phase processes, with the energy required for melting and freezing affecting both temperature and precipitation type. A major freezing rainstorm occurred in early April 2023 over Eastern Canada, causing damage to infrastructure and impacting the economy. The goal of this study is to investigate the impact of the latent heat release associated with freezing rain on the 2-m air temperature and the type of precipitation that reaches the surface. To illustrate the impacts of latent heat, the April storm was simulated using the Global Environmental Multiscale (GEM) model with the modified Predicted Particle Properties (P3) scheme. It was observed that the release of latent heat from freezing rain led to a rise in the 2-m air temperature, with rain recorded when temperatures exceeded 0°C. The median cumulative freezing rain showed a 34.4 % decrease, while time for the median temperature to reach 0°C decreased by 2.5 h. The results from the model suggest that temperature advection played a role in balancing the precipitation phase change. This study contributes to our knowledge of processes associated with maintaining or stopping freezing rain and improves our ability to mitigate its hazards.

3.1 Introduction

Freezing rain can have significant social, environmental, and economic consequences (Degelia et al., 2016). The ice buildup that accompanies freezing rain can cause power outages, disrupt transportation, and lead to dangerous driving conditions, causing traffic accidents. The cost of repairing damage caused by freezing rain can be substantial. The 1998 ice storm in southern Quebec and eastern Ontario resulted in 28 deaths and a near billion-dollar loss in repairing transmission lines alone (Lecomte et al., 1998). Zarnani et al. (2012) stated that ice storms cost an annual average of $313 million in the United States. In 2017, a prolonged freezing event resulted in significant damage to utility infrastructure resulting in power outages that damaged 133,000 homes in the province of New Brunswick, Canada (Thériault et al., 2022).

There are two different mechanisms that can lead to the formation of freezing rain. In the first process, solid precipitation falls into a melting layer aloft (air temperature, $T > 0°C$). The melting layer then completely melts the snow into liquid precipitation. As the liquid drops pass through the subfreezing layer ($T < 0°C$), the drops do not refreeze due to a lack of ice nuclei, freezing instead when the drops strike a cold surface (Brooks, 1920; Forbes et al., 1987). The second process occurs through a supercooled warm rain process, whereby droplets grow by collision and coalescence without the presence of ice particles aloft (Huffman and Norman, 1988; Rauber et al., 2000). The droplets then freeze upon contact with the surface. However, this process typically produces freezing drizzle rather than freezing rain (Rauber et al., 2000).

The phase change from liquid to ice releases latent heat. When freezing rain occurs, latent heat is released into the subfreezing layer as the supercooled droplets freeze upon contact with a subfreezing surface. A slow erosion of the freezing layer near the surface then occurs, and depending on atmospheric conditions, an isothermal layer of 0°C can form (e.g., Lackmann et al., 2002), changing freezing rain to rain. Studies have found freezing rain episodes where the surface temperatures have increased because of the release of latent heat (Stewart, 1985). Freezing raindrops move the 2-m temperature towards 0°C and increase the occurrence of near-0°C conditions (i.e., 2-m temperatures between $-2°C$ and $+2°C$). During the 2017 New Brunswick storm, a large proportion of the precipitation occurred as freezing rain when the temperature was near 0°C (Thériault et al., 2022). Cardinal et al. (2023) conducted a climatology study in Terrace,

British Colombia and noted that on average, the near-0°C events are longer when freezing rain is involved. Unlike other forms of precipitation, the high occurrence of freezing rain also correlates to areas where the annual temperature is just above 0°C (Mekis et al., 2020).

Lackmann et al. (2002) suggested that the latent heat released during the freezing rain event in February 2001 increased the temperature profile by about 3°C over several hours in the Carolinas. In a comprehensive study across the United States and Canada, Cortinas et al. (2004) found that only 11 % of freezing rain events lasted more than four hours. McCray et al. (2019) stated that the majority of stations in North America experience fewer than one long-duration event every two years. Henson et al. (2011) concluded that the phase change during the freezing rain event in the 1998 ice storm impacted the severity and longevity of the icing event. Neglecting the presence of warming associated with latent heat can contribute to cold bias in the weather model (Lackmann et al., 2002; Degelia et al., 2016; Thériault et al., 2022). Although small temperature errors in models are often considered acceptable, they can also be disastrous because they can change the model precipitation type, including ice accretion on roads and electric poles. This is especially true when other processes such as temperature advection and evaporative cooling are weak (McCray et al., 2020). Other studies have also discussed latent heat exchange aloft when snowflakes fall into a warm layer and latent heat is extracted from the surrounding air. In some cases, the melting layer is completely eroded within hours (Wexler and Hasegawa, 1954; Kain et al., 2000).

Past studies (Lackmann et al., 2002; McCray et al., 2020; Thériault et al., 2022; Stewart et al., 2023) have discussed the importance of latent heat resulting from phase change, but to our knowledge no studies have implemented this process in the model. Despite the possible impact of the latent heat release during freezing rain on the atmospheric stability near the surface (Lackmann et al., 2002; McCray et al., 2020), no studies have quantified its contribution to the warming of environmental conditions to 0°C (e.g., Thériault et al., 2022; Stewart et al., 2023). Furthermore, ignoring the influence of freezing rain in the land surface model can also impact the model's representation of snow cover, which can be particularly disastrous in mountainous regions (Quéno et al., 2018). Currently, many land surface models treat supercooled rainwater as solid precipitation (e.g., McTaggart-Cowan et al., 2019). The goal of this study was to quantify the contribution of the freezing of supercooled drops at the surface on the near surface air temperature. To achieve this,

the extreme, high-impact ice storm on April 5–6, 2023 in southeastern Canada (Figure 3.1) was examined using high-resolution simulations with the Global Environmental Multiscale (GEM) model (Milbrandt et al., 2016; McTaggart-Cowan et al., 2019). The storm brought up to 35 mm of freezing rain, ice pellets, snow, and rain over the area. A large amount of accretion (~ 9 mm) was recorded in the downtown Montreal area, and ice pellets (~ 26 mm) were reported 60 km north of Montreal.

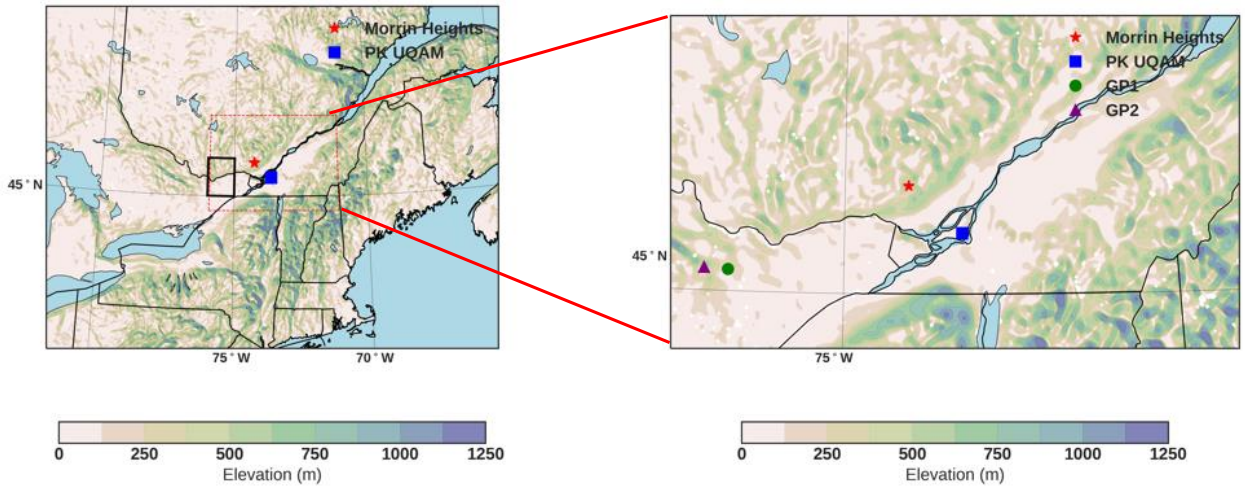

Figure 3.1: (a) Model domain (outer rectangle) of the study area and the location of the analysis domain (inner dotted red rectangle). The black rectangle inside the red rectangle is the domain shown in Figure 3.10. (b) Location of the two weather stations used, PK-UQAM (blue square) and Morin-Heights (red star), as well as grid points GP1 (green circle) and GP2 (purple triangle).

The paper is organized as follows. Section 3.2 describes the experimental design and the model configuration, including the observation data. Section 3.3 gives an overview of the synoptic conditions that led to the April 2023 freezing rain event. The results are presented in Section 3.4 and discussed in Section 3.5. Finally, the conclusions are summarized in Section 3.6.

3.2 Methods

3.2.1 Model description and simulation configuration

The Global Environmental Multiscale (GEM) model version 5.1.1 was used to conduct high-resolution simulations of the 2023 April ice storm. GEM is a numerical weather prediction model developed by Environment and Climate Change Canada (ECCC) and the Canadian Centre for Meteorological and Environmental Prediction (CCMEP) (Girard et al., 2014; McTaggart-Cowan

et al., 2019). The vertical coordinates are based on the log-hydrostatic pressure and vary according to the terrain. Our study has 64 hybrid vertical levels that separate thermodynamic equations from motion equations (Girard et al., 2014).

The domain of the simulation (Figure 3.1) encompasses the southern region of Quebec, extending into a portion of the Great Lakes and Maine in the United States. It has 1330 × 1004 horizontal grid points and a 1-km horizontal grid spacing. The simulation started at 0000 UTC 04 April 2023 and ran until 0000 UTC 07 April 2023, which included the duration of the storm. The model was initiated 38 h before the onset of precipitation in Montreal. The model time step was 30 s, and hourly outputs were archived. The simulation was initialized with Canadian Meteorological Centre (CMC) analysis data and driven at the lateral boundaries with hourly data from European Centre for Medium-Range Weather Forecasts Reanalysis (ERA5) (Hersbach et al., 2020).

The physical parameterization includes the Predicted Particle Properties (P3) cloud and precipitation scheme (Morrison and Milbrandt, 2015), the Canadian land surface scheme (CLASS, Verseghy et al., 1993), correlated-k terrestrial and solar radiation scheme (Li and Barker, 2005), Kuo-transient shallow convection parameterization (Kuo, 1965; Bélair et al., 2005), and the turbulent kinetic energy closure planetary boundary layer and vertical diffusion (Benoit et al., 1989; Delage and Girard, 1992; Delage, 1997).

3.2.1.1 Cloud and precipitation properties

The Predicted Particle Properties (P3; Morrison and Milbrandt, 2015) include three hydrometeor categories. The two liquid categories are cloud and rain, which have two prognostic variables: mass and number mixing ratio. The ice category has five prognostic variables: total mass, rime mass, rime volume, liquid on ice mass, and total number mixing ratios. For the ice category, the parametrized microphysical processes are sublimation, contact freezing, melting, heterogeneous and homogeneous freezing, collection, and sedimentation. The version of P3 used in this study also includes the parametrization of secondary ice production processes with two free-ice categories (Lachapelle et al., 2024) and prediction of the liquid fraction (Cholette et al., 2020).

The precipitation types in P3 are diagnosed based on the properties of the hydrometeor at the lowest level. When the mass-weighted mean density of ice particles is greater than 700 kg m−3, the precipitation is classified as ice pellets, while a density less than 700 kg m−3 indicates snow. Hail and ice pellets are grouped together as ice pellets in this study. When the precipitation is liquid, it is considered rain if the lowest model temperature is above 0°C and freezing rain if it is below 0°C. When an ice particle has melted almost completely (more than 99 %), the model considers it to be fully melted and treats it as rain category rather than ice category (Cholette et al., 2020). If liquid remains in the solid precipitation distribution when reaching the surface, we assumed that the liquid does not warm the near-surface air since it is still part of the ice-phase hydrometeor. In this study, rain and drizzle are grouped into a single category as rain.

3.2.1.2 The land surface properties

CLASS is designed to simulate exchanges between the land and atmosphere. Atmospheric data are used to drive the water and energy balance of the land surface (Bartlett et al., 2006). Seven meteorological forcing variables are used: precipitation, lowest model level temperature, incoming shortwave radiation, incoming longwave radiation, wind speed, specific humidity, and pressure. In our study, we used reanalysis data from ERA5 to initiate canopy, soil and snow temperatures, liquid and ice water content, snow mass, density and albedo. The CLASS configuration in our study used 16 soil layers.

Grid cells in CLASS have sub-areas belonging to four subareas: bare soil, snow-covered soil, vegetation, and snow on vegetation patches (Davison et al., 2006). The vegetation types included in the simulation are needleleaf tree, broadleaf tree, crops, and grass. The bare soil fraction can change over the course of the year due to crops being harvested or plants dying in winter. Albedo, roughness length, minimum and maximum leaf area index, and rooting depth all vary depending on the type of vegetation present. These variations also affect the energy balance and surface temperature. The surface energy fluxes are calculated over these sub-areas individually, and the surface temperature, which is the temperature at the surface–atmosphere interface, is then estimated for each sub-area by solving their respective surface energy balance equation. This process requires an iterative approach that proceeds until the canopy and surface temperature converge. Finally, the

surface temperature for a grid cell is calculated by combining the relative fractions of each sub-area. The surface temperature is then substituted back into the equation to determine the energy balance terms.

3.2.2 Description of the energy partitioning method

Lackmann et al. (2002) suggested that the latent heat released from the freezing of supercooled drops at the surface is distributed between the surface and the atmosphere (Figure 3.2). For the surface, CLASS was modified to take this process into account. The steps to achieve this are as follows. For the surface, CLASS was modified to take this process into account. The steps to achieve this are as follows.

First, for a non-vegetated area, the surface temperature is calculated by solving a surface energy balance that relies on surface energy fluxes (W m^{-2}) as shown in Equation 3.1.

$$K\downarrow - K\uparrow + L\downarrow - L\uparrow - Q_H - Q_E - G = 0 \quad (3.1)$$

where $K\uparrow$ is the outgoing shortwave radiation, $K\downarrow$ is the incoming shortwave radiation, $L\uparrow$ is the outgoing longwave radiation, $L\downarrow$ is the incoming longwave radiation, Q_H is the sensible heat flux, Q_E is the latent heat flux, and G is the ground flux. The energy budget can be represented as energy flux per unit area and is measured in W m^{-2}. Fluxes are positive when there is any energy gain at the surface.

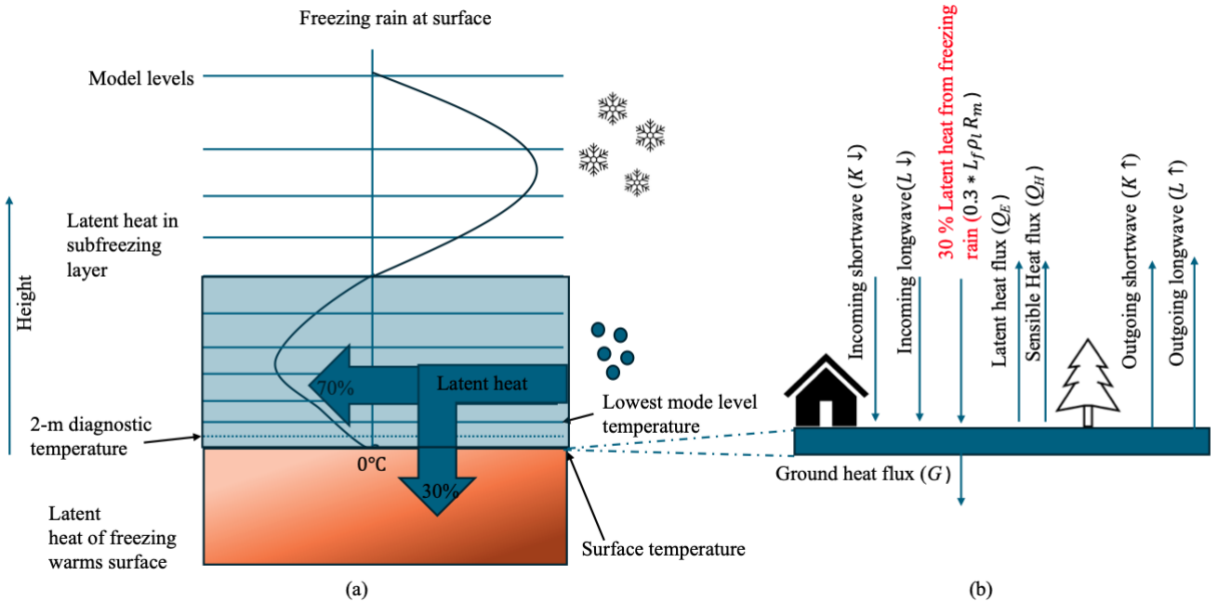

Figure 3.2: Schematic diagram showing how the latent heat is distributed between the surface and atmosphere. (a) Vertical temperature profile of a freezing rain event with warm front aloft and a subfreezing layer (blue block) below. Of the latent heat energy, 70% goes to the subfreezing layer and 30% goes to the surface (brown block). (b) Components of the surface energy balance in CLASS with the incoming ($K\downarrow$, $L\downarrow$, $0.3 * L_f \rho_l R_m$) and outgoing (QH, QE, G, $K\uparrow$, $L\uparrow$) fluxes.

Second, CLASS 3.6 only considers partitioning of precipitation between rainfall and snowfall without considering freezing rain (Verseghy, 2012). Precipitation type is identified based on the P3 microphysics scheme. The amount of freezing rain is then used in CLASS to estimate the amount of heat released from freezing rain.

Third, the heat (H) required to change the phase of a mass (m) is given by the following:

$$H = mL_f \tag{3.2}$$

where m is the mass of supercooled drops of freezing rain and L_f is the latent heat of fusion. Equation 3.2 can be represented in terms of the precipitation rate, which is a variable diagnosed by GEM. The heating rate due to the freezing of freezing rain (ΔQ, J s^{-1}) is

$$\Delta Q = X_i L_f \rho_l R_m \tag{3.3}$$

where Xi is the quantitative estimate of the amount of energy that is partitioned/divided between air and surface, ρ_l is the density of liquid water, R_m is the precipitation rate of freezing rain in (m s^{-1}), and. Based on Lackmann et al. (2002), we assumed that 70% of the energy is going to heat the atmosphere (i.e., $X_i = 0.7$)The corresponding increase in temperature (ΔT) from the release of latent heat per unit of time of a column of air with mass (M) can be calculated by rewriting the first law of thermodynamics.

$$\Delta T = \frac{\Delta Q}{M C_p} \tag{3.4}$$

where C_p is the specific heat at constant pressure. Additional details are provided in Appendix A. The column of air above a grid point is divided into multiple model levels. Seventy percent of the latent heat generated by freezing rain is evenly distributed across the lowest 10 levels. However, the temperature change is not uniform across levels, since, according to Equation 3.4, the temperature change is inversely related to the mass of air in each model level.

Finally, the remaining energy ($0.3 L_f \rho_l R_m$), where $X_i = 0.3$, goes to the surface, which can be bare soil or canopy. The latent heat released from the freezing of supercooled drops that reach the surface (Eq. 3) was added as one of the incoming energy fluxes, and the energy balance (Eq. 1) became:

$$K\downarrow - K\uparrow + L\downarrow - L\uparrow + 0.3 * L_f \rho_l R_m - Q_H - Q_E - G = 0 \tag{3.5}$$

Although Equation. 3.5 applies to bare soil, we made a similar modification for the vegetation patches in the grid cell.

We explore two additional configurations: (a) an equal split with 50% of the energy going to the atmosphere and 50% to the surface (EXP-50), and (b) 30% of the energy going to the atmosphere and 70% to the surface (EXP-30).

3.2.3 Data and data anlysis

Data analysis was conducted using observations and high-resolution simulation outputs. We used measurements collected during the storm at the Université du Québec à Montréal (UQAM) weather station located in downtown Montreal (PK-UQAM) and at Morin-Heights (Thériault et al., 2022). Using two sites captures the spatial contrast in precipitation type, allowing us to observe how the storm produced different precipitation at the two locations. Manual observations were conducted during the event at 10-min intervals to identify precipitation type. First, to verify model performance during the storms, the hourly 2-m temperatures and hourly precipitation were retrieved from the Environment and Climate Change Canada (ECCC) archives. Simulated hourly values for precipitation, temperature, and freezing rain were obtained from the averaging the grid points closest to the observation stations within a 1-km radius. ECCC stations in the simulation's domain that had missing values during the freezing rain event were excluded from the analysis. The closest available soundings during the event were available from Maniwaki, Quebec. The vertical profile of temperature and moisture at Maniwaki before and during the storm was used to understand the meteorological factors that contributed to the storm. ERA5 reanalysis data was compared with the observed data at Maniwaki. This comparison allowed the ERA5's vertical profile to be evaluated against simulations at other locations. Because ERA5 is a reanalysis product, it includes observations such as latent heat production during the freezing rain event.

Second, two simulations were performed. The first simulation used the original configuration, hereafter referred to as CTRL. The second simulation included a modification to account for the process of latent heat that accompanies freezing rain, hereafter referred to as EXP. Our study compared precipitation amounts following the simulation. We compared the simulated CTRL and EXP vertical temperature and moisture profiles and used ERA5 as a reference to check the model performance. We investigated impacts on the 2-m temperature, surface temperature, precipitation amount for rain and freezing rain, and the time taken for the 2-m-temperature to reach >0°C over the subregion of interest.

Finally, we investigated situations in which latent heat affected the transition from freezing rain to rain. In particular, latent heat that accompanied freezing rain was compared against the hourly temperature advection in the lowest model level.

3.3 Evaluation of the control (CTRL) simulation

3.3.1 Meteorological conditions at PK-UQAM and Morin-Heights

Surface observations in downtown Montreal (Figure 3.3) indicated that the onset of precipitation was at 1300 UTC 05 April 2023, initially consisting of a mix of ice pellets and freezing rain. This mixed precipitation persisted until approximately 1710 UTC 05 April 2023, after which it transitioned into freezing rain only. Following a prolonged period of freezing rain, temperatures increased to above 0°C at 2350 UTC 05 April 2023, when the precipitation shifted to rain.

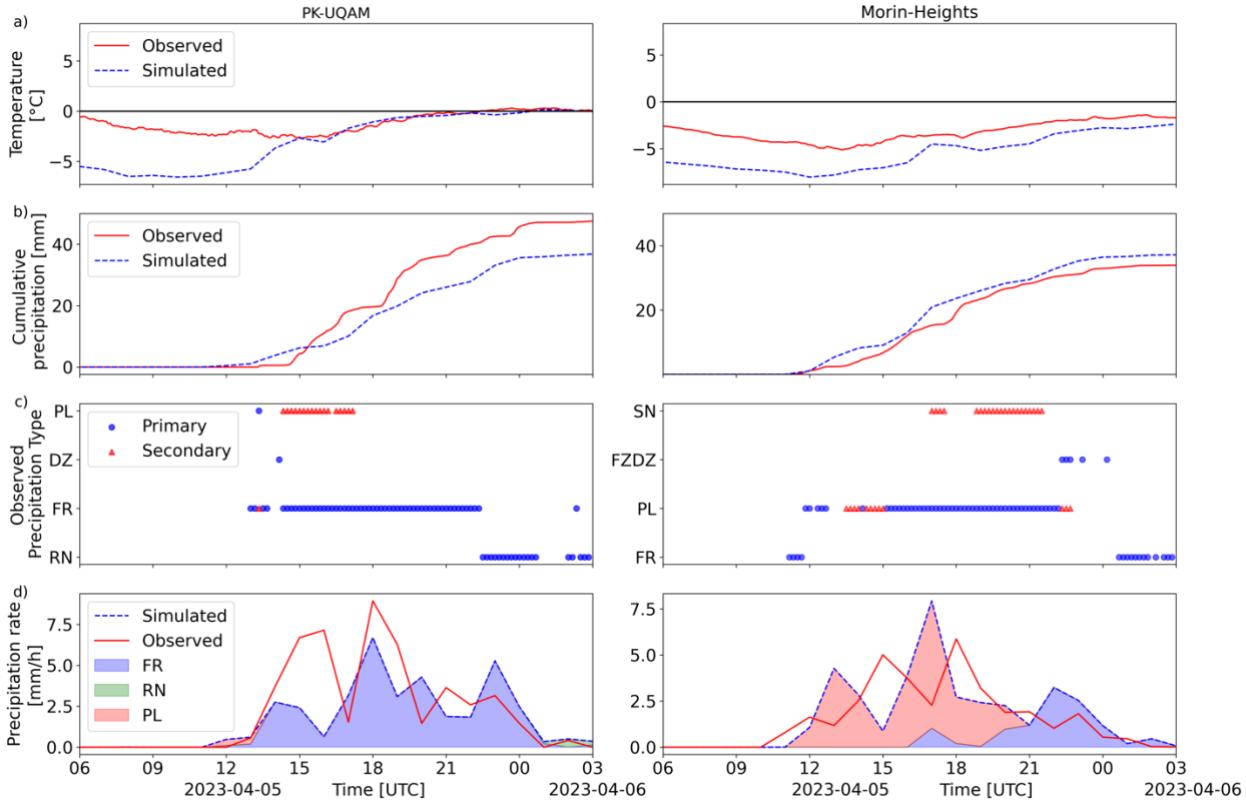

Figure 3.3: Summary of PK-UQAM and Morin-Heights measurements of (a) temperature and (b) cumulative observed precipitation measured by laser-optical disdrometer, along with cumulative simulated precipitation. (c) Observed surface precipitation types during the event. The main type of precipitation (primary) and the subordinate one (secondary) are shown. (d) Simulated precipitation types and precipitation rates. Snow (SN), freezing rain (FR), rain (RN), ice pellets (PL), simulated precipitation, and observed precipitation.

Similarly, the onset of precipitation at Morin-Heights occurred at 1150 UTC 05 April 2023 and was characterized by a mixture of ice pellets and freezing rain. Subsequently, around 1700 UTC 05 April 2023, the precipitation transitioned to primarily ice pellets with some snowfall. That period ended with freezing drizzle that eventually became freezing rain. Unlike at PK-UQAM, no rainfall was reported at Morin-Heights during this event.

The total observed precipitation amounts recorded at PK-UQAM and Morin-Heights were 47.6 mm and 34.6 mm, respectively. At PK-UQAM, CTRL produced 37.0 mm of precipitation, including 35.1 mm of freezing rain. Meanwhile it produced 37.4 mm at Morin-Heights, with most of the precipitation presenting as ice pellets (26.1 mm). CTRL was better at reproducing the total precipitation amount at Morin-Heights compared to Montreal. Precipitation was probably underestimated at PK-UQAM because the model was unable to capture the high precipitation rates measured.

For precipitation types, CTRL simulations (Figure 3.3d) aligned well with manual observations (Figure 3.3c) and followed a similar pattern of transitions. At PK-UQAM, CTRL simulated a brief period of ice pellets, followed by an extended period of freezing rain, before transitioning into rain. Similarly, in Morin-Heights, the simulated precipitation type transitioned from ice pellets to freezing rain, but later in the storm than the observed transition.

3.3.2 Precipitation amounts and types

Total precipitation and total freezing rain in the CTRL simulation were compared with 39 and 8 meteorological stations, respectively. Montreal mainly received freezing rain, with solid precipitation to the north and rain to the south of the city. The highest measured precipitation amount recorded was 64.1 mm in Kemptville, Ontario, which seemed to be well-reproduced in the model (Figure 3.4a). The highest amount of simulated freezing rain was reported to the west of Kemptville, but no observations on precipitation type are available at that station. The highest observed amount of freezing rain was at PK-UQAM (40.5 mm). The bias of the total precipitation is 1.9 mm and the bias of the freezing rain was 6.1 mm (Figure 3.5).

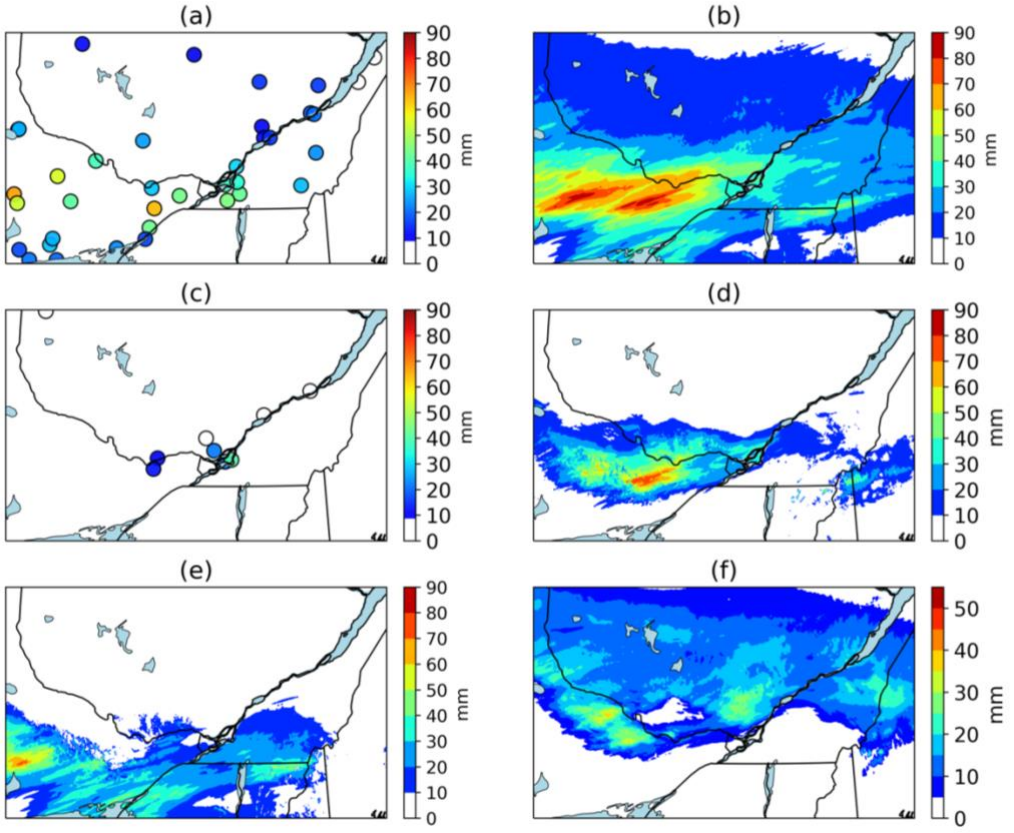

Figure 3.4: (a) Observed total precipitation amount. (b) Total precipitation from the CTRL simulation. (c) Observed freezing rain. (d) CTRL freezing rain. (e) CTRL rain. (f) CTRL total solid precipitation. All panels show the period 0000 UTC 04 April 2023–0000 UTC 07 April 2023. All amounts are in mm.

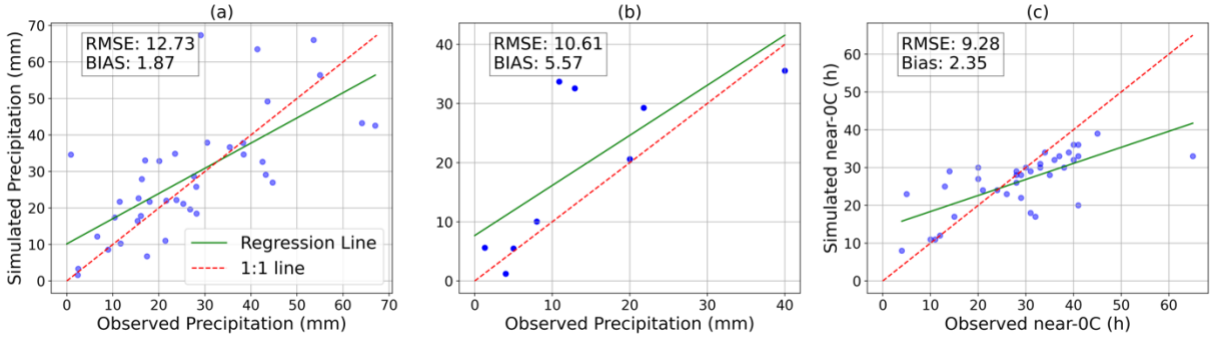

Figure 3.5: Comparison of the simulated (CTRL) and observed precipitation over the period 0000 UTC 04 April 2023–0000 UTC 07 April 2023 for (a) total precipitation, (b) total freezing rain, and (c) total number of near-0°C hours.

3.3.3 2-m air temperature

The 2-m temperature continued to evolve before, during, and after the ice storm. Before the storm, the 2-m temperature was > 0°C in the area surrounding Montreal. Cold air advection decreased the air temperature to < −2°C at 1200 UTC 5 April 2023, which made conditions favorable for freezing rain. Following a southerly wind regime, the air temperature increased to >0°C at 0100 UTC 6 April 2023. Over a 13-h period across Quebec and Ontario weather stations (Figure 3.6), the simulation exhibited a 2-m temperature mean bias of 0.05°C and an RMSE of 1.36°C across 41 stations. A small, colder bias was observed north of the Montreal region, while a slight warmer bias was observed to the south of the Montreal region.

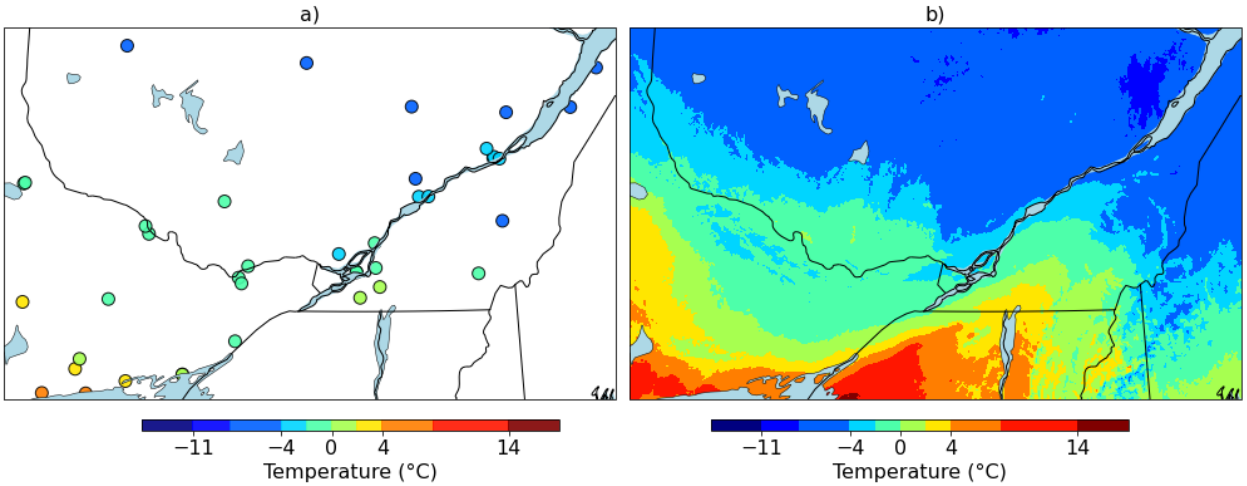

Figure 3.6: (a) Observed and (b) simulated 2-m temperature averaged from 0012 UTC 5 April 2023 to 0000 UTC 6 April 2023.

3.3.4 Near-0°C conditions

Figure 3.7 shows the cumulative hours during which the 2-m temperature was at near-0°C conditions, between −2°C and + 2°C (Mekis et al., 2020). During winter storms, near-0°C conditions are commonly observed (Stewart et al., 2023). In our study, among the 37 stations, the greatest number of hours of near-0°C conditions was 67 h at Ottawa Gatineau Airport. Ottawa International Airport and Montreal International Airport recorded 34 h and 41 h, respectively. The CTRL run simulated 34 h and 36 h for Ottawa and Montreal International Airports respectively, revealing that the model has a good ability to simulate the average occurrences of near-0°C conditions. The model results show an RMSE of 9.28 h and bias of 2.35 h (Figure 3.5). However, the model underestimated the maximum number of hours at Gatineau Airport. The CTRL

simulations showed that the areas experiencing the most near-0°C hours also coincide with the regions where freezing rain occurred.

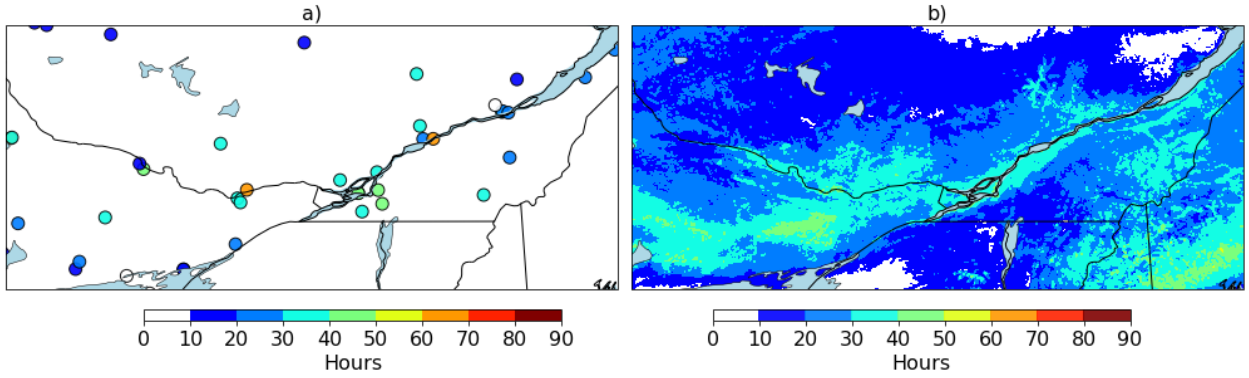

Figure 3.7: Number of near-0°C (−2°C ≤ T ≤ +2°C) hours (a) observed and (b) simulated from 0000 UTC 04 April 2023 to 0000 UTC 07 April 2023.

3.3.5 Vertical temperature structure

The vertical temperature structure at PK-UQAM and Morin-Heights, along with the observed temperature profiles before and during the storm at Maniwaki, are shown in Figure 3.8. The two soundings are characterized by a refreezing layer near the surface and a melting layer aloft, which is typical for freezing rain and ice pellets. The temperature profiles are generally well simulated except that the refreezing layer at PK-UQAM was warmer in CTRL simulation compared to Morin-Heights. At 1000 hPa, the CTRL temperature was −3.89°C, the ERA5 temperature was −2.17°C, and the observed value for the 2-m temperature was −2.57°C. Morin-Heights had a colder minimum temperature in the refreezing layer compared to PK-UQAM, and this temperature was well captured by the model. The coldest ERA5 temperatures in the refreezing layer were −2.9°C at PK-UQAM and −7.5°C at Morin-Heights, while CTRL produced temperatures in the refreezing layer of −5.6°C and −7.7°C, respectively. The warmest ERA5 temperatures in the melting layer were 3.7°C at PK-UQAM and 3°C at Morin-Heights, while temperatures were 2°C warmer in the CTRL simulations (5.6°C and 5°C, respectively). The observed 2-m temperature at Morin-Heights was −4.27°C.

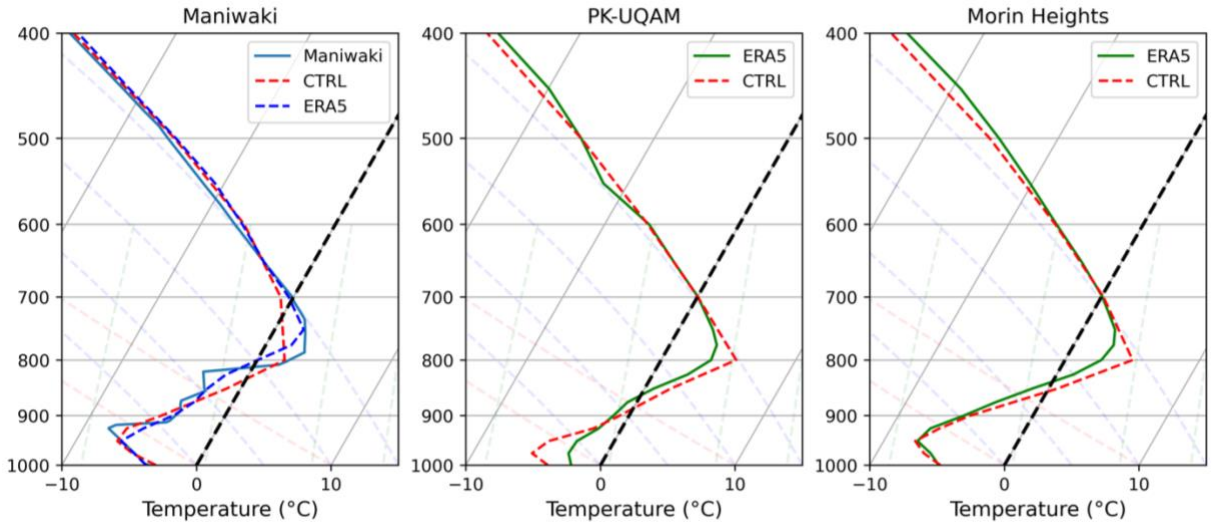

Figure 3.8: (a) Temperature profile of ERA5 reanalysis (blue dashed), CTRL (red dashed) and observed (blue) at Maniwaki at 1200 UTC 5 April 2023. ERA5 reanalysis (green) and CTRL (red dotted) vertical profiles of temperatures (°C) at (b) PK-UQAM and (c) Morin-Heights at 1500 UTC 5 April 2023.

3.4 Impact of the latent heat of freezing

This section investigates the impacts of modifying the temperature in the sub-freezing layer on simulated precipitation amount and type. There was an overall decrease in accumulated freezing rain and an increase in accumulated rain in the EXP run relative to CTRL (Figure 3.9).

In southern Ontario, EXP displayed a decrease of up to 50 mm of freezing rain accumulation, but an increase of up to 50 mm of rain, relative to CTRL (EXP-CTRL). The maximum difference occurred for the highest values of cumulative freezing rain in CTRL. The difference in freezing rain at PK-UQAM was only 3 mm. The bias in the total precipitation did not change after the modification (i.e., from 1.9 mm to 2.2 mm), but there was an improvement in the simulation of freezing rain (i.e., from 5.6 mm to 3.0 mm).

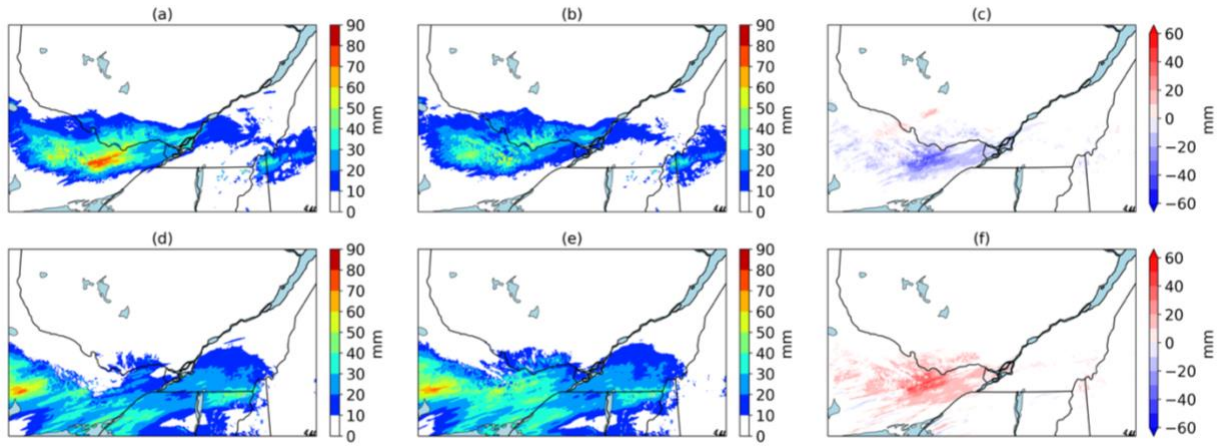

Figure 3.9: (a) CTRL accumulated freezing rain, (b) EXP accumulated freezing rain, (c) EXP-CTRL accumulated freezing rain, (d) CTRL accumulated rain, (e) EXP accumulated rain, and (f) EXP-CTRL accumulated rain over the period 0000 UTC 04 April 2023–0000 UTC 07 April 2023. All amounts are in mm.

Precipitation transition times can vary depending on the latent heat release, impacting the accumulation of freezing rain and rain. Figure 3.10 shows the ranges of simulated values for 2-m temperature, cumulative freezing rain, cumulative rain, and surface temperature over the domain that received the highest amount of freezing precipitation. As soon as freezing rain occurred (1200 UTC 5 April 2023), there was an increase in both the surface and 2-m temperatures. The difference between the median 2-m temperatures for the two simulations reached 1.2°C. The median temperature of the EXP run reached 0°C 2.5 h earlier than the CTRL model. The median total rain amounts for the CTRL and EXP runs were 10 mm and 19.1 mm, respectively. Similarly, the median total freezing rain amounts for CTRL and EXP were 28.5 mm and 18.7 mm, respectively, indicating a 34.4 % decrease in freezing rain for EXP. This corresponded to 35.1 % of area experiencing less freezing rain due to the earlier transition in the domain. At the grid point location, where the maximum freezing rain was observed in the CTRL run, the time taken for the 2-m temperature to reach 0°C was 3 h less in the EXP than in CTRL. The mean bias among the stations that recorded freezing rain was −0.84°C in the CTRL simulation and −0.49°C in the EXP simulation.

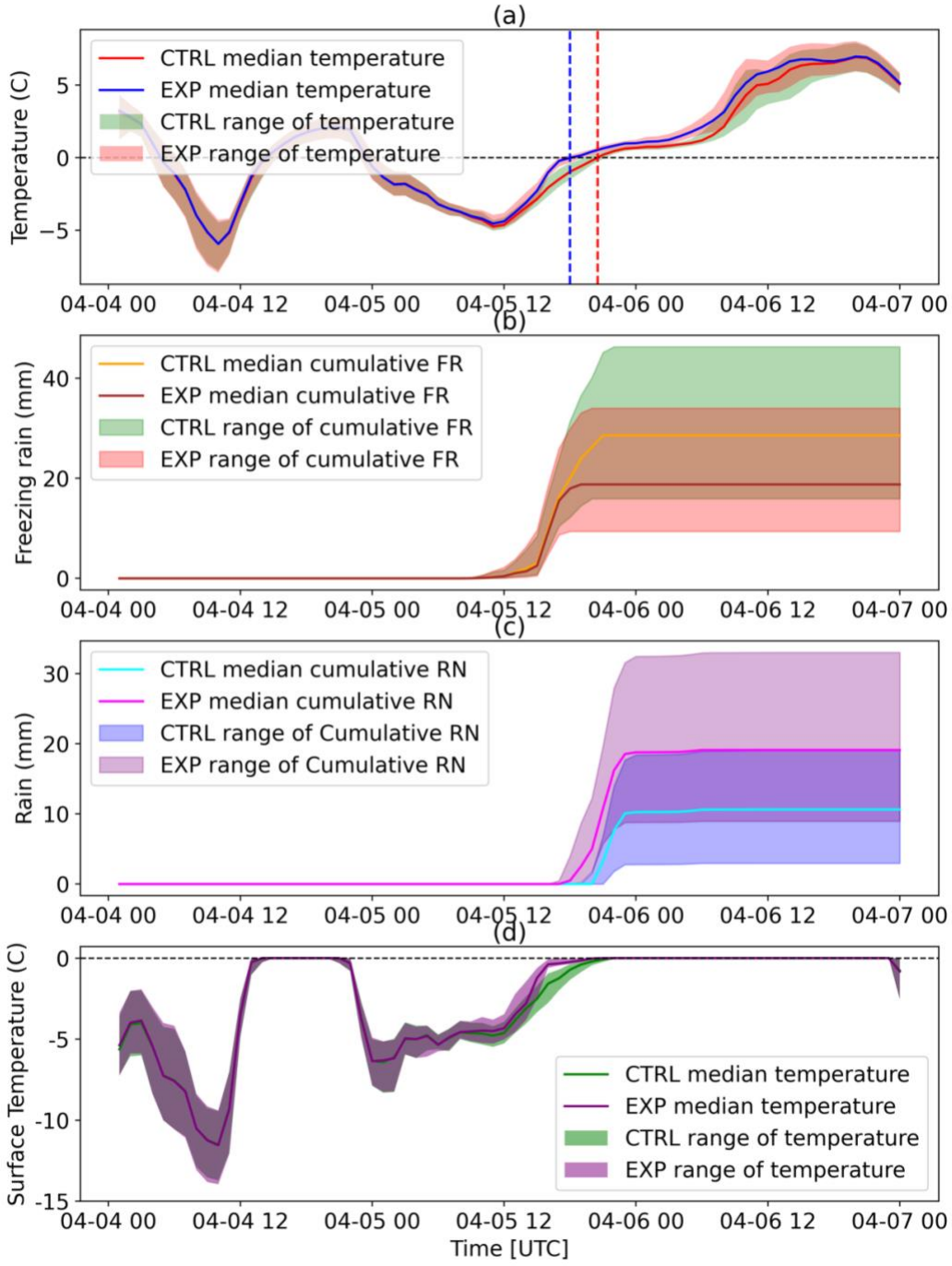

Figure 3.10: The range of (a) the 2-m temperature (°C), (b) CTRL and EXP accumulated freezing rain (mm), (c) CTRL and EXP accumulated rain (mm), and (d) CTRL and EXP surface temperatures (°C). The shading represents the 25th and 75th percentile values for the area indicated by the black rectangle in Figure 3.1a. The red and blue vertical dashed lines in (a) represent the time when temperatures reached 0°C in CTRL and EXP, respectively.

The upper air temperatures at PK-UQAM and Ottawa Gatineau Airport at various pressure levels are shown in Figure 3.11. These two sites were chosen because among the available sites in our

study, the simulation produced the two highest amounts of freezing precipitation at these sites. The difference in temperature between CTRL and EXP was greatest in the lower levels because this is where the latent heat was added. The EXP was closest to both ERA5 and the measured surface temperature. The freezing rain rates at both the sites were similar, leading to a similar heating distribution. Even though the modification was applied to the sub-freezing layer, the peak of the warm nose was also slightly impacted at both the sites.

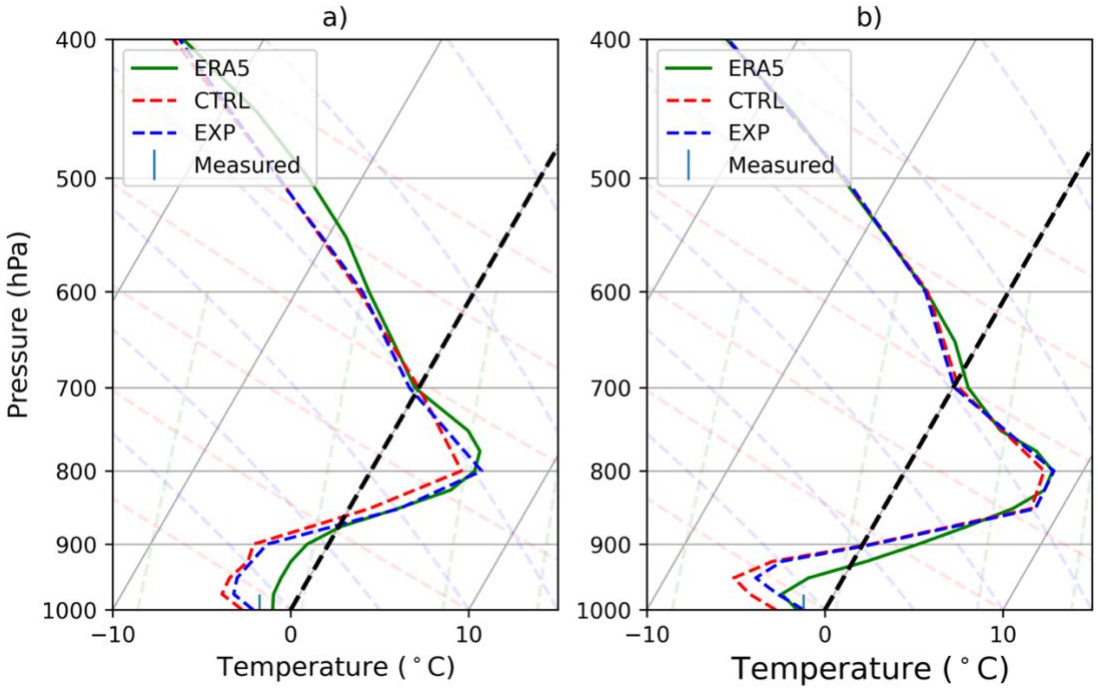

Figure 3.11: Vertical temperature profiles (°C) from EXP (dashed blue), CTRL (dashed red), and ERA5 (green), and the 2-m measured temperature (vertical solid blue) at stations (a) PK-UQAM and (b) Ottawa Gatineau Airport at 1700 UTC 05 April 2023.

The temperature tendency at PK-UQAM is shown Figure 3.12. The temperature rose at the lowest model level (N_1), which is closest to the surface, reaching a maximum 1.3°C. Conversely, the greatest temperature increase occurred at the fifth lowest model level (N_5), at 0.44°C. This pattern indicates a decreasing trend in the temperature increase with each successive model level away from the surface. The difference in air temperature between the model levels also starts to decrease with altitude. The bias for the time it took for the 2-m temperature to reach >0°C following the transition from freezing rain to rain decreased by 45 min.

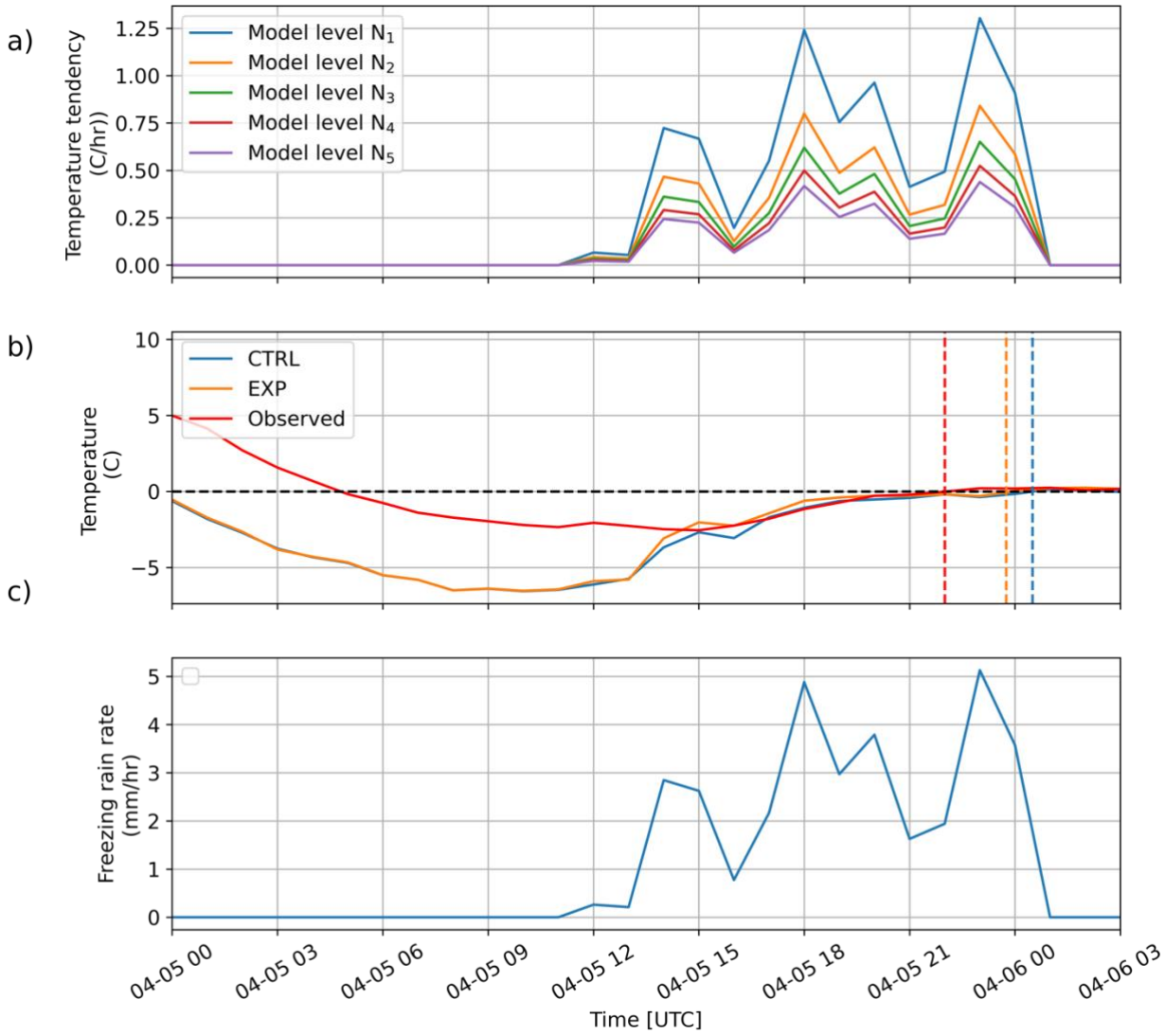

Figure 3.12: (a) Latent heat temperature tendency (°C h-1) at the lowest five model levels using Eq. A.1 (in Appendix A). (b) 2-m temperature for CTRL, EXP, and the observed temperature (°C). Vertical dashed lines show the time when the temperature reached 0°C. (c) Freezing rain rate (mm h-1) at PK-UQAM. In (a), N1 (lowest level) to N5 (highest level) refer to the first five model levels).

The 2-m temperature is a diagnostic term in the model, as a weighted function of surface temperature and the lowest model level. When adding a heating rate, such as 1.5°C h^{-1}, to the lowest model level, the full increase is not directly observed at the 2-m diagnostic temperature. This is due to vertical mixing redistributing some of the added heat to higher atmospheric levels, and to the surface drag coefficient for heat leading to some heat loss during the transfer to the 2-m level. Due to these redistribution and loss processes, the actual temperature increase at 2-m will be less than the initial heating rate of 1.5°C h^{-1} that is applied at the lowest model level.

Since 70 % of the energy is distributed in the atmosphere, we compared thermal advection at the lowest model level with latent energy from freezing rain. The impact of the latent heat release was investigated at three sites: PK-UQAM and two other grid points, hereafter referred as GP1 and GP2 (locations shown in Figure 3.1). A large amount of freezing rain occurred at GP1 and GP2 (Figure 3.13). Although GP1 and GP2 appear geographically close, there are also differences between their onset temperature. At GP1 during the freezing rain period over 13 h, the cumulative latent heat term in the lowest model level was an order of magnitude higher compared to cumulative thermal advection (+15.8°C compared to −3.79°C), so we see a transition occur. In contrast, at PK-UQAM during the freezing rain period over 13 h, the cumulative thermal advection term was −32.5°C and the cumulative latent heat term was +24.3°C, thus the same order of magnitude. Consequently, EXP shortened the transition from freezing rain to rain by 0.5 h at PK-UQAM, while the transition was shortened by 5.5 h at GP1. At GP2, although the magnitude of the latent heat of freezing rain was similar, the colder temperature at the onset of the freezing rain event made it difficult to transition to rain. The coldest temperature at GP1 was −4.6°C, while the coldest temperature at GP2 was −5.8°C. This difference of 1.2°C is enough to impact the transition from freezing rain to rain. Thus, the impact of latent heat generated from freezing rain transitioning to rain can be offset by the onset temperature and thermal advection.

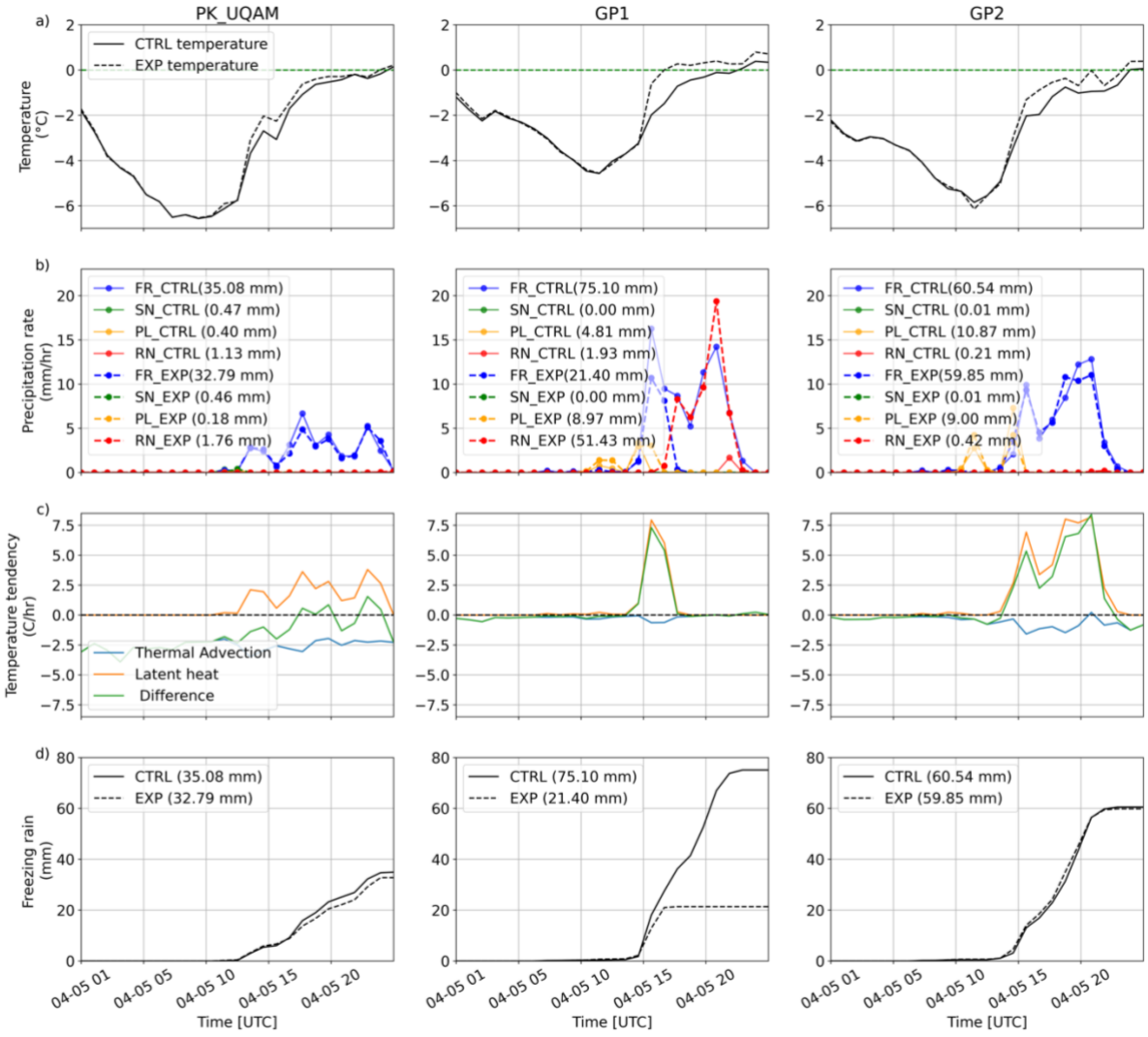

Figure 3.13: (a) 2-m temperature (°C), (b) CTRL precipitation rate for the various precipitation types, and (c) latent heat and thermal advection at the lowest model level from the simulation. “Difference” is the latent heat minus the thermal advection. (d) Cumulative freezing rain for EXP and CTRL. The cumulative precipitation amounts are inside the parenthesis in (b) and (d) in mm. GP1 and GP2 are two grid points from the map (shown in Figure 3.1a). Freezing Rain (FR), Snow (SN), Ice pellets (PL), Rain (RN).

3.5 Discussion

We demonstrated that adding the latent heat produced by freezing rain in the model impacted the simulated temperature and simulated precipitation amount at various regions. Previous studies (Cholette et al., 2020; Thériault et al., 2022) that have used baseline P3 to simulate precipitation found that freezing rain was overestimated in the model. Our CTRL-run RMSE and bias values were comparable to those of the previous studies. Modifying the scheme to include the freezing

fragmentation drops (Lachapelle et al., 2024) slightly improved the simulation of freezing rain precipitation. Lackmann et al. (2002) stated that the thermodynamic impact of freezing rain can contribute to bias in lower-tropospheric temperatures. Adding latent heat distribution in the lowest level of the atmosphere during the April 2023 ice storm increased mean 2-m temperatures by up to 3°C and improved air temperature distribution in the sub-freezing layer near the surface.

The role of warming due to the latent heat release from freezing rain varied during the April 2023 storm. Sometimes, the latent heat was insufficient to warm the near-surface cold layer to 0°C and transition freezing rain to rain. To better understand this effect, we investigated the local temperature tendency equation, which is formed from horizontal thermal advection and diabatic heating. In the refreezing layer, the magnitude of cold-air advection played a role in the transition between precipitation types (Thériault et al., 2022). Persistent low-level cold air advection helps maintain the temperature of the refreezing layer (McCray et al., 2019). Our study showed that, if in contrast, the magnitude of the latent heating term is higher, meaning that the precipitation rate is also higher, the transition can occur quickly as the 2-m temperature increases to above 0°C. In the simulation at GP1, the latent heat term was approximately four times higher than cold air advection, causing the freezing rain to quickly transition to rain. The highest freezing rain rate at this site in the simulation was 15 mm h^{-1}, significantly higher than the 8 mm h^{-1} observed in the simulated 2017 New Brunswick storm (Thériault et al., 2022). McTaggart-Cowan et al. (2019) stated that the warming from the latent heat from freezing rain can be important when the magnitude of the thermal advection and latent heat are comparable. Henson et al. (2011) also discussed the role of horizontal temperature advection in balancing atmospheric warming due to precipitation phase change at the surface during the 1998 ice storm.

The relatively colder onset of the 2-m air temperature also played a role in the persistence of the freezing rain event in some regions during the April 2023 storm. At GP2, the cold onset temperature of −5.8°C delayed the transition from freezing rain to rain, despite freezing rain rates reaching as high as 12 mm h^{-1}. The colder the onset temperature, the later the beginning of the erosion of the cold layer due to the release of latent heat at the surface. The colder the 2-m temperature, the longer it will take for the surface to reach 0°C for a given heating rate. McCray et al. (2019) pointed out

that a relatively cold onset 2-m temperature was particularly important for prolonging a freezing rain event in the Northeastern United states.

Figure 3.14 illustrates the impact of varying energy partitioning scenarios between the atmosphere and the surface for the same domain shown in Figure 3.10. The total freezing rain amount varied depending on the amount of heat added to the atmosphere during freezing. Greater amounts of heat being released in the atmosphere led to a larger decrease in freezing rain at the surface. More specifically, the mean decreases in freezing rain amounts were 21 %, 22 %, and 34 % when 30 %, 50 %, and 70 % of the heat was released in the atmosphere, respectively. Similarly, the total amount of rain increased by 39 %, 49 %, and 80 % when 30 %, 50 %, and 70 % of the heat was released in the atmosphere, respectively.

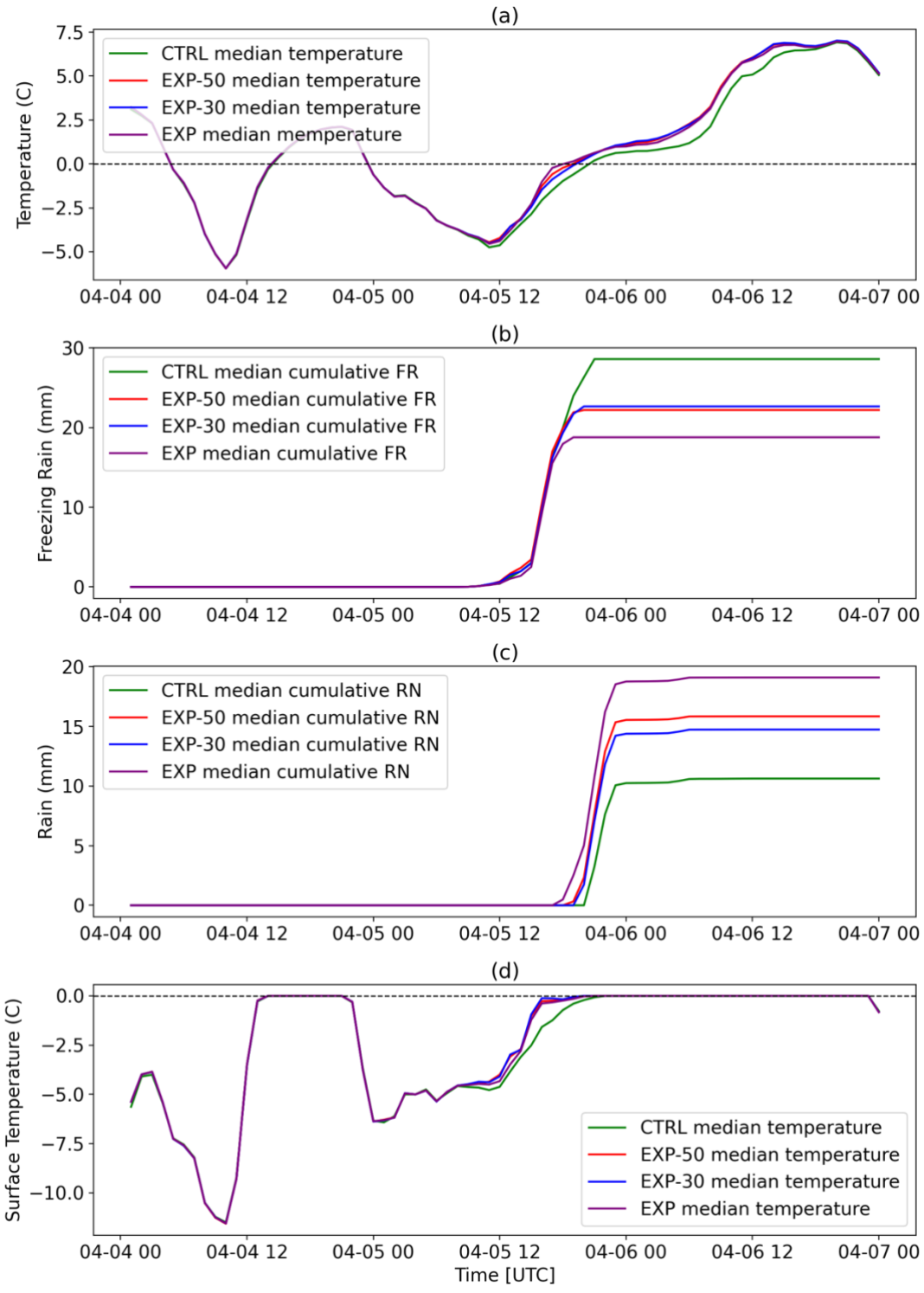

Figure 3.14: (a) Median 2-m temperature, (b) median cumulative freezing rain, (c) median cumulative rain, and (d) median surface temperature for CTRL (green), EXP (purple), and EXP with 50% (red) or 30% (blue) partitioning.

Implementing the latent heat distribution in the model was challenging. First, our implementation somewhat differed from the calculations proposed by Lackmann et al. (2002) and McCray et al. (2019). They assumed that latent heat from freezing rain was distributed across the entire refreezing layer, and that it would only cease when the mean/median temperature of the entire refreezing layer exceeded 0°C. However, in our implementation, as shown in Figure 3.12a, the temperature increase from latent heat was different at each model level because they are not separated equally due to the model structure. The thickness of each layer is given Appendix A. Furthermore, in our model, latent heat from freezing rain only ceases when the 2-m temperature exceeds 0°C. Second, the number of model levels used can impact the distribution of the heat and, in turn, the simulated air temperature. We conducted a sensitivity experiment to find the number of levels that produced the most realistic temperature profile. If we had constrained the heat to the lowest three model levels, or even just the lowest model level, the heating would be distributed to a small mass. The result would be a temperature increase at the corresponding model level that would produce a rise in air temperature at 2-m, which is unrealistic. We found that using 10 model levels to distribute the heat produced a more realistic temperature field. Third, the percentage of latent heat distributed between the surface and atmosphere, as explored in simulations EXP, EXP-30, and EXP-50, affects the simulation of freezing rain and rain due to its impact on the evolution of the 2-m temperature. When latent heat is distributed among multiple model levels, the energy received by the level closest to the surface varies depending on the total amount of latent heat available. If less heat is available to be distributed in the atmosphere, the energy at the lowest level decreases proportionally. Since the energy at the lowest level is crucial for determining the 2-m temperature, the differences between the EXP-30 and EXP-50 simulations were less pronounced, reflecting the relatively small variation in energy at this critical level. The differences were more evident between EXP and EXP-50.

The 2-m air temperature is influenced by multiple factors, including the surface temperature, lowest model level temperature, stability corrections, and surface roughness length. As seen in Figure 3.14, an increase in latent heat within the surface energy balance contributes to surface warming but does not necessarily lead to a corresponding increase in the 2-m air temperature. This may be because the added energy is used to melt frozen ground or snow, and limiting surface temperature to increase beyond 0°C. Instead, 2-m air temperature is more strongly influenced by changes in the lowest model level temperature, as also indicated in Figure 3.14. Additionally, while surface

temperature is calculated using the surface energy balance, some components of the energy balance, such as sensible heat flux and evapotranspiration, also depend on the temperature at the lowest model level. Stability corrections, further regulate how the 2-m air temperature responds to surface and atmospheric changes in temperature.

Finally, other factors can also impact air temperature at the lowest level of the atmosphere. The 2-m temperature biases that occurred in the model could be due to a combination of factors. The treatment of the radiative terms in the surface energy balance (Lackmann et al., 2002), albedo, sensible heat from precipitation, planetary boundary layer parameterization scheme, soil moisture and temperature, as well as synoptic-scale errors, can all introduce biases into the model. Furthermore, the type of soil and its degree of freezing can also influence the partitioning of latent heat between the atmosphere and the surface (Lackmann et al., 2002). Other effects that might impact the surface temperature include representation of terrain features such as wind-channeling effects that maintain the relatively cold air near the surface and impact the duration of freezing rain events. Studies have shown that wind channeling supports cold air advection for long-duration freezing rain events (Carrera et al., 2009; Ressler et al., 2012).

3.6 Conclusion

We investigated the contribution of the latent heat released from the freezing of supercooled drops at the surface during the April 2023 ice storm. We made modifications to lower model levels as well as CLASS to account for atmospheric heating in the sub-freezing layer and the surface energy balance at the surface respectively. Multiple experiments were conducted using a high-resolution GEM simulation (1-km grid spacing) and using different heat partitioning between the ground and the lower atmosphere.

These analyses led to several conclusions:

- Latent heat from the freezing rain of supercooled drops contributed to an increase in the 2-m temperature to > 0°C, which eliminated freezing rain. Where transition between precipitation types was possible, the EXP simulation showed an overall decrease in freezing rain and an increase in rain.

- The transition of precipitation varied across southern Quebec and southern Ontario. In the EXP simulation, the largest amount of transition from freezing rain to rain was observed at the southern region of Ontario. This is also where the largest amount of freezing rain occurred in the CTRL run.
- The magnitude of thermal advection was compared to the latent heat that was generated from the freezing rain. Advection combined with the onset 2-m temperature and freezing precipitation rate played a role in determining whether the 2-m temperature rose to 0°C and whether precipitation transitioned from freezing rain to rain.

Future work could assess how latent heat from freezing rain can reduce freezing and/or produce temperatures near 0°C during other freezing rain events. Further investigation is needed to understand how urban surfaces respond to latent heat, particularly in densely built-up areas with a high concentration of electrical infrastructure. Stewart et al. (2023) showed that near-0°C temperatures would still occur in warmer climate conditions, and the latent heat process may play a role. A comparison of climatological studies with and without this modification could help us understand the impact of this process in determining freezing rain duration in the current and future climate.

Overall, our study represents the first comprehensive evaluation of the impact of latent heat from freezing during a freezing rain event on both the 2-m temperature and the temperature of the subfreezing layer. Although the impact of latent heat from freezing rain is small, even a few degrees can significantly alter precipitation type. The latent heat released during a freezing rain event can suppress its further formation and cause it turn into rain. Length of a freezing rain event is an important factor that defines the severity of an event. Thus, it is important to examine such transitions, which can reduce the adverse impacts of freezing rain, including infrastructure damage and hazardous travel conditions.

CHAPTER 4

Evolution of extreme freezing rain events in the CTRL and PGW climate in Eastern North America

This chapter is presented in the format of a scientific article that will be submitted to the Journal of Geophysical Research: Atmospheres.

Basnet, S and Thériault, J.M. Evolution of extreme freezing rain events in the CTRL and PGW climate in Eastern North America.

Abstract

Long-duration freezing rain events, defined in this study as six hours or more, can lead to severe societal and infrastructure impacts. This study investigates the thermodynamic evolution of long-duration freezing rain under warmer atmospheric conditions using the CRCM6-GEM5 regional climate model, run for both a historical (CTRL) period and a pseudo-global warming (PGW) scenario over the southeastern United States, southern Quebec, and the province of New Brunswick for the 2012–2022 period. Results show a decrease in the frequency of long-duration freezing rain events under PGW, with a shift toward rain during and after events, particularly in New Brunswick and southern Quebec. Onset surface temperatures are warmer in PGW across all regions, with southern Quebec experiencing the largest increase at 4.18°C. In southern Quebec, drier onset surface conditions in PGW enhance evaporative cooling, helping to maintain subfreezing temperatures. Melting layer depth and maximum temperatures decrease in all regions under PGW, indicating a cooler melting layer aloft. Latent heat release during freezing rain remains a key factor in limiting event duration in both climates. Latent heat suppresses freezing rain in 84% of events in the southeastern U.S. under the current climate, and in 90% of events in southern Quebec under a future warming scenario. These findings highlight regional thermodynamic changes that affect the persistence of freezing rain and provide insight into future risks and improved forecasting potential.

4.1 Introduction

Freezing rain is a significant meteorological hazard in mid-latitude regions, particularly in Canada, where it is among the costliest hydrometeorological disasters. It can cause extensive damage to power lines (Jeong et al., 2018), communication infrastructure (Mulherin, 1998), trees (Seidl et al., 2017), and agriculture due to ice accumulation, even in small amounts. An example of its devastating impact was the 1998 Ice Storm, which left over a million people without power, caused infrastructure collapse, and resulted in significant human casualties (Henson et al., 2007). Although freezing rain is relatively rare globally, certain regions such as eastern Canada, the northeastern U.S., and parts of southeastern U.S. are particularly vulnerable to these hazardous events. Regions such as eastern Newfoundland (Stuart and Isaac, 1999), the Ottawa River Valley (Cheng et al., 2004), and the St. Lawrence River Valley in southern Quebec (Henson et al., 2011) experience frequent freezing rain events, often due to warm air layers above shallow sub-freezing surfaces.

Freezing precipitation forms through two main processes: the melting process and the supercooled warm rain process (Rauber et al., 2000). The melting process occurs when ice crystals fall into a warm (> 0°C) layer, melt into liquid droplets, and then pass through a subfreezing layer, becoming supercooled before freezing on contact with surfaces. This process is primarily responsible for freezing rain. In contrast, the supercooled warm rain process involves liquid droplets growing through collision and coalescence without an elevated warm layer, often producing freezing drizzle. Environmental conditions for freezing rain and ice pellets depend on the presence of both a melting layer aloft and a subfreezing layer near the surface (Zerr, 1997). If hydrometeors completely melt in the warm layer, they are more likely to remain supercooled as freezing rain, while incomplete melting can lead to refreezing as ice pellets. Studies show that while the melting process has traditionally been considered the dominant cause of freezing rain, the collision–coalescence process plays a significant role, particularly in clouds with high liquid water content and cloud-top temperatures above -10°C (McCray et al., 2019).

Freezing rain is influenced by diabatic processes, in which the release of latent heat during phase changes affects both temperature and precipitation type (Stewart, 1985). As snowflakes melt aloft, the extraction of latent heat cools the air, potentially eroding the warm layer, whereas when rain freezes upon contact with the surface, the release of latent heat warms the air to 0°C, potentially

transitioning freezing rain to rain. Studies have shown that latent heat can cause surface warming, with an increase in 2-m air temperature, as seen in the 2023 ice storm in southern Quebec and Ontario (Basnet et al., 2025). This effect can be counteracted by evaporative cooling, particularly in dry conditions (Lackmann et al., 2002). The release of latent heat from freezing rain can also increase the occurrence of near-0°C temperatures, which prolongs freezing rain events. These processes are crucial for forecasting freezing rain events, as they can either maintain or erode the cold and warm layers, making it difficult to predict precipitation phase changes. McCray et al. (2019) and Thériault et al. (2022) emphasize the importance of understanding this thermodynamic evolution to better mitigate the hazards associated with freezing rain.

Recent studies on freezing precipitation have examined freezing rain processes under present and warmer climates using observations, reanalysis, and high-resolution regional models. A study examined ten major freezing precipitation events in Manitoba and found that they were influenced by low topographic features (Tropea et al., 2021). Under a pseudo-global warming scenario, the locations of these events shifted. Another study by Cheng et al. (2011) estimated the potential impacts of climate change on future freezing rain events over eastern Canada. The results showed that the region could experience more freezing rain during the colder months (December–February) and less during the warmer months (November, April, and October in the north) due to climate change. Comparison of the 1998 Ice Storm to the Weather Research and Forecasting (WRF) model with current and pseudo-global warming scenarios shows that microphysical processes involved in precipitation are also affected (Cholette et al., 2021). In the scenario, warmer atmospheric conditions led to increased ice mass and enhanced riming aloft, resulting in higher liquid precipitation rates.

Past studies have presented the thermodynamic conditions for the current climate (Cortinas, 2000; McCray et al., 2019). Some studies have also looked at case studies of the impacts of warmer atmospheric conditions on specific ice storm events (Cholette et al., 2021; Marinier et al., 2023). Further investigation is needed to better understand the fine-scale processes that determine the evolution of freezing rain in warmer conditions. Our study builds on this previous work in two key aspects. First, this climatological study provides a regional comparison of upper-air profiles between the current climate and a warmer future climate, looking at all long duration freezing rain

events. Second, while recent studies have investigated the impact of latent heat release from freezing rain at the surface during single storms, the climatological role of this process in suppressing freezing rain events remains largely unquantified. The objective of this study is to characterize the thermodynamic conditions required for long duration (LD) freezing rain events, and to assess whether these conditions change in a warmer climate.

This paper is organized as follows. Section 4.2 outlines the methodology, including model configuration, the study domain, and the data analysis. Section 4.3 presents the climatology of freezing rain events across the selected region. Section 4.4 examines the thermodynamic evolution of freezing rain events in the CTRL and PGW simulations. Section 4.5 presents the discussion and Section 4.6 offers concluding remarks.

4.2 Methodology

4.2.1 Study area and model description

The study employed the CRCM6-GEM model version 5.1.1 with a 2.5-km horizontal resolution (Roberge et al., 2024). The model domain of this simulation covers eastern North America, between 31°N and 66°N. The coverage is displayed in Figure 4.1. The simulation spans the period from January 2012 to December 2022. The analysis focuses on three key regions, southeastern U.S., southern Quebec and New Brunswick, as these areas have been identified as vulnerable to freezing rain impacts based on past studies. We limit most of our analysis to these three regions because each exhibit relatively uniform climatological characteristics, which allows for a more robust assessment of freezing rain patterns. Moreover, these areas have historically experienced high-impact ice storms, such as the January 2017 event in New Brunswick and the 1998 storm in southern Quebec, which have caused widespread damage to infrastructure, disrupted transportation networks, and significantly impacted communities (Thériault et al., 2022). Ice storms have also proven to be dangerous and economically costly events in the southeastern United States, particularly given the high population density in the region (McCray et al., 2019).

A two-step nesting approach is used to achieve the convection-permitting resolution of 2.5 km. In the first step, intermediate simulations are conducted at 12-km resolution using CRCM6-GEM5

with spectral nudging applied in the interior of the domain. These 12-km simulations then serve as lateral boundary conditions for the convection-permitting 2.5-km simulations, which are the basis for all analyses in this study.

At the 12-km resolution, a pair of continuous 11-year simulations (2012–2022) was performed, consisting of a control (CTRL) and a pseudo-global warming (PGW) experiment. The CTRL simulation is forced by ERA5 reanalysis, representing present-day climate conditions. The PGW experiment follows the same configuration but incorporates a climate change perturbation computed as the difference between a future period (2076–2100) and a historical baseline (1990–2014), based on monthly means from an ensemble of 30 CMIP6 models under the high-emission SSP5-8.5 scenario. This delta is applied to temperature, winds, geopotential, specific humidity, sea surface temperature, sea ice fraction, sea level pressure, and soil temperature. The model configuration follows Roberge et al. (2024), with 66 vertical levels extending up to 25 hPa and a time step of 60 seconds.The outputs from both the 12-km CTRL and PGW simulations are used to drive their respective 2.5-km simulations. The driving data for the 2.5km resolution are temperature, wind, surface geopotential, surface pressure, specific humidity, sea surface temperature, and sea ice fraction.

Both the CTRL and PGW simulations used the same parameterizations. Cloud and precipitation processes were represented using the Predicted Particle Properties (P3; Morrison and Milbrandt 2015) bulk microphysics scheme. Unlike traditional schemes, P3 treats ice particles as a continuum with evolving properties rather than having fixed categories such as snow, graupel, or hail. It predicts three main hydrometeor types: liquid cloud droplets, rain, and ice phase particles. The ice characteristics are predicted using ice mass mixing ratio, ice number mixing ratio, ice mass from rime growth and bulk rime volume. The Canadian Land Surface Scheme (CLASS, version 3.6; Verseghy, 2000) was used to represent land-surface processes. Other parameterizations included the Kuo-transient shallow convection scheme (Kuo 1965; Bélair et al. 2005), the correlated-k terrestrial and solar radiation scheme from Li and Barker (2005), a turbulent kinetic energy closure scheme for the planetary boundary layer and vertical diffusion (Benoit et al. 1989; Delage and Girard 1992; Delage 1997).

4.2.2 Available observed and modelled data

Temperature and precipitation data were collected from 83 hydrometeorological stations across the study domain (Figure 4.1). While temperature records were available from all 83 stations, only 31 had sufficiently complete precipitation records. Following the criteria used by Cortinas et al. (2004) and McCray et al. (2019), stations were selected based on having at least 80% data availability over the 11-year study period. All hydrometeorological observational data were obtained from the Integrated Surface Database (ISD; Smith et al., 2011) maintained by the National Centers for Environmental Information (NCEI) of the National Oceanic and Atmospheric Administration (NOAA). For model comparison, 2-m air temperature and precipitation amounts were extracted from the grid points nearest to each station location.

The model outputs used in this study include 2-m air temperature and precipitation amount and type. Precipitation analysis is based on hourly data, using a threshold of at least 0.2 mm liquid water equivalent to define precipitation occurrence (e.g., Chartrand et al., 2022; Marinier et al., 2023). Freezing rain was identified when rain occurred while 2-m air temperature was below 0°C. Hourly 3-D variables were also available for both the CTRL and PGW simulation. These variables include geopotential height and temperature at 16 specific pressure levels.

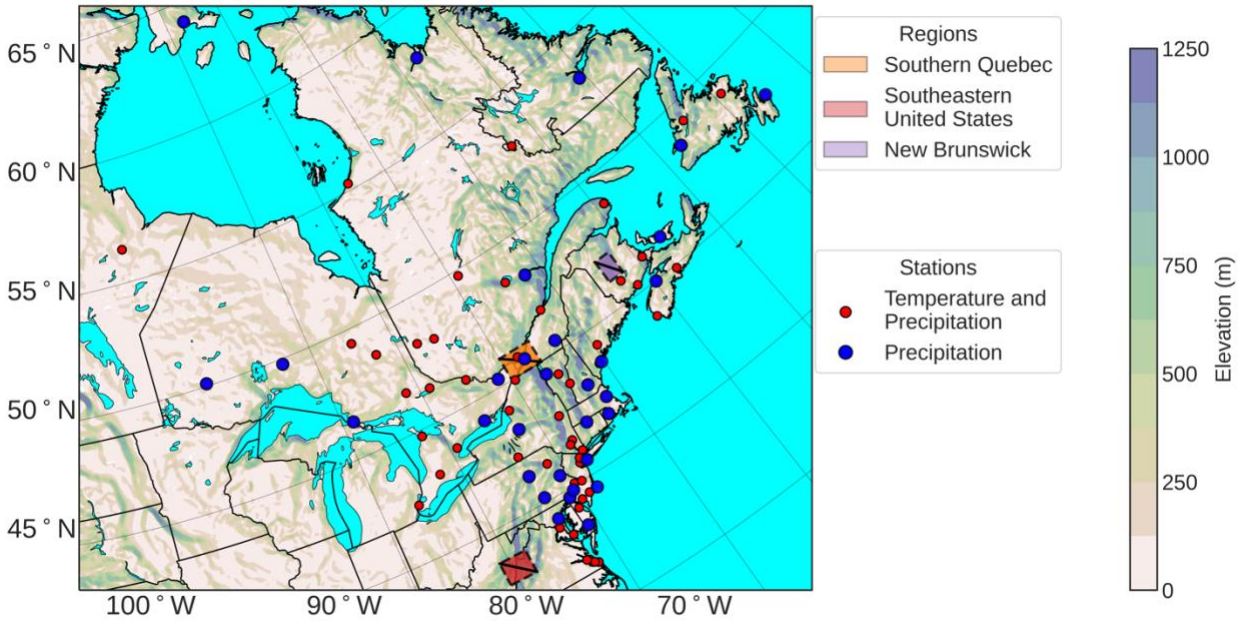

Figure 4.1: Map of the study domain along with station locations for temperature and precipitation data (red and blue dots) with shaded topography (m). Locations of the three study regions: southern Quebec (orange), southeastern U.S. (red), and New Brunswick (purple). The cross section of each region is shown starting from the top left corner to the bottom right corner of each region.

4.2.3 Definition and data analysis

Freezing rain events were first identified by grouping consecutive hourly observations at each station. To ensure events are synoptically independent, we then merged any separate groups that are less than 6 hours apart. The duration of an event is defined as the total number of hours with freezing rain observations between its start and end, excluding any intermittent hours without freezing rain.

Since freezing rain is light in intensity, its severity is defined by the length of an event. We define LD events as those with six or more hours of observed freezing rain, a threshold consistent with prior studies (Cortinas et al., 2000; Marinier et al., 2022). Short-duration (SD) events are defined as those with less than six hours of freezing rain. One-hour events are excluded from the study. We also omit five-hour events to maintain a clear distinction between SD and LD categories, following the McCray et al. (2019).

After identifying events, we compared temperature and dew point depression at onset for LD events as well as the progression of precipitation phase before, during, and after each event across regions. The precipitation phase before and after the event includes all precipitation occurring within the six hours preceding and following the event. The precipitation type output is provided at an hourly resolution. However, multiple types of precipitation often appear within the same hour, since the model diagnoses precipitation at 60-second intervals, with the hourly output aggregating these sub-hourly diagnostics. Thus, percentages for each precipitation type (Rain, Snow, Ice pellets, No Precipitation) may sum to more than 100%, as freezing rain events can be accompanied by multiple types of precipitation.

For LD events, we also examine upper-air temperature profiles at the time of event onset. The warm layer is defined as the atmospheric layer aloft where the temperature exceeds 0°C, and must be located above a near-surface cold layer, where the temperature is at or below 0°C. For both the warm and cold layers, we compute their respective depths, the maximum temperature in the warm layer (T_{max}), and the minimum temperature in the cold layer (T_{min}).

We used the equation from Lackmann et al. (2002) to estimate the temperature increase resulting from latent heat release during the freezing of supercooled drops.

$$\Delta T = \frac{F_A L_f \rho_l R_m}{M C_p} \tag{4.1}$$

where T is the dry bulb temperature, F_A is the fraction of latent heat that goes to the surface, L_f is the latent heat of vaporization, ρ_l is the density of liquid water, R_m is the depth of liquid equivalent precipitation, M is the mass of air per unit area through which the heat is transferred to the air, and C_p is the specific heat of air at constant pressure. Based on past studies F_A is estimated to be 0.7.

The mass of air per unit area is calculated based on the depth of the air column. Basnet et al. (2025) estimated this depth to be approximately 1,000 m. Other studies, such as McCray et al. (2019) and Thériault et al. (2022), estimated the depth influenced by latent heat release using the depth of the subfreezing layer, which varies by region. To assess how sensitive our results are to this assumption, we also tested an alternative approach. Instead of using a fixed depth, we used the climatological median depth of the subfreezing layer observed during the events.

The current version of the CRCM6-GEM5 does not explicitly account for the release of latent heat that occurs when supercooled water freezes during events such as freezing rain. To investigate whether including this physical process could alter the outcome of an event, we conducted a theoretical analysis similar to the example in Lackmann et al. (2002). For each freezing rain event, we first calculated how much the air temperature would increase if all of the available latent heat from freezing were released. This is referred to as the latent heat induced temperature change, or ΔT. We then compared this value to the temperature deficit, which we define as the difference between 0°C and the actual air temperature at the end of the freezing rain event (shown in Figure 4.2 by the green double-headed arrow). In other words, the temperature deficit tells us how far below freezing the air still is. By comparing the latent heat-induced ΔT to the temperature deficit, we can assess whether the latent heat was sufficient to raise the temperature above freezing. If so, it could erode the cold layer and enable a transition from freezing rain to rain.

Based on this comparison, we classified each event into one of three categories: 'T' (Transition), the temperature remained below 0°C, but the latent heat induced temperature change was large enough to fully eliminate the temperature deficit, suggesting that the air could have surpassed 0°C if latent heat were included; 'E' (Equilibrium), the temperature was already above 0°C, so latent heat release would influence the event's evolution by shortening its duration; and 'F' (Failed), the temperature remained < 0°C , and the latent heat was not sufficient to bridge the temperature deficit. This classification allowed us to assess, in a systematic way, how often latent heat could meaningfully influence the outcome of freezing rain events. We used this classification for both the CTRL and PGW simulation.

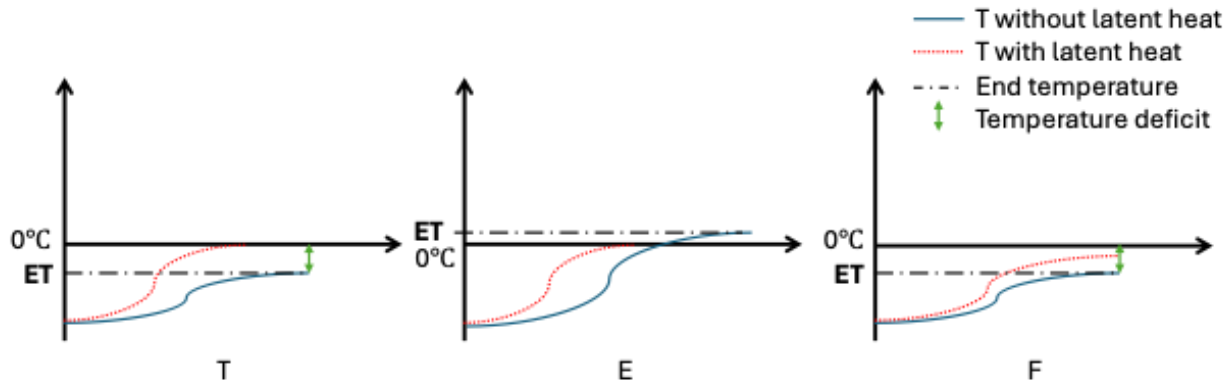

Figure 4.2: Schematic diagram illustrating the classification of freezing rain transition events. In each plot, the x-axis represents time evolution, and the y-axis represents the 2-m temperature during the freezing rain event. The blue line shows the temperature evolution without latent heat, while the red line shows the temperature evolution with latent heat. ET refers to the temperature at the end of the freezing rain event, without latent heat. The green double-headed arrow indicates the temperature deficit needed to reach 0°C. T, E, and F are described in the methods section.

4.3 Results

4.3.1 Evaluation

The model simulation for the CTRL scenario were evaluated using the temperature and precipitation data for the meteorological stations as shown in Figure 4.3. The model accurately reproduced the mean annual 2-m temperature for the 11 years (R2 = 0.97), and also captured the average amount of precipitation with reasonable accuracy (R2 = 0.77). Among the stations used in the study, St. John's International Airport recorded the highest observed mean yearly precipitation at 1422 mm, with the model closely matching at 1450 mm. In contrast, Coral Harbour Airport had the lowest observed mean precipitation at 269 mm, with the model estimating 356 mm, indicating

a noticeable overestimation. Additional information on model evaluation is provided in Appendix B.

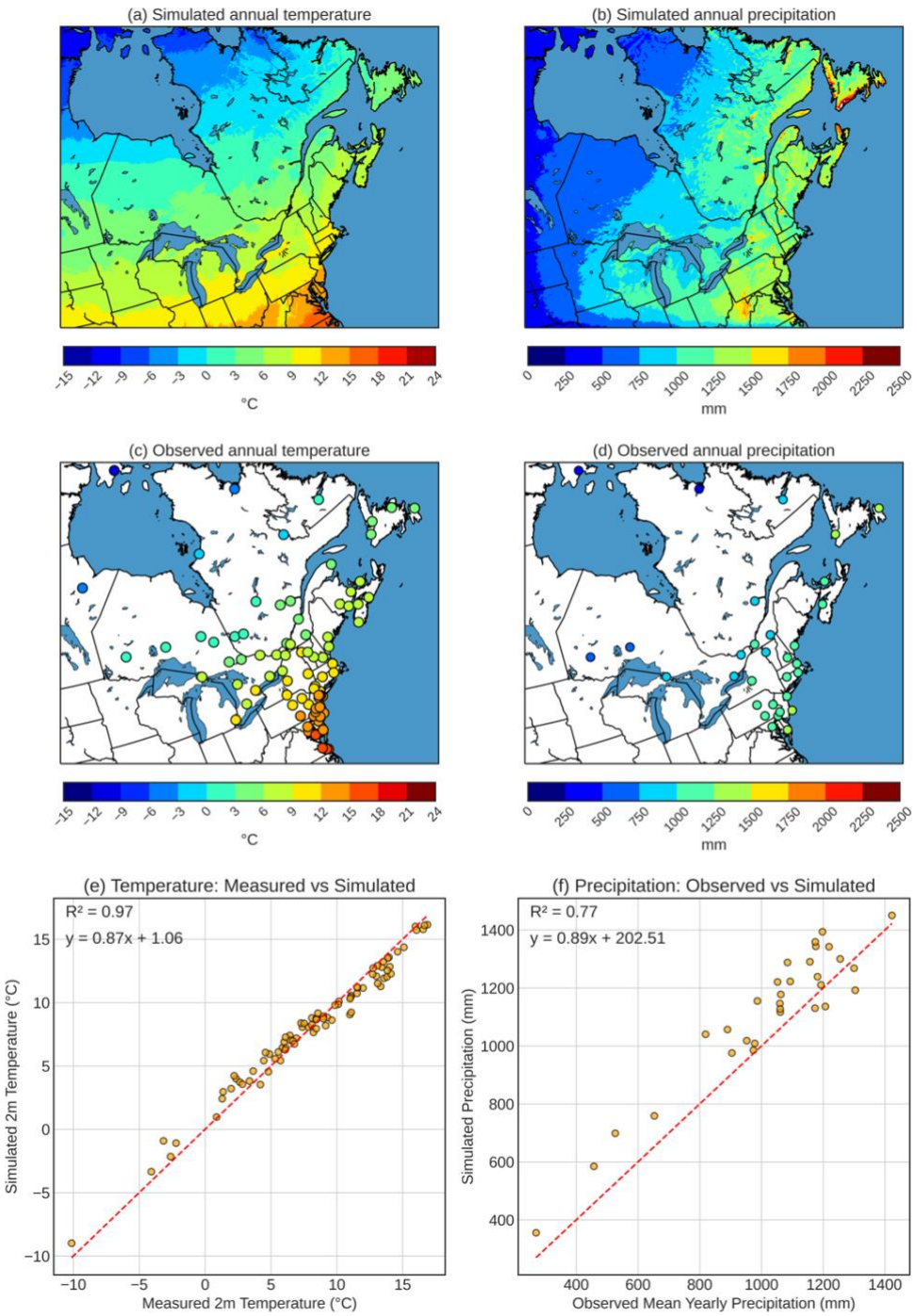

Figure 4.3: Comparison of the simulations (CTRL) and observations over the January 2012–December 2022 period: (a) CTRL mean annual 2-m temperatures, (b) CTRL mean annual precipitation, (c) observed mean annual 2-m temperature, (d) observed annual precipitation, comparison of observed versus simulated (at the nearest grid point to the observation (e) annual mean 2-m temperature, (f) annual mean precipitation. The red dashed line represents a 1:1 slope for reference.

4.3.2 Climatology

4.3.2.1 Climatology of freezing rain in the CTRL simulation

Past studies have shown that freezing rain is observed throughout eastern Canada and the U.S. (Cortinas et al., 2004; McCray et al., 2019; Marinier et al., 2023). The climatology of freezing rain events in our three regions of interest shows distinct regional patterns. We observed the highest median values of freezing rain duration in Newfoundland, with totals exceeding 60 h, as shown in Figure 4.4. However, this region was excluded from the study due to high spatial variability caused by complex terrain and proximity to the ocean. The median number of freezing rain events per year is comparable in southern Quebec and the southeastern U.S., with approximately 5 events per year. In contrast, New Brunswick experiences approximately 10 events per year. Results for total hours mirrors those of number of events. Annually, the median number of hours of freezing rain is notably higher in New Brunswick (39 h) compared to southern Quebec (18 h) and the southeastern U.S. (21 h). The two stations with the highest observed freezing rain hours are St. John's (65 h) and Gander (55 h), which matches well with the simulation results.

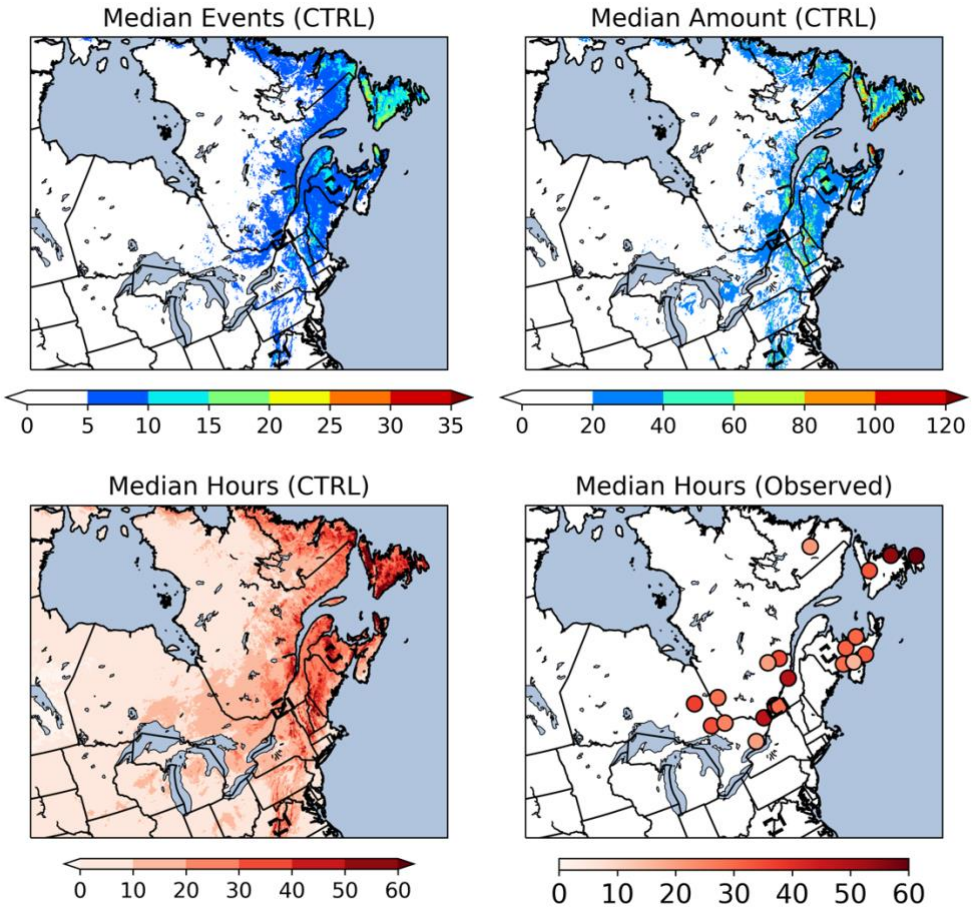

Figure 4.4: Climatology of freezing rain from 2012–2022 showing (a) median annual number of events, (b) median annual amount (mm), (c) median annual hours, for CTRL, and (d) median annual hours, observed.

4.3.2.2 Comparison of climatology between CTRL and PGW

The spatial distribution of mean annual 2-m temperature in the two simulations are compared in Figure 4.5. The largest temperature increases are observed in the northern regions, while the southern areas exhibit comparatively smaller changes. Regionally, the median temperature increase in PGW is 6.69°C in New Brunswick, 6.47°C in southern Quebec, and 4.55°C in the southeastern U.S. Under CTRL, LD freezing rain accounts for highest proportion of events in the southeastern U.S. (40%), followed by New Brunswick (35.4%). LD events are less common in southern Quebec (32.6%). Even if the freezing rain events occur less frequently in southeastern U.S., a higher proportion of the events are of long-duration. Under PGW, all regions show a decline in LD events, which become quite rare. This change is most pronounced in southern Quebec, where LD events account for only 14.2% of freezing rain events in PGW.

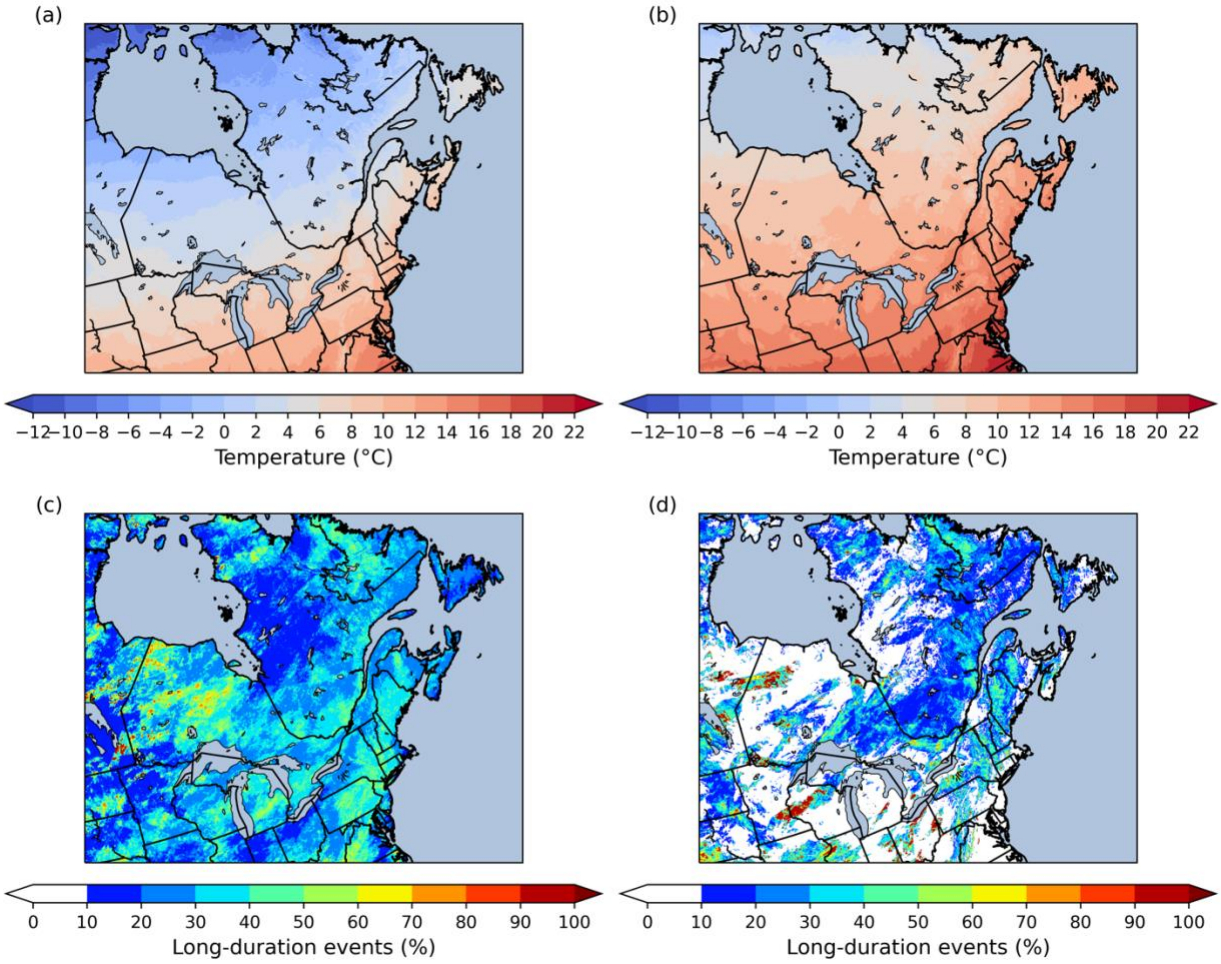

Figure 4.5: Comparison between CTRL and PGW simulations: mean annual temperature in (a) CTRL, and (b) PGW, and LD events (≥ 6 h) as percentage of total freezing rain events in (c) CTRL, and (d) PGW.

Figure 4.6 shows the mean annual total amounts of freezing rain, rainfall, and snowfall from the CTRL and PGW simulations for the 2012–2022 period. Orographic enhancement of precipitation causes some areas to receive more precipitation in our selected regions. The presence of mountains may cause cold-air damming, which directs cold, dense air against the Appalachian slopes and contributes to more persistent freezing rain in the southeastern U.S. (Robbins et al., 2002). The Appalachians also enhance the development of strong temperature inversions, leading to increased amounts of freezing rain in central and southern New Brunswick (Chartrand et al., 2023). Additionally, wind channeling in the St. Lawrence River Valley (SLRV) influences freezing rain occurrences in southern Quebec (e.g., Marinier et al., 2023). The snowfall distribution in New Brunswick follows the orography, with more snow produced at higher elevations, as seen in Figure 4.6. Out of all three types of precipitation, the strongest peak associated with orography was found

for freezing rain. This peak is largely mirrored in both the CTRL and PGW simulations, though its amplitude varies. In general, snow and freezing rain decrease substantially, while rain increases across all regions. If the peak values of the cross section are compared between CTRL and PGW, the sharpest decline in southern Quebec is in freezing rain (83%), followed by a 56% drop in snow, while rain increases by 45%. Similarly, New Brunswick sees a 55% decrease in freezing rain, a 47% decrease in snow, and a 41% increase in rain.

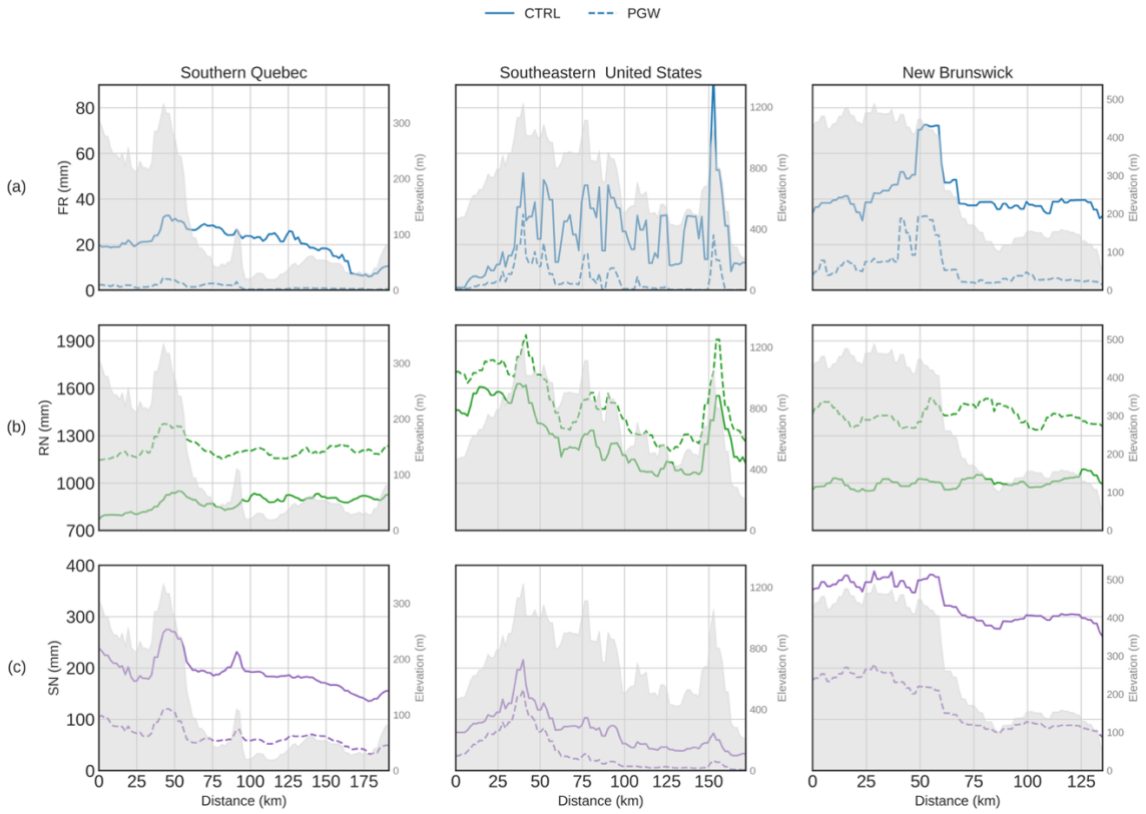

Figure 4.6: Vertical cross-sections showing the annual average (mm year^{-1} in liquid equivalent) of (a) freezing rain (FR), (b) rain (RN), and (c) snow (SN) during 2012–2022, based on the CTRL (solid line) and PGW (dashed line) simulations, with the topography shown for each study region (grey shading). On the x axis, 0 km refers to the left top corner of the cross section shown in Figure 4.1

4.3.3 Evolution of long duration of freezing rain events

4.3.3.1 Precipitation evolution

Different types of precipitation may occur before, during and after LD freezing rain events across southern Quebec, the southeastern U.S., and New Brunswick (Table 1). Snow is the dominant precipitation type before a freezing rain event in New Brunswick (67.2%) and southern Quebec (54.3%), while the southeastern U.S. sees a more even mix of snow, rain, and no precipitation

conditions. During the event, snow remains prevalent in New Brunswick (62.1%) and southern Quebec (52.4%), whereas the southeastern U.S. experiences more rain (40.2%). After the event, rain becomes more common than snow in all regions, especially in New Brunswick (46.6%) and the southeastern U.S. (40.2%). No precipitation is the most common after freezing rain in southern Quebec (40.3%) and the southeastern U.S. (43.4%).

Under PGW conditions, LD freezing rain events show shifts in precipitation type before, during, and after the events across all regions. Snow remains the dominant type before freezing rain in New Brunswick (79.5%), while no precipitation is dominant in southern Quebec (68.5%). The southeastern U.S. continues to have an even balance of precipitation types. During freezing rain, rain becomes more prominent, especially in New Brunswick (55.6%), while snow remains high across all regions, suggesting more mixed-phase precipitation. After freezing rain, rain dominates in all regions, particularly in New Brunswick and the southeastern U.S., while southern Quebec shows a more balanced mix of rain, snow and no precipitation. Under PGW, there are increases in rain during and after freezing rain events, particularly in New Brunswick. Additionally, periods of no precipitation before freezing rain events become more frequent in southern Quebec under PGW, contrasting with more snow-dominated precursors in CTRL.

Table 4.1: Percentage of LD freezing rain events that are preceded by, occurred with, or were followed by rain, snow, or no precipitation (NP) in southern Quebec, the southeastern U.S., and New Brunswick under the CTRL and PGW simulations.

Region	Phase	CTRL (%)			PGW (%)		
		Rain	Snow	NP	Rain	Snow	NP
Southern Quebec	Before	9.5	54.3	39.3	4.9	27.1	68.5
	During	28.6	52.4	32.5	38.0	53.4	23.7
	After	36.3	26.8	40.3	36.2	36.8	30.3
Southeastern U. S	Before	21.1	41.1	41.0	20.8	38.8	45.8
	During	40.2	44.6	29.2	40.0	56.2	25.5
	After	40.2	18.2	43.4	45.1	40.8	26.7
New Brunswick	Before	9.4	67.2	24.2	15.6	79.5	9.2
	During	34.9	62.1	23.1	55.6	74.6	8.5
	After	46.6	25.0	32.3	54.4	47.0	9.8

4.3.3.2 Onset air temperature

We examined the 2-m air temperature during LD freezing rain events because it plays a role in determining the type and amount of precipitation. Basnet et al. (2025) showed that the onset 2-m air temperature can influence the amount of freezing rain during an event. In the CTRL simulation, the southeastern U.S. had the highest proportion of freezing rain events with an onset temperature between -2°C and 0°C (54.7%), followed by New Brunswick (31.1%), and southern Quebec (20.9%) (Figure 4.7). Freezing rain events in the southeastern U.S. are more likely to occur near the 0°C threshold, whereas in southern Quebec they tend to occur under colder near-surface air conditions. Under PGW conditions, all regions shift more strongly toward near-0°C onset temperatures. The proportion between -2°C and 0°C rises to 79.7%, 66.2%, and 88.2%, in the southeastern U.S., New Brunswick, and southern Quebec, respectively. These changes reflect a consistent trend toward freezing rain events becoming concentrated at near 0°C in a warmer climate, with the most pronounced shift occurring in southern Quebec. The median temperature difference between CTRL and PGW freezing rain events varies by region, with southern Quebec experiencing the largest increase at approximately 4.2°C. In comparison, New Brunswick and the southeastern U.S. show smaller increases of about 2.4°C and 1.2°C, respectively.

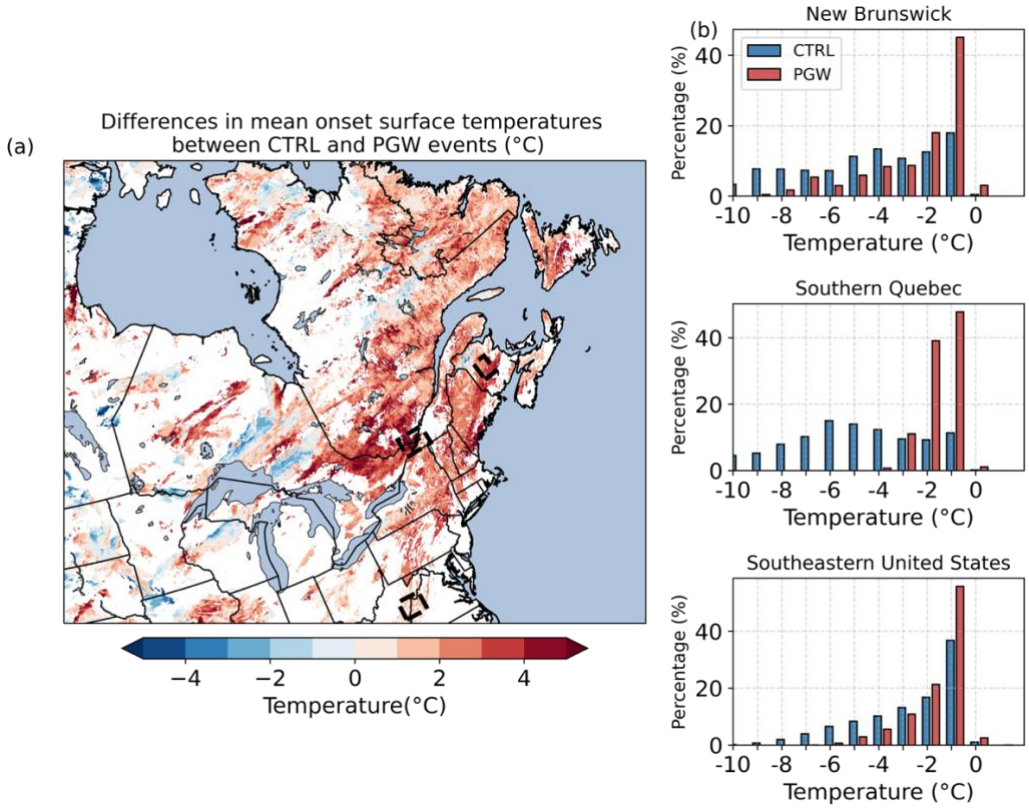

Figure 4.7: (a) Mean 2-m air temperature difference (PGW − CTRL) at the onset of LD freezing rain events. (b) Distribution of 2-m air temperature at the onset of LD freezing rain events under PGW and CTRL climates for each region.

Dew point depression plays a role in the thermodynamic conditions that support the formation of freezing rain (McCray et al., 2019). When dew point depression is large, there is more evaporative cooling (Lackmann et al., 2002). Figure 4.8 presents the distribution of onset dew point depression temperatures at the surface across regions and between CTRL and PGW scenarios. In southern Quebec, the proportion of temperatures in the 0 to 2°C range decreases from 72.4% in CTRL to 45.7% in PGW, indicating a broader spread of temperature distributions under PGW. In the southeastern U.S., the proportion within this range increases from 79.4% to 91.7%, showing that the temperature range in PGW remains narrow. In New Brunswick, onset dew point depression temperatures are concentrated between 0 and 2°C in both CTRL and PGW simulations. The median temperature difference between CTRL and PGW events varies by region. In southern Quebec, the median increases by about 1.3°C, while in the southeastern U.S. and New Brunswick, the median decreases by approximately -0.5°C and -0.3°C, respectively. Therefore, under PGW conditions,

freezing rain events in southern Quebec occur in relatively dry air, which promotes stronger evaporative cooling from precipitation.

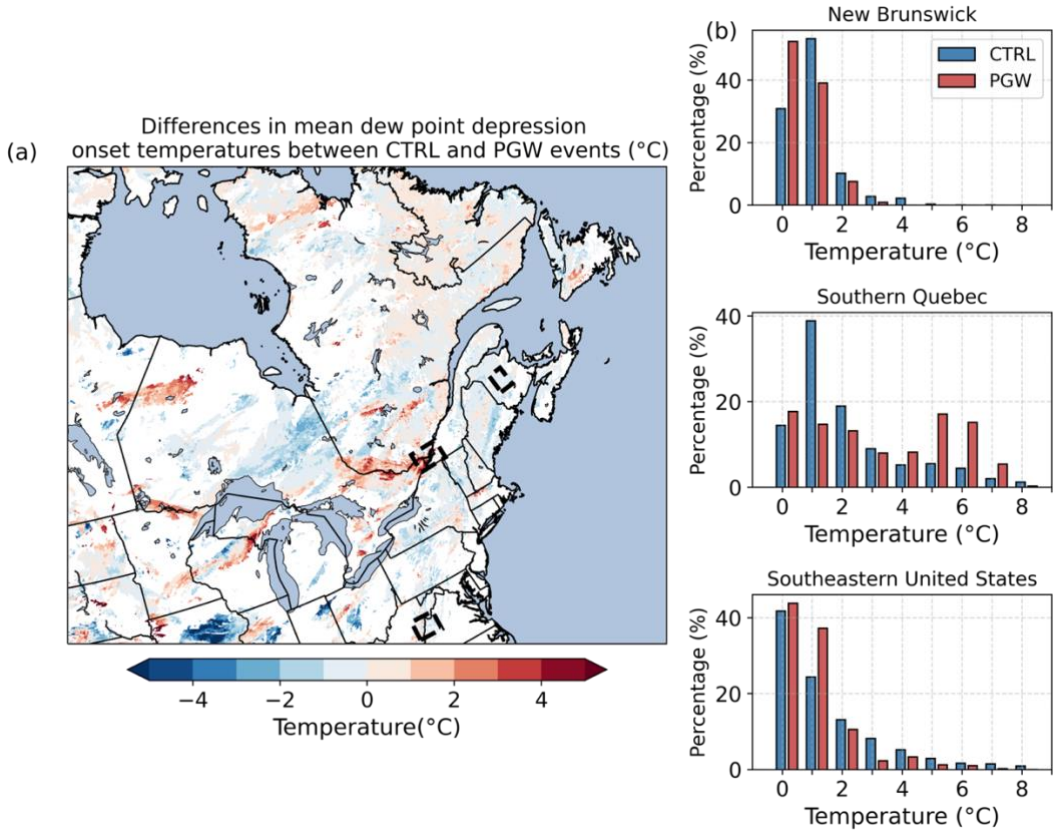

Figure 4.8: (a) Mean dew point depression temperature difference (PGW − CTRL) at the onset of LD freezing rain events. (b) Distribution of dew point depression temperatures associated with the onset of LD freezing rain events under PGW and CTRL climates for southern Quebec, southeastern U.S., and New Brunswick.

4.3.3.3 Upper air profiles

We examined key thermodynamic characteristics of the vertical temperature structure at the onset of freezing rain events (Figure 4.9). These include the depth of the melting layer, the depth of the subfreezing layer, the maximum temperature within the melting layer, and the minimum temperature within the subfreezing layer. Our analysis focuses on the median values of these variables across different regions for both the CTRL and PGW simulations.

In the CTRL, the subfreezing layer is shallowest in southern Quebec, with a median depth of 784 m, and deepest in New Brunswick, reaching 975 m. The southeastern United States exhibits a depth of 928 m. Under PGW conditions, the subfreezing layer deepens notably in New Brunswick to

1379 m and slightly increases in southern Quebec to 804 m, whereas it shallows considerably in the southeastern U.S. to 695 m. The minimum temperatures within the subfreezing layer follow a similar regional pattern. New Brunswick experiences the coldest minima in both scenarios, with -4.5°C in CTRL and -4.0°C in PGW. Southern Quebec has slightly warmer minima, at -3.8°C in CTRL and -3.2°C in PGW, while the southeastern U.S. records the warmest minima, with -3.2°C in CTRL and -2.3°C in PGW.

The melting layer exhibits a contrasting pattern. In CTRL, southern Quebec has the deepest melting layer at 1487 m, followed by the southeastern U.S. at 1155 m, and New Brunswick at 1090 m. Under PGW conditions, the melting layer becomes shallower in all regions, most dramatically in southern Quebec (969 m) and New Brunswick (885 m), while the southeastern U.S. reaches 945 m. Maximum temperatures within the melting layer also decrease under PGW. Southern Quebec maintains the highest maximums, at 2.9°C in CTRL and 1.5°C in PGW. The southeastern U.S. and New Brunswick exhibit lower maxima, with 2.1°C and 2.0°C in CTRL, decreasing to 1.7°C and 1.0°C in PGW, respectively.

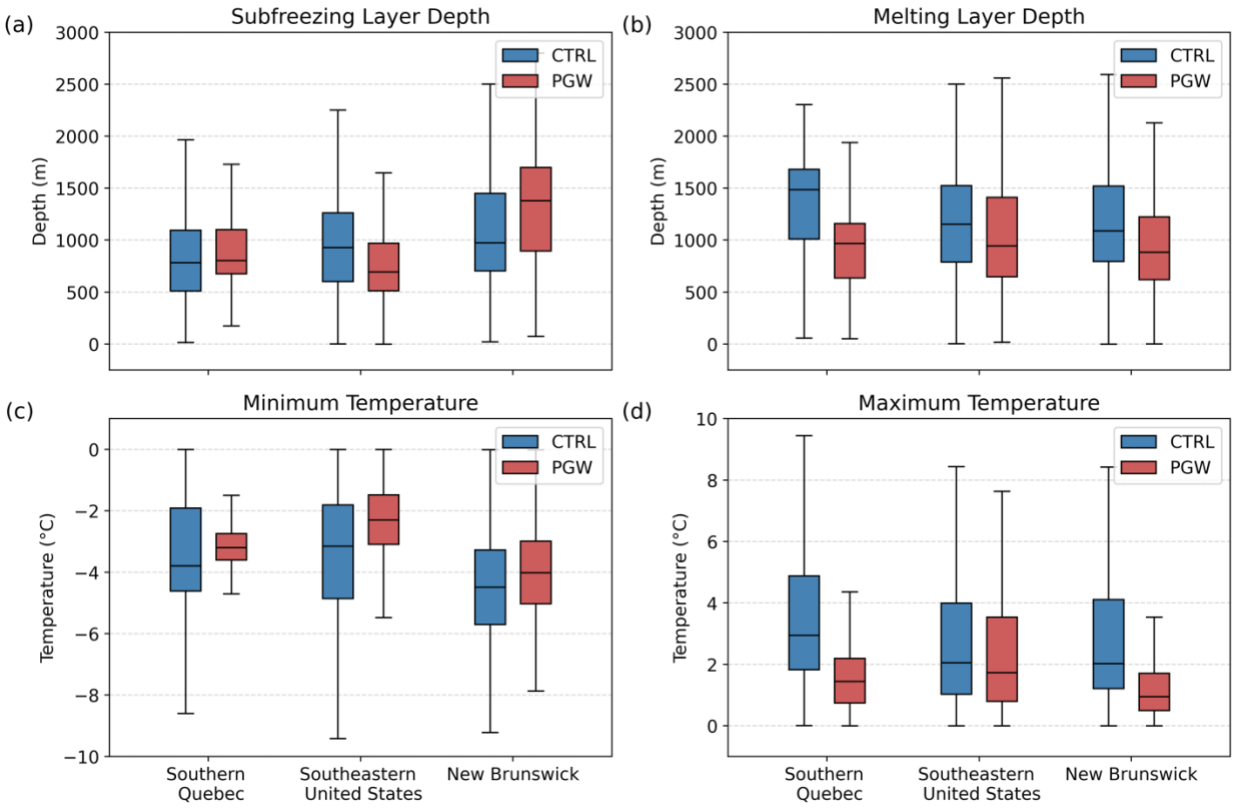

Figure 4.9: Boxplots of (a) subfreezing layer depth, (b) melting layer depth, (c) minimum temperature, and (d) maximum temperature for each region at LD event onset for CTRL (red) and PGW (blue) runs.

4.3.3.4 Latent heat from freezing rain

We investigated the contribution of the latent heat of freezing during freezing rain events. This is linked to the intensity of the precipitation.

First, the distribution of precipitation rates is shown Figure 4.10a. Under CTRL, most freezing rain events in southern Quebec are associated with precipitation rates in the 0.5–1.5 mm h^{-1} range, with 38.6% in 0.5–1.0 mm h^{-1} and 29.2% in 1.0–1.5 mm h^{-1}. In the PGW scenario, this shifts markedly, with 45.4% of events falling in the 1.0–1.5 mm h^{-1} range, suggesting more intense precipitation. In the southeastern U.S., the distribution of freezing precipitation rates remains relatively stable between CTRL and PGW. In New Brunswick, there is a modest increase in the frequency of higher ranges (e.g., from 2.6% in 2.5–3.0 mm h^{-1} in CTRL to 6.5% in PGW). Median freezing rain rates vary regionally between CTRL and PGW. In southern Quebec, the median rate increases from 1.1 mm h^{-1} in CTRL to 1.2 mm h^{-1} in PGW, while in New Brunswick it rises from 1.2 mm h^{-1} to

1.5 mm h^{-1}. In contrast, the southeastern U.S. shows a slight decrease from 1.2 mm h^{-1} in CTRL to 1.1 mm h^{-1} in PGW.

Second, the estimated latent heating rate at the surface calculated using Equation 4.1 is shown in Figure 4.10b, replacing the precipitation amount with precipitation rate. Most latent heat rates are concentrated in the 0.0–0.3°C h^{-1} range across all regions and both scenarios. Under PGW in New Brunswick, the frequency of events in the lowest range decreases, from 63.2% to 51.1%, while the frequency in the higher ranges 0.6–0.9°C h^{-1} and 0.9–1.2°C h^{-1} increases. In contrast, southern Quebec shows little change, whereas in the southeastern U.S. the 0.0–0.3°C h^{-1} range increases (64.9% to 71.4%) accompanied by decreases in the higher ranges. The latent heat shift in New Brunswick follows the changes in freezing rain rates, while southern Quebec and the southeastern U.S. show minimal changes in both, because freezing rain rate there remains concentrated in low-rate bins.

Third, the impact of latent heat in each region is shown in Figure 4.10c, following the methodology detailed in Section 4.2. For each region, we categorize freezing rain events based on whether latent heat release could eliminate the subfreezing layer, with three categories: transitions ('T'), failed ('F'), and equilibrium ('E'). Under CTRL conditions, southern Quebec has the highest proportion of freezing rain events where latent heat is insufficient to erode the subfreezing layer, classified as failed events ('F'), at 43%. Transition events ('T'), where latent heat would be sufficient to fully eliminate the temperature deficit, account for 28% of events, while 29% of events conclude with temperatures already at or above 0°C ('E'), typically due to surface warming from other processes such as warm-air advection or mixing during the event. Under PGW conditions, southern Quebec shows a major shift: transition events nearly double to 57%, failed events drop to just 10%, and equilibrium events increase marginally to 33%. This pattern suggests that under future warming, latent heat has a substantially greater capacity to erode the subfreezing layer and potentially terminate freezing rain earlier. In New Brunswick, T events remain nearly constant between CTRL and PGW, but F events decrease from 27% to 18%. In contrast, in the southeastern U.S., failed events increase marginally from 16% to 19%, equilibrium events decrease from 32% to 29%, and transition events stay at approximately 52%.

To quantify how often latent heat has the potential to influence the duration of a freezing rain event, we define a simple metric: latent heat influence fraction = 1 – F, which is equivalent to E + T. This metric represents the proportion of events where latent heat could either erode the cold layer or contribute to early termination of the event. Under this metric, southern Quebec shows the largest increase under PGW, indicating that the role of latent heat in altering freezing rain outcomes strengthens most in this region, compared to more modest changes in New Brunswick and the southeastern U.S.

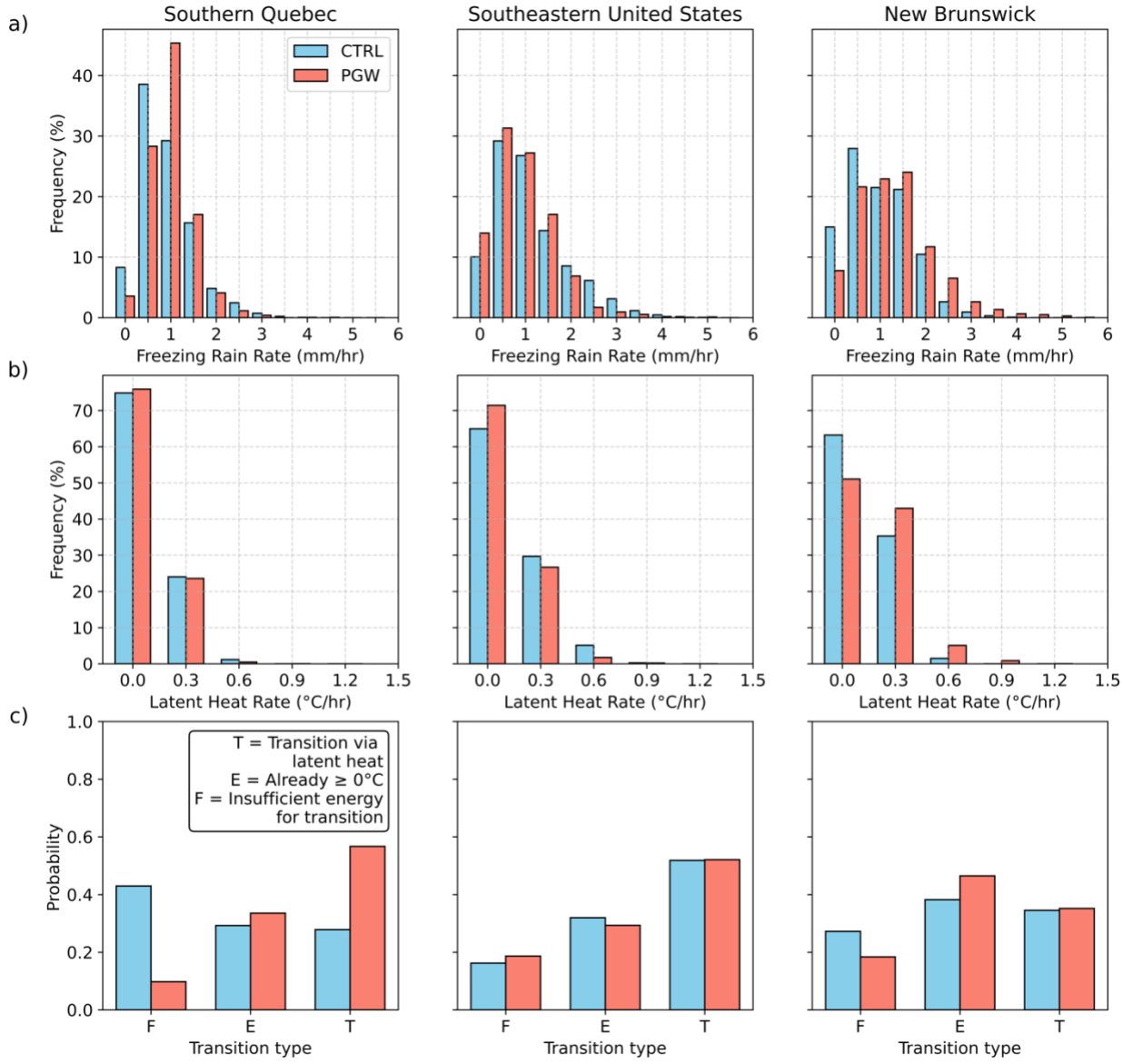

Figure 4.10: Relative frequencies of (a) freezing rain rates (mm h^{-1}) and (b) latent heat-induced warming rates (°C h^{-1}), where each bin value represents the range from its lower edge up to the next bin (e.g., 0 = 0–0.5 mm h^{-1} for freezing rain, 0 = 0–0.3°C h^{-1} for latent heat). Panel (c) shows the probability of events categorized by the impact of latent heat (F, E, or T) for CTRL (blue) and PGW (red) simulations in each study region discussed in the text.

The relative changes in T, F, and E events across regions are closely linked to the depth of the subfreezing layer impacted by latent heating (M in Equation 4.1). To assess the sensitivity of our results to assumptions about this depth, we compared outcomes using a fixed depth of 1000 m and region-specific median depths, as calculated in Section 4.3.3.3. These medians represent the typical depth of the subfreezing layer during freezing rain events in each region and determine the mass of air impacted by latent heat release. In the CTRL scenario, the fixed depth was replaced with median values of 784.1 m for southern Quebec, 928.0 m for the southeastern U.S., and 974.8 m for New Brunswick. Under PGW conditions, these values changed to 803.6 m, 694.9 m, and 1378.7 m, respectively. As shown in Figure 4.11, using region-specific median depths generally increased the proportion of freezing rain events classified as T. However, the impact is minimal, with the most noticeable change in southern Quebec, with a ~3.8% increase in T. E in which temperatures are already at or above freezing without latent heating, remained largely unchanged by choice of depth. Under PGW, using region-specific median depths increases the proportion of T events by ~ 4–5% in southern Quebec and the southeastern U.S., but decreases it by ~5 % in New Brunswick due to the much deeper subfreezing layer in this region.

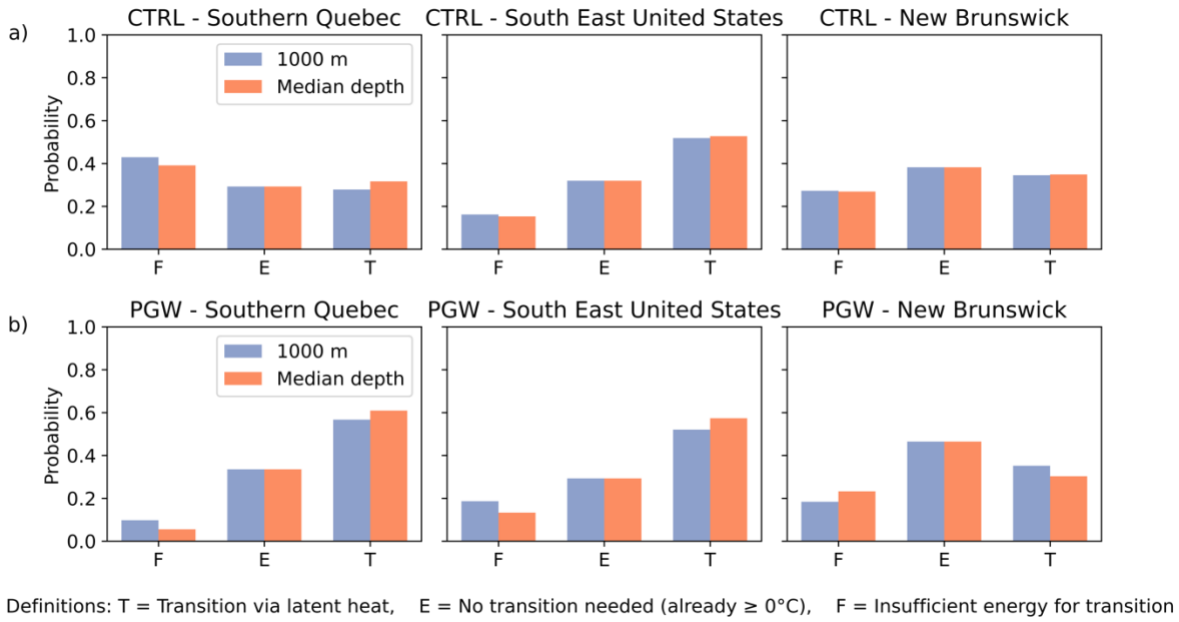

Figure 4.11: Probability of events categorized by the impact of latent heating (F, E, or T) using a subfreezing layer depth of either 1000 m (blue) or the median depth for the region (orange) in (a) the CTRL scenario, or (b) the PGW scenario.

4.4 Discussion

The study compares the atmospheric processes that support the thermodynamic structures associated with freezing rain across the three regions. Many studies have examined the characteristics of upper-air profiles during freezing rain events (Zerr, 1997; Robbins and Cortinas, 2002; McCray et al., 2019). We demonstrated that latent heat plays an important role in the freezing of supercooled drops at the surface, affecting near-surface air temperature climatologically and suppressing freezing rain.

Zerr (1997) found that the surface precipitation type is more strongly influenced by the melting layer characteristics than by the subfreezing layer. Similar findings were reported by Stewart and King (1987) and Czys et al. (1996). In our study, the median depth of melting layer aloft at freezing rain event onset in southern Quebec was ~1.5 km. This is comparable to the depth that was simulated for the 1998 ice storm over southern Quebec (Cholette et al., 2020). Zerr (1997) has stated that depths greater than 1.5 km are not common during freezing rain events. In comparison, the median depth in New Brunswick was around 1 km, which is shallower than the simulated 1.5 km depth reported by Thériault et al. (2022) for the January 2017 ice storm over New Brunswick. Marinier et al. (2022) reported both observed and simulated melting layer depths of 1 km for the February 2008 freezing rain event in New Brunswick.

The mean onset 2-m air temperature during freezing rain events was colder in the CTRL, while in the PGW it was warmer and closer to 0°C. A colder onset temperature can help sustain freezing rain for a longer time before it transitions to rain, as shown in Basnet et al. (2025). This is likely one reason for the decline in the percentage of LD events in the PGW climate. This trend is especially evident in southern Quebec, where most onset temperatures are close to 0°C in the PGW simulation and transitions due to latent heat release are more frequent compared to other regions. Although the near-surface air is typically saturated during freezing rain events, evaporative cooling from falling precipitation can still contribute to maintaining the subfreezing layer and extending the duration of freezing rain. As raindrops fall into a subsaturated cold layer, partial evaporation cools the air, offsetting some of the warming associated with latent heat release when the drops freeze upon contact with the surface. Previous studies (Bell and Bosart, 1988; McCray et al., 2019) have identified this process as a key mechanism in the southeastern United States. In our study,

larger dew point depressions at onset were observed in southern Quebec, particularly under PGW conditions, where evaporative cooling played a more important role, while its influence was minimal in New Brunswick.

The impact of latent heat release at the surface on the number of freezing rain events is noticeable across all regions and cannot be ignored in either the CTRL or PGW simulations. Another process to consider is cold-layer advection which helps maintain subfreezing temperatures. Depending on the balance between warming from latent heat and cooling from cold layer advection, the subfreezing layer near the surface may either persist or be eroded. A surface cold-air advection rate of 0.41°C over a 3-hour period was observed during freezing rain events in the southeastern U.S. (McCray et al., 2019). Although this rate is lower than the corresponding latent heat warming from freezing rain in our simulation (Figure 4.10b), it still represents a meaningful cooling contribution. Basnet et al. (2025) noted that the warming from latent heat accompanying freezing rain in Montreal during the ice storm of April 2023 was offset by the cold air advection. Previous research (Carrera et al. 2009; Ressler et al. 2012) has shown that cold air advection played a major role in maintaining freezing rain events in southern Quebec.

4.5 Conclusion

An investigation of LD freezing rain events across southeastern U.S., southern Quebec and New Brunswick was carried out for a 11-year period (2012–2022) by using CRCM6-GEM5 model output in the current (CTRL) climate and in a pseudo-global warming (PGW) future. The analysis yielded several key insights.

- In all regions, the percentage of events that are of long duration decreases in PGW in comparison to CTRL.
- Under PGW, LD freezing rain events are more likely to be associated with snow during and after the event in New Brunswick, compared to CTRL. Snowfall preceding freezing rain events declines in southern Quebec under PGW.
- Onset temperatures of LD freezing rain events are warmer in the PGW simulation than in the CTRL across all regions, with the largest increase in southern Quebec. In this region, onset dew point depression is also higher, while it is less pronounced in New Brunswick and the southeastern United States.

- Under PGW conditions, the melting layer depth decreases across all regions, accompanied by a corresponding decrease in maximum temperature.
- In the warmer PGW climate, freezing rain exhibits higher precipitation rates in northern regions, while these rates decrease slightly in the southeastern U.S.
- Latent heat from freezing rain plays a key role in the suppression of freezing rain in the current climate. This impact continues to be important in the warmer climate, especially in southern Quebec.

A limitation of this study is that we did not assess the role of horizontal advection during each event, leaving its contribution to the thermodynamic evolution unquantified. Advection can modify temperature profiles and potentially influence both the onset and persistence of freezing rain. Additionally, we did not explicitly quantify the cooling associated with evaporation or compare it with the warming produced by the freezing of supercooled liquid, which could alter the balance of thermodynamic processes during these events. However, it is important to note that both advection and evaporative cooling are already represented in the model, meaning their effects are implicitly accounted for, even if not individually analyzed.

The focus of this study was on long-duration freezing rain events, which pose the greatest hazards due to their widespread impacts on infrastructure, transportation, and public safety. Since the severity of freezing rain depends largely on how long it lasts and how much ice accumulates, understanding the factors that control event duration is crucial. By analyzing the thermodynamic conditions governing the evolution of freezing rain under both current and future warmer climates, this study provides a basis for improving the prediction of such events. These insights into the associated thermodynamic patterns may ultimately assist forecasters in identifying and anticipating prolonged freezing rain episodes more effectively.

5 Discussion and Conclusion

5.1 Summary and main conclusion

The main objective of this thesis was to improve our understanding of episodes of near-0°C conditions and the processes leading to and maintaining near-0°C, including precipitation over eastern Canada. This work was carried out in three chapters, each with distinct sub-objectives. The objective of the second chapter was to characterize near-0°C temperature pathways across Eastern Canada and the United States under both current and warmer climate scenarios, using high-resolution regional climate simulations. The objective of the third chapter was to quantify the impact of latent heat release from freezing rain on near-surface air temperature and precipitation phase transitions by explicitly implementing this process in the models. Finally, the objective of the fourth chapter is to examine the climatological thermodynamic conditions of long-duration freezing rain events, with particular focus on the role of surface latent heat in modulating event persistence and transitions. Together, these studies provided a comprehensive understanding of the processes that generate and sustain near-0°C conditions, highlighting the influence of latent heat and thermodynamic interactions on freezing rain formation, duration, and phase transitions. The findings also offer insight into how near-0°C events may evolve under future warmer climates, improving our ability to model, forecast, and manage the impacts of hazardous winter weather.

In Chapter 2, high-resolution (2.5-km) regional climate simulations using the Canadian Regional Climate Model version six based on the Global Environmental Multiscale (GEM) model, version 5.1.1 (CRCM6-GEM5) were employed to examine near-0°C temperature pathways over an 11-year period. Two 11-year simulations were conducted, representing the current climate and a warmer future warmer climate under pseudo-global warming conditions. Validation against meteorological station data demonstrates the model's skill in capturing near-0°C conditions across Eastern Canada and the United States. The results show a northward shift of the 0°C annual temperature isotherm in the warmer climate, with the highest number of near-0°C hours occurring in Newfoundland and Nova Scotia under CTRL, and in northern Quebec under PGW, and a general increase in near-0°C hours in northern regions and a decrease in southern regions. Pathways P3 (cooling followed by warming) and P4 (warming followed by cooling) dominate, with P3 prevalent

in the south and P4 in the north, and the dividing boundary between them shifting northward under PGW. Onset of near-0°C events occur later in fall, while their cessation occurs earlier in spring, particularly in northern Quebec, with many spring pathways in CTRL now occurring in winter under PGW, except for P4, which remains winter-dominated. Precipitation events near 0°C last longer than non-precipitation events, with rain, snow, and freezing rain preferentially associated with P3, P4, and P2 pathways, respectively. P1 and P2 events are influenced by diurnal heating, while P4 events are primarily linked to snow-covered surfaces. Near-0°C temperature peaks persist in a warmer climate, with increases in primary and no peaks, and many secondary peaks in Canada transitioning to primary peaks, whereas those in the United States transition to no peaks.

Chapter 3 investigated the role of latent heat released during the freezing of supercooled drops at the surface during the extreme April 5–6, 2023 ice storm in southeastern Canada. The storm produced 35.1 mm of freezing rain in downtown Montreal, while approximately 26 mm of ice pellets were recorded 60 km north of the city, leading to major disruptions in transportation and infrastructure. The warming effect from latent heat released during the freezing of supercooled liquid is often neglected in atmospheric models. This study is the first to explicitly incorporate this process, aiming to quantify how the freezing of supercooled drops at the surface influences near-surface air temperature and the transition between precipitation types. High-resolution (1-km) GEM simulations were conducted, with modifications to lower atmospheric levels and the CLASS land surface scheme to represent latent heat release at the surface, and multiple experiments (EXP) explored different heat partitioning between the ground and the lower atmosphere. The results demonstrated that latent heat from freezing supercooled drops raised 2-m air temperatures above 0°C, eliminating freezing rain in regions where transitions were possible. In the EXP simulations, this led to an overall decrease in freezing rain and an increase in rain. The spatial pattern of precipitation transitions varied across southern Quebec and southern Ontario, with the largest conversion observed in southern Ontario, which also experienced the most intense freezing rain in the CTRL simulation. The analyses further revealed that thermal advection, combined with the onset 2-m temperature and the freezing precipitation rate, was critical in determining whether the near-surface temperature reached 0°C and whether freezing rain transitioned to rain. Although the temperature changes due to latent heat were relatively modest, they were sufficient to significantly alter precipitation type, reduce the duration of freezing rain, and modify local surface energy

balances. This highlights the importance of including latent heat effects in high-resolution models, as they not only influence near-surface atmospheric stability but also the precipitation type and amount. Overall, this study demonstrates that even small energy contributions from latent heat during phase change can have substantial impacts on precipitation evolution, surface conditions, and hazard outcomes during high-impact ice storms.

In Chapter 4 the objective was to conduct a climatological examination of the thermodynamic conditions associated with extreme freezing rain events in both the current and future warmer climate, with a particular emphasis on the warming influence of latent heat released during freezing rain at the surface. Long-duration freezing rain events (≥6 hours) were analyzed across southeastern U.S., southern Quebec, and New Brunswick using high-resolution (2.5-km) simulations from the CRCM6-GEM5 for both current (CTRL) and pseudo-global warming (PGW) climates. The analyses revealed that the frequency of long-duration freezing rain events generally decreased under PGW, accompanied by a marked shift toward rain during and following events, particularly in southern Quebec and New Brunswick. Warmer onset temperatures in PGW contributed to this shift, while dew point depression emerged as a more significant factor in sustaining freezing rain in southern Quebec due to enhanced evaporative cooling in drier sub-freezing layers. The simulations also indicated a reduction in the depth of the melting layer and lower maximum temperatures aloft under PGW, reflecting a cooler warm layer that affects precipitation phase transitions. Latent heat release continued to play a suppressive role on freezing rain formation in both CTRL and PGW simulations; however, its influence was modulated by cold-air advection and the onset temperature, demonstrating that multiple thermodynamic processes interact to control freezing rain persistence. Latent heat acted as a limiting factor, suppressing freezing rain in 84% of events in the southeastern U.S. under the current climate and in 90% of events in southern Quebec in a future warming scenario, underscoring its consistent role in shaping event duration across regions. These results suggest that future warming will alter the structure and occurrence of long-duration freezing rain events by reducing their frequency, modifying the vertical thermal profile, and shifting the balance between freezing rain and rain. The findings underscore the importance of accurately representing latent heat, moisture processes, and warm-layer dynamics in high-resolution regional climate models to improve our understanding of hazardous ice storm events.

Temperatures near 0°C hold critical importance from both scientific and societal perspectives. Scientifically, they represent a threshold where precipitation phase changes occur, giving rise to complex thermodynamic interactions that govern the onset, evolution, and persistence of near-0°C events. This thesis has shown how temperatures transition into and out of near-0°C conditions, how latent heat release can fundamentally alter precipitation types during storms, and how specific thermodynamic environments determine the duration of freezing rain. Societally, these processes translate into risks for transportation, infrastructure, and public safety, particularly in regions regularly exposed to hazardous winter weather. By connecting these physical mechanisms with their broader consequences under both present and warmer climates, this thesis provides a more complete framework for understanding and anticipating near-0°C events in the face of a changing climate.

5.2 Limitation of the work

The results obtained in this thesis have limitations, which are discussed below. These limitations are linked to the three chapters of the thesis, along with potential ways to address them.

Chapter 2 assessed temperature pathways in the current and future warmer climate. Marquis et al. (2022) showed that internal climate variability can shift the timing of the last spring frost by up to 46 days in southern Quebec. Future studies could use large ensembles of high-resolution regional climate models to better quantify the probability and dynamics of temperature pathways. The study also looked the near 0°C temperature peaks in both the climates. A limitation of using kernel density estimation (KDE) to identify temperature peaks near 0°C lies in the sensitivity of the method to bandwidth selection. The choice of bandwidth directly affects the smoothness of the estimated distribution, where a small bandwidth may create spurious peaks due to noise in the data, while a large bandwidth may over smooth the distribution and obscure meaningful features around 0°C. As a result, the exact location and prominence of peaks near 0°C may be influenced as much by methodological choices as by the underlying data. To assess robustness, one option is to compare KDE results with varying bin size and examining differences in the peaks. In addition, more rigorous approaches such as cross-validation methods for bandwidth selection could be applied, even though they may be computationally expensive for large datasets.

In chapter 3 we implemented a latent heat process associated with the freezing of supercooled drops at the surface in the model. A limitation of this study is the presence of internal variability in regional climate model (RCM) simulations. Internal variability arises from the chaotic nature of the climate system and can contribute to differences between control and perturbed simulations that are not directly related to the imposed perturbation like the latent heat release from freezing rain. As a result, part of the signal attributed to the perturbation may in fact reflect this inherent variability like the upper air temperature in the perturbed simulation. A more robust approach would involve conducting ensembles of simulations with different initial conditions for both control and perturbed cases, allowing the isolation of the true physical effect from model variability. Another limitation of this study is that the partitioning of latent heat from freezing rain between the atmosphere and the soil has not been quantified. A small fraction of the latent heat may be transferred to warming the soil, but a quantitative estimate requires a robust approach that accounts for soil type, temperature, and moisture content. Soil temperature well below freezing can offset the latent warming. Such information is necessary to determine how much latent heat is absorbed by the soil versus how much remains in the atmosphere, which could influence the evolution during freezing rain events.

The fourth chapter examined the thermodynamics of the long duration freezing rain events in the current and future warmer climate. A limitation of this study is that we did not assess the role of horizontal advection during each event, leaving its contribution to the thermodynamic evolution unquantified. Advection can modify temperature profiles and potentially influence both the onset and persistence of freezing rain. Additionally, we did not explicitly quantify the cooling associated with evaporation or compare it with the warming produced by the freezing of supercooled liquid, which could alter the balance of thermodynamic processes during these events. However, it is important to note that both advection and evaporative cooling are already represented in the model, meaning their effects are implicitly accounted for, even if not individually analyzed. Our analysis focused primarily on the characteristics at the onset of each event to infer the role of latent heat release, rather than examining its continuous effect throughout the entire duration. As a result, the temporal evolution of latent heat and other key processes during freezing rain events remains incompletely characterized, leaving aspects of their dynamics and climatology unresolved.

Chapters 2 and 4 use the PGW method, which has limitations. Because PGW adds a climate-change delta to boundary conditions from a historical control simulation, it preserves the historical synoptic-scale weather patterns and cannot capture changes in storm tracks or synoptic variability that may occur in a warmer climate (Brogli et al., 2023). The PGW delta typically has no interannual variability, so the same climate change signal is applied to every simulated year, preventing PGW from representing changes in year-to-year fluctuations or shifts in the frequency and timing of extreme events. Studies have conflicting reports on the future changes in atmospheric circulation (Shepherd, 2014). These limitations mean PGW should not replace multi-model ensembles, which capture uncertainty from different GCMs and provide the full range of possible futures needed for robust probabilistic projections. Instead, PGW is best used as a complement for storyline assessments (Hazeleger et al., 2015; Shepherd, 2019) or high-resolution simulations where computational cost makes large ensembles prohibitive (e.g., Pichelli et al., 2021).

It is important to recognize the uncertainty associated with future climate scenarios, which arise from three main sources: internal variability, model response, and forcing (Hawkins and Sutton 2009; Tebaldi and Knutti 2007). Internal variability includes processes intrinsic to the atmosphere, ocean, and the coupled atmosphere-ocean system, which produce natural fluctuations independent of any external forcing. Model uncertainty arises because models differ in their physical parameterizations, grid resolution, and how they handle processes such as clouds or soil-vegetation interactions. Finally, forcing uncertainty stems from incomplete knowledge of external factors that drive the climate system, including land use change, ozone concentration, and greenhouse gas emissions.

5.3 Future work

The findings and methods developed in this chapter 2 offer several promising directions for future research and practical applications. One important direction would be to investigate the implications of near-0°C pathways on urban snow management practices, particularly in densely populated cities where winter maintenance has both economic and safety implications. Optimizing salt usage to match shorter and more variable freezing events could reduce environmental impacts

and improve operational efficiency. Modelling future snowmelt scenarios would help improve our understanding on risk of runoff, ice formation, and infrastructure stress.

Building on the findings of this thesis, further research could explore the broader environmental and societal impacts of near-0°C conditions, particularly in relation to agriculture and flooding. Near-0°C temperatures play a critical role in determining the timing of freeze–thaw cycles, which directly affect soil structure, planting schedules, crop viability, and pest dynamics. Shifts in the onset and cessation of near-0°C events, as observed in the PGW simulations, may lead to earlier thaws and delayed freezes, potentially disrupting traditional growing seasons and increasing vulnerability to frost damage. Future studies could integrate climate projections with agricultural models to assess potential impacts on food security and to identify effective adaptation measures for farmers.

Aditionally, there is scope for interdisciplinary research that links climate simulations with socioeconomic studies. For instance, investigating how near-0°C conditions influence energy consumption, transportation safety, and public health could provide a more holistic understanding of the societal consequences of climate change. Such work would support the development of targeted adaptation and mitigation strategies, ensuring that both infrastructure and communities remain resilient under future climate scenarios.

The methodology developed in Chapter 3 to assess the impact of latent heat release during freezing rain events offers a valuable foundation for future research. By accounting for latent heat effects, this approach can be applied to additional freezing rain case studies to test its robustness and transferability across different meteorological conditions and geographical regions. Expanding the application of this methodology would allow researchers to evaluate how latent heat influences surface temperature, precipitation phase transitions, and the persistence of near-0°C environments under diverse climate scenarios.

Future studies could also adapt this methodology to explore how different types of land cover and urban infrastructure respond to latent heat release. This is particularly important in urbanized regions where dense electrical grids, transportation systems, and critical services are highly

vulnerable to ice accretion. Incorporating land-surface and urban canopy considerations into the methodology could help quantify how factors such as urban heat islands, road materials, and building density modulate the impact of latent heat on freezing rain duration and severity. Such advances would improve our understanding of how freezing rain affects cities and could inform more effective adaptation strategies.

Beyond individual case studies, applying this methodology in a climatological context is an essential next step. Conducting a climatology of freezing rain events that incorporates latent heat effects would help determine the broader importance of this process across regions. As Stewart et al. (2023) demonstrated, near-0°C temperatures are expected to remain common even under warmer climate scenarios, suggesting that the role of latent heat in prolonging freezing rain may persist into the future. By comparing climatological studies with and without the latent heat methodology, researchers could quantify its influence on freezing rain duration and frequency in both present and projected climates.

Chapter 4 focused on long duration freezing rain events, which represent the most hazardous cases due to their widespread impacts on infrastructure, transportation, and public safety. The analysis of thermodynamic conditions associated with these events provides an important foundation, but future research could expand on several key aspects to deepen understanding and improve prediction capabilities.

Parameters such as warm-layer depth, cold-layer temperature, and dew point depression are important for assessing the potential longevity of an event. Future research should also consider the integration of observational data with high-resolution model simulations. While modelling provides detailed insight into atmospheric structure, it is computationally expensive, and observed datasets remain limited, particularly for precipitation rates and upper-air soundings, which are typically available only every 6 hours and are sometimes located far from freezing rain sites. A hybrid approach combining the strengths of both observations and simulations could offer a more complete picture of event evolution and duration, improving confidence in results. Applying statistical analyses and machine learning techniques to this hybrid framework could then help uncover patterns and thresholds in onset conditions that serve as predictors of long-duration events,

ultimately supporting the development of predictive tools that enhance forecasting and enable more proactive risk management.

Another direction is the examination of synoptic-scale conditions associated with long-duration freezing rain. Large-scale atmospheric patterns, including troughs, ridges, cyclones, and anticyclones, likely play a central role in sustaining prolonged near-0°C conditions. Studying these features alongside thermodynamic conditions would provide a more complete view of the mechanisms that sustain extreme events and could help determine whether certain synoptic environments consistently favor long-duration freezing rain.

While this chapter focused only on extreme long-duration events, future work should also investigate shorter-duration freezing rain events to place these cases in a broader context. Comparing short and long-duration events would not only help clarify their similarities and differences, but particularly reveal how the release of latent heat from the freezing of supercooled liquid can act to suppress freezing rain, with its influence likely varying by event duration. Such analyses would provide a more complete picture of freezing rain climatology, especially considering that our results indicate an increase in the number of short-duration events under future warmer climate scenarios. These insights are crucial for quantifying future risks, as even modest shifts in event duration could have significant societal consequences.

5.4 Implication of the findings

The results from these chapters provide a comprehensive understanding of near-0°C temperature pathways and the dynamics of freezing rain across Eastern North America. By integrating high-resolution modelling with extensive observational datasets, this research establishes a robust framework for examining the processes that lead to and sustain near-0°C conditions, as well as the subsequent impacts on precipitation type and intensity. The insights gained are particularly relevant for improving the accuracy of precipitation phase forecasts, which is critical for anticipating and mitigating the hazards associated with freezing rain and mixed-phase precipitation events. The research further highlights potential shifts in the timing of seasonal hydrological events, with implications for flood management, water resource planning, and agricultural operations such as crop selection, planting schedules, and soil management practices.

The pseudo-global warming (PGW) approach employed in the study gives us a storyline perspective, providing a physically consistent depiction of how a past high-impact event might unfold under a warmer future climate rather than estimating the probability of such events occurring. While this makes PGW less suited for direct probabilistic risk assessments, the findings nonetheless advance our understanding of near-0°C pathways and long duration freezing rain events. It is important to recognize, however, that these results are subject to the assumptions inherent to the PGW framework, including its limited representation of changes in storm frequency and dynamics, as well as uncertainties in observational datasets used for model validation.

APPENDIX A

With $0.7L_f \rho_l R_m$ energy available for the atmosphere, this energy will be evenly distributed among the 10 lowest model levels in the subfreezing layer during the freezing rain event, resulting in $(0.7L_f \rho_l R_m)/10$ energy allocated to each level. Each model level will receive this amount of energy, contributing to a temperature increase for each level. The approximate height of the 10 lowest model levels, from the surface are: 30, 47, 61, 76, 91, 105, 117, 129,142, 157 m.

For model level *i*, with the mass of the air in the model level M_i, the temperature increase would be:

$$\Delta T_i = \frac{0.7 L_f \rho_l R_m}{10 M_i C_p} \tag{A.1}$$

This temperature increase from latent heat is then added to the initial temperature of each respective model level, updating the temperature profile across each sub-freezing layer.

$$T_i = T_i + \frac{0.7 L_f \rho_l R_m}{n M_i C_p} \tag{A.2}$$

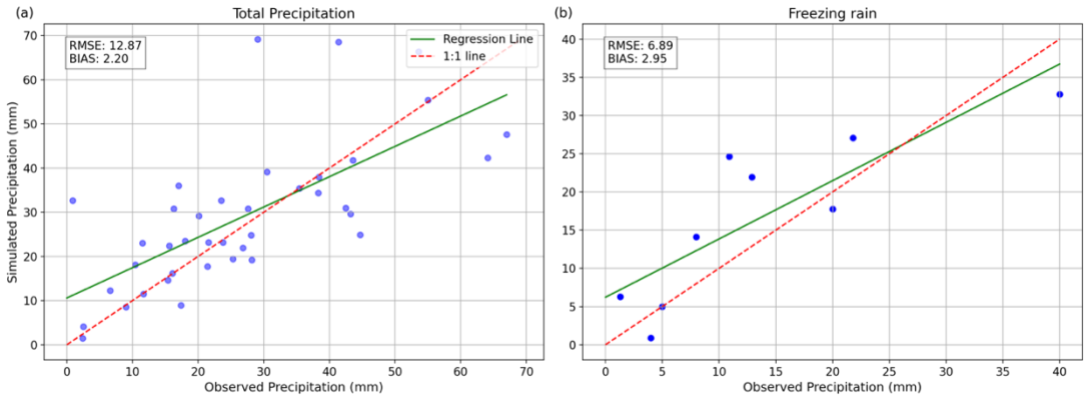

Figure A1. Comparison of simulated (EXP) and observed precipitation over the period 0000 UTC 04 April 2023–0000 UTC 07 April 2023 for (a) total precipitation and (b) total freezing rain.

APPENDIX B

This section provides additional information on the data used for chapter 2 and chapter 4.

Root Mean Square Error (RMSE) = $\sqrt{\frac{1}{n}\sum_{i=1}^{n}(S_i - O_i)^2}$

Mean Bias (BIAS) = $\frac{1}{n}\sum_{i=1}^{n}(S_i - O_i)$

Pearson Correlation Coefficient (R) = $\frac{\sum_{i=1}^{n}(O_i - \bar{O})(S_i - \bar{S})}{\sqrt{\sum_{i=1}^{n}(O_i - \bar{O})^2 \cdot \sum_{i=1}^{n}(S_i - \bar{S})^2}}$

Percent Bias (PBIAS) = $100 \times \frac{\sum_{i=1}^{n}(S_i - O_i)}{\sum_{i=1}^{n} O_i}$

Normalized Root Mean Square Error (NRMSE) = $\frac{100 \times \sqrt{\frac{1}{n}\sum_{i=1}^{n}(S_i - O_i)^2}}{\bar{O}}$

Variable Definitions

S_i — Simulated (model) value at station

O_i — Observed (measured) value at station

n — Total number of observations

i — Index of each observation (1 to n)

$\bar{O}$ — Mean of all observed values

$\bar{S}$ — Mean of all simulated values

Table B.1: Seasonal Temperature for 83 Stations

Season	RMSE (°C)	BIAS (°C)	R
DJF	1.3	-0.6	0.96
MAM	1.2	-0.8	0.95
JJA	1.2	0.7	0.89
SON	0.9	0.3	0.95

Table B.2: Annual near-0°C hours for 83 Stations

	NRMSE (%)	PBIAS (%)	R
Annual near 0°C hours	17.9%	-12.1	0.92

Table B.3: Annual precipitation near-0°C hours for the 31 stations

	NRMSE (%)	PBIAS (%)	R
Annual precipitation	11.8%	8.7%	0.95

Table B.4: Annual freezing rain hours for 20 stations.

	RMSE	Bias	R
Annual Freezing Rain hours (h)	12.34	-10.3	0.85

The model demonstrates strong overall performance across all evaluation metrics. Seasonal temperature (Table B.1) is reproduced with low errors (RMSE of 0.9–1.3°C) and high correlation, with the model tending to underestimate temperatures in winter/spring (cold bias) and overestimate in summer/fall (warm bias). Near-0°C hours (Table B.2) show a moderate underestimation (PBIAS = −12.1%) but a good correlation of 0.92. Annual precipitation (Table B.3) is also well captured (NRMSE = 11.8%, PBIAS = 8.7%, R = 0.95), with the strong correlation showing that spatial and temporal patterns are well reproduced. Freezing rain hours (Table B.4) are more challenging to simulate, with the bias indicating that the model underestimates freezing rain hours, though the correlation remains acceptable (R = 0.85).

RÉFÉRENCES

Atlas, D., Tatehira, R., Srivastava, R.C., Marker, W., Carbone, R.E., 1969. Precipitation-induced mesoscale wind perturbations in the melting layer. Quarterly Journal of the Royal Meteorological Society 95, 544–560. https://doi.org/10.1002/qj.49709540508

Atlas, D., Ulbrich, C., 2006. Drop size spectra and integral remote sensing parameters in the transition from convective to stratiform rain. Geophysical research letters 33.

Banfield, C.E., Jacobs, J.D., 1998. Regional Patterns of Temperature and Precipitation for Newfoundland and Labrador During the Past Century. Canadian Geographies / Géographies canadiennes 42, 354–364. https://doi.org/10.1111/j.1541-0064.1998.tb01351.x

Bartlett, P.A., MacKay, M.D., Verseghy, D.L., 2006. Modified Snow Algorithms in the Canadian Land Surface Scheme: Model Runs and Sensitivity Analysis at Three Boreal Forest Stands. Atmosphere-Ocean 44, 207–222. https://doi.org/10.3137/ao.440301

Basnet, S., Thériault, J.M., 2025. Quantification of the impact of latent heat associated with the freezing of supercooled drops at the surface during freezing rain. Atmospheric Research 108120. https://doi.org/10.1016/j.atmosres.2025.108120

Bélair, S., Mailhot, J., Girard, C., Vaillancourt, P., 2005. Boundary Layer and Shallow Cumulus Clouds in a Medium-Range Forecast of a Large-Scale Weather System. Monthly Weather Review 133, 1938–1960. https://doi.org/10.1175/MWR2958.1

Bell, G.D., Bosart, L.F., 1988. Appalachian Cold-Air Damming. Monthly Weather Review., 116, 137-161.

Beltaos, S., Tang, P., Rowsell, R., 2012. Ice jam modelling and field data collection for flood forecasting in the Saint John River, Canada. Hydrological Processes 26, 2535–2545. https://doi.org/10.1002/hyp.9293

Benoit, R., Côté, J., Mailhot, J., 1989. Inclusion of a TKE Boundary Layer Parameterization in the Canadian Regional Finite-Element Model. Monthly Weather Review 117, 1726–1750. https://doi.org/10.1175/1520-0493(1989)117%253C1726:IOATBL%253E2.0.CO;2

Bernstein, B.C., Omeron, T.A., Politovich, M.K., McDonough, F., 1998. Surface weather features associated with freezing precipitation and severe in-flight aircraft icing. Atmospheric Research 46, 57–73. https://doi.org/10.1016/S0169-8095(97)00051-3

Bonsal, B.R., Prowse, T.D., 2003. Trends and Variability in Spring and Autumn 0 °C-Isotherm Dates over Canada. Climatic Change 57, 341–358. https://doi.org/10.1023/A:1022810531237

Boone, A., Masson, V., Meyers, T., Noilhan, J., 2000. The Influence of the Inclusion of Soil Freezing on Simulations by a Soil–Vegetation–Atmosphere Transfer Scheme. Journal of Applied Meteorology and Climatology 39, 1544–1569. https://doi.org/10.1175/1520-0450(2000)039%253C1544:TIOTIO%253E2.0.CO;2

Bourgouin, P., 2000. A method to determine precipitation types. Weather and Forecasting 15, 583–592.

Brandes, E.A., Ikeda, K., Zhang, G., Schönhuber, M., Rasmussen, R.M., 2007. A statistical and physical description of hydrometeor distributions in Colorado snowstorms using a video disdrometer. Journal of applied meteorology and climatology 46, 634–650.

Brooks, C.F., 1920. The Nature of Sleet and How it is Formed. Monthly Weather Review 48,69–72.

Cardinal, É., Thériault, J.M., Stewart, R.E., Thompson, H.D., Déry, S.J., 2024. Climatology of and Factors Contributing to Occurrences of Near-0°C Temperatures and Associated Precipitation at and near Terrace, British Columbia, Canada. Atmosphere-Ocean 62, 145–164. https://doi.org/10.1080/07055900.2023.2270560

Carrera, M.L., Gyakum, J.R., Lin, C.A., 2009. Observational Study of Wind Channeling within the St. Lawrence River Valley. https://doi.org/10.1175/2009JAMC2061.1

Chartrand, J., Thériault, J.M., Marinier, S., 2023. Freezing Rain Events that Impacted the Province of New Brunswick, Canada, and Their Evolution in a Warmer Climate. Atmosphere-Ocean 61, 40–56. https://doi.org/10.1080/07055900.2022.2092444

Chen, B., Hu, W., Pu, J., 2011. Characteristics of the raindrop size distribution for freezing precipitation observed in southern China. Journal of Geophysical Research: Atmospheres 116.

Cheng, C.S., Auld, H., Li, G., Klaassen, J., Tugwood, B., Li, Q., 2004. An automated synoptic typing procedure to predict freezing rain: An application to Ottawa, Ontario, Canada. Weather and Forecasting 19, 751–768.

Cheng, C.S., Li, G., Auld, H., 2011. Possible Impacts of Climate Change on Freezing Rain Using Downscaled Future Climate Scenarios: Updated for Eastern Canada. Atmosphere-Ocean 49, 8–21. https://doi.org/10.1080/07055900.2011.555728

Cholette, M., Thériault, J.M., 2021. Precipitation Type Distribution and Microphysical Processes During the 1998 Ice Storm Simulated Under Pseudo-Warmer Conditions. Journal of Geophysical Research: Atmospheres 126, e2020JD033577. https://doi.org/10.1029/2020JD033577

Cholette, M., Thériault, J.M., Milbrandt, J.A., Morrison, H., 2020. Impacts of Predicting the Liquid Fraction of Mixed-Phase Particles on the Simulation of an Extreme Freezing Rain Event: The 1998 North American Ice Storm. Monthly Weather Review 148, 3799–3823. https://doi.org/10.1175/MWR-D-20-0026.1

Cortinas, J., 2000. A Climatology of Freezing Rain in the Great Lakes Region of North America. Monthly Weather Review 128, 3574–3588. https://doi.org/10.1175/1520-0493(2000)128<3574:ACOFRR>2.0.CO;2

Cortinas Jr, J.V., Bernstein, B.C., Robbins, C.C., Walter Strapp, J., 2004. An analysis of freezing rain, freezing drizzle, and ice pellets across the United States and Canada: 1976–90. Weather and Forecasting 19, 377–390.

Côté, J., Gravel, S., Méthot, A., Patoine, A., Roch, M., Staniforth, A., 1998. The Operational CMC–MRB Global Environmental Multiscale (GEM) Model. Part I: Design Considerations and Formulation. Monthly Weather Review 126, 1373–1395. https://doi.org/10.1175/1520-0493(1998)126%253C1373:TOCMGE%253E2.0.CO;2

Crawford, R.W., Stewart, R.E., 1995. Precipitation type characteristics at the surface in winter storms. Cold Regions Science and Technology 23, 215–229. https://doi.org/10.1016/0165-232X(94)00014-O

Czys, R.R., Scott, R.W., Tang, K.C., Przybylinski, R.W., Sabones, M.E., 1996. A Physically Based, Nondimensional Parameter for Discriminating between Locations of Freezing Rain and Ice Pellets.

Davison, B., Pohl, S., Domes, P., Marsh, P., Pietroniro, A., MacKay, M., 2006. Characterizing snowmelt variability in a land-surface-hydrologic model. Atmosphere-Ocean 44, 271–287. https://doi.org/10.3137/ao.440305

Degelia, S.K., Christian, J.I., Basara, J.B., Mitchell, T.J., Gardner, D.F., Jackson, S.E., Ragland, J.C., Mahan, H.R., 2016. An overview of ice storms and their impact in the United States. International Journal of Climatology 36, 2811–2822. https://doi.org/10.1002/joc.4525

Delage, Y., 1997. Parameterising Sub-grid Scale Vertical Transport in Atmospheric Models Under Statically Stable Conditions. Boundary-Layer Meteorology 82, 23–48. https://doi.org/10.1023/A:1000132524077

Delage, Y., Girard, C., 1992. Stability functions correct at the free convection limit and consistent for for both the surface and Ekman layers. Boundary-Layer Meteorol 58, 19–31. https://doi.org/10.1007/BF00120749

Eira, I.M.G., Oskal, A., Hanssen-Bauer, I., Mathiesen, S.D., 2018. Snow cover and the loss of traditional indigenous knowledge. Nature Clim Change 8, 928–931. https://doi.org/10.1038/s41558-018-0319-2

EK, M., Cuenca, R.H., 1994. Variation in soil parameters: Implications for modeling surface fluxes and atmospheric boundary-layer development. Boundary-Layer Meteorol 70, 369–383. https://doi.org/10.1007/BF00713776

Fan, X., 2009. Impacts of Soil Heating Condition on Precipitation Simulations in the Weather Research and Forecasting Model. Monthly Weather Review 137, 2263–2285. https://doi.org/10.1175/2009MWR2684.1

Findeisen, W., 1940. The formation of the 0 C isothermal layer and fractocumulus under nimbostratus. Meteor. Z 57, 49–54.

Forbes, G.S., Thomson, D.W., Anthes, R.A., 1987. Synoptic and Mesoscale Aspects of an Appalachian Ice Storm Associated with Cold-Air Damming. Monthly Weather Review 115, 564–591. https://doi.org/10.1175/1520-0493(1987)115%253C0564:SAMAOA%253E2.0.CO;2

Fujibe, F., 2001. On the Near-0 °C Frequency Maximum in Surface Air Temperature under Precipitation: A Statistical Evidence for the Melting Effect. 気象集誌. 第 2 輯 79, 731–739. https://doi.org/10.2151/jmsj.79.731

Furukawa, Y., Yamamoto, M., Kuroda, T., 1987. Ellipsometric study of the transition layer on the surface of an ice crystal. Journal of Crystal Growth 82, 665–677. https://doi.org/10.1016/S0022-0248(87)80012-X

Gagnon, A.S., Gough, W.A., 2005. Trends in the Dates of Ice Freeze-up and Breakup over Hudson Bay, Canada. ARCTIC 58, 370–382. https://doi.org/10.14430/arctic451

Garrett, T.J., Yuter, S.E., 2014. Observed influence of riming, temperature, and turbulence on the fallspeed of solid precipitation. Geophysical Research Letters 41, 6515–6522.

Gasset, N., Fortin, V., Dimitrijevic, M., Carrera, M., Bilodeau, B., Muncaster, R., Gaborit, É., Roy, G., Pentcheva, N., Bulat, M., Wang, X., Pavlovic, R., Lespinas, F., Khedhaouiria, D., Mai, J., 2021. A 10 km North American precipitation and land-surface reanalysis based on the GEM atmospheric model. Hydrology and Earth System Sciences 25, 4917–4945. https://doi.org/10.5194/hess-25-4917-2021

Girard, C., Plante, A., Desgagné, M., McTaggart-Cowan, R., Côté, J., Charron, M., Gravel, S., Lee, V., Patoine, A., Qaddouri, A., Roch, M., Spacek, L., Tanguay, M., Vaillancourt, P.A., Zadra, A., 2014. Staggered Vertical Discretization of the Canadian Environmental Multiscale (GEM) Model Using a Coordinate of the Log-Hydrostatic-Pressure Type. Monthly Weather Review 142, 1183–1196. https://doi.org/10.1175/MWR-D-13-00255.1

Gough, W.A., 2008. Theoretical considerations of day-to-day temperature variability applied to Toronto and Calgary, Canada data. Theor Appl Climatol 94, 97–105. https://doi.org/10.1007/s00704-007-0346-9

Guan, W., Jiang, X., Ren, X., Chen, G., Lin, P., Lin, H., 2020. The Leading Intraseasonal Variability Mode of Wintertime Surface Air Temperature over the North American Sector. https://doi.org/10.1175/JCLI-D-20-0096.1

Gunn, K.L.S., Marshall, J.S., 1958. The Distribution with Size of Aggregate Snowflakes. Journal of the Atmospheric Sciences 15, 452–461. https://doi.org/10.1175/1520-0469(1958)015%253C0452:TDWSOA%253E2.0.CO;2

Hanesiak, J.M., Stewart, R.E., 1995. The Mesoscale and Microscale Structure of a Severe Ice Pellet Storm. Monthly Weather Review 123, 3144–3162. https://doi.org/10.1175/1520-0493(1995)123%253C3144:TMAMSO%253E2.0.CO;2

Hanson, K.J., 1961. The Albedo of Sea-Ice and Ice Islands in the Arctic Ocean Basin. Arctic 14, 188–196.

Harrington, J.Y., Reisin, T., Cotton, W.R., Kreidenweis, S.M., 1999. Cloud resolving simulations of Arctic stratus: Part II: Transition-season clouds. Atmospheric Research 51, 45–75.

Henson, W., Stewart, R., Kochtubajda, B., 2007. On the precipitation and related features of the 1998 Ice Storm in the Montréal area. Atmospheric Research 83, 36–54. https://doi.org/10.1016/j.atmosres.2006.03.006

Hersbach, H., Bell, B., Berrisford, P., Hirahara, S., Horányi, A., Muñoz-Sabater, J., Nicolas, J., Peubey, C., Radu, R., Schepers, D., Simmons, A., Soci, C., Abdalla, S., Abellan, X., Balsamo, G., Bechtold, P., Biavati, G., Bidlot, J., Bonavita, M., De Chiara, G., Dahlgren, P., Dee, D., Diamantakis, M., Dragani, R., Flemming, J., Forbes, R., Fuentes, M., Geer, A., Haimberger, L., Healy, S., Hogan, R.J., Hólm, E., Janisková, M., Keeley, S., Laloyaux, P., Lopez, P., Lupu, C., Radnoti, G., de Rosnay, P., Rozum, I., Vamborg, F., Villaume, S., Thépaut, J.-N., 2020. The ERA5 global reanalysis. Quarterly Journal of the Royal Meteorological Society 146, 1999–2049. https://doi.org/10.1002/qj.3803

Huffman, G.J., Norman, G.A., 1988. The Supercooled Warm Rain Process and the Specification of Freezing Precipitation. Monthly Weather Review 116, 2172–2182. https://doi.org/10.1175/1520-0493(1988)116%253C2172:TSWRPA%253E2.0.CO;2

Ishizaka, M., Motoyoshi, H., Nakai, S., Shiina, T., Kumakura, T., Muramoto, K., 2013. A new method for identifying the main type of solid hydrometeors contributing to snowfall from measured size-fall speed relationship. Journal of the Meteorological Society of Japan. Ser. II 91, 747–762.

Iwai, K., 1970. Size distributions of raindrops fallen as surface temperature below 0°C. Bull. Inst. of Natural Educ., Shiga Heights, Shinshu Univ. 9, 93–99.

Jahn, M., 2015. Economics of extreme weather events: Terminology and regional impact models. Weather and Climate Extremes 10, 29–39. https://doi.org/10.1016/j.wace.2015.08.005

Jeong, D.I., Cannon, A.J., Zhang, X., 2019. Projected changes to extreme freezing precipitation and design ice loads over North America based on a large ensemble of Canadian regional climate model simulations. Natural Hazards and Earth System Sciences 19, 857–872. https://doi.org/10.5194/nhess-19-857-2019

Jiang, H., Cotton, W.R., 2000. Large eddy simulation of shallow cumulus convection during BOMEX: Sensitivity to microphysics and radiation. Journal of the atmospheric sciences 57, 582–594.

Jin, M., Dickinson, R.E., 2010. Land surface skin temperature climatology: benefitting from the strengths of satellite observations. Environ. Res. Lett. 5, 044004. https://doi.org/10.1088/1748-9326/5/4/044004

Kain, J.S., Goss, S.M., Baldwin, M.E., 2000. The Melting Effect as a Factor in Precipitation-Type Forecasting. Weather and Forecasting 15, 700–714. https://doi.org/10.1175/1520-0434(2000)015%253C0700:TMEAAF%253E2.0.CO;2

Kelly, D.L., Schaefer, J.T., Doswell, C.A., 1985. Climatology of Nontornadic Severe Thunderstorm Events in the United States.

Kerguillec, R., 2015. Seasonal distribution and variability of atmospheric freeze/thaw cycles in Norway over the last six decades (1950–2013). Boreas 44, 526–542. https://doi.org/10.1111/bor.12113

Kjellström, E., Bärring, L., Nikulin, G., Nilsson, C., Persson, G., Strandberg, G., 2016. Production and use of regional climate model projections – A Swedish perspective on building climate services. Climate Services 2–3, 15–29. https://doi.org/10.1016/j.cliser.2016.06.004

Knight, D.H., Weaver, S.W., Starr, C.R., Romme, W.H., 1979. Differential response of subalpine meadow vegetation to snow augmentation. Rangeland Ecology & Management/Journal of Range Management Archives 32, 356–359.

Kumjian, M.R., Tobin, D.M., Oue, M., Kollias, P., 2020. Microphysical Insights into Ice Pellet Formation Revealed by Fully Polarimetric Ka-Band Doppler Radar. Journal of Applied Meteorology and Climatology 59, 1557–1580. https://doi.org/10.1175/JAMC-D-20-0054

Kuo, H.L., 1965. On Formation and Intensification of Tropical Cyclones Through Latent Heat Release by Cumulus Convection.

Lachapelle, M., Cholette, M., Thériault, J.M., 2024. Effect of Secondary Ice Production Processes on the Simulation of ice pellets using the Predicted Particle Properties microphysics scheme. EGUsphere 1–30. https://doi.org/10.5194/egusphere-2024-594

Lachapelle, M., Thériault, J.M., 2022. Characteristics of Precipitation Particles and Microphysical Processes during the 11–12 January 2020 Ice Pellet Storm in the Montréal Area, Québec, Canada. Monthly Weather Review 150, 1043–1059. https://doi.org/10.1175/MWR-D-21-0185.1

Lackmann, G.M., Keeter, K., Lee, L.G., Ek, M.B., 2002. Model Representation of Freezing and Melting Precipitation: Implications for Winter Weather Forecasting. Weather and Forecasting 17, 1016–1033. https://doi.org/10.1175/1520-0434(2003)017%253C1016:MROFAM%253E2.0.CO;2

Larouche, P., Galbraith, P.S., 2016. Canadian Coastal Seas and Great Lakes Sea Surface Temperature Climatology and Recent Trends. Canadian Journal of Remote Sensing 42, 243–258. https://doi.org/10.1080/07038992.2016.1166041

Lecomte, E.X., Pang, A.W., Russell, J.W., 1998. Ice Storm'98. Institute for Catastrophic Loss Reduction. ICLR Research Paper Series 1.

Leduc, M., Logan, T., 2025. The impact of climate change on the annual cycle of freeze-thaw events in eastern North America. https://doi.org/10.1175/JAMC-D-24-0190.1

Legault, S., Houle, D., Plouffe, A., Ameztegui, A., Kuehn, D., Chase, L., Blondlot, A., Perkins, T.D., 2019. Perceptions of U.S. and Canadian maple syrup producers toward climate change, its

impacts, and potential adaptation measures. PLOS ONE 14, e0215511. https://doi.org/10.1371/journal.pone.0215511

Li, J., Barker, H.W., 2005. A Radiation Algorithm with Correlated-k Distribution. Part I: Local Thermal Equilibrium. Journal of the Atmospheric Sciences 62, 286–309. https://doi.org/10.1175/JAS-3396.1

Liu, C., Ikeda, K., Rasmussen, R., Barlage, M., Newman, A.J., Prein, A.F., Chen, F., Chen, L., Clark, M., Dai, A., Dudhia, J., Eidhammer, T., Gochis, D., Gutmann, E., Kurkute, S., Li, Y., Thompson, G., Yates, D., 2017. Continental-scale convection-permitting modeling of the current and future climate of North America. Clim Dyn 49, 71–95. https://doi.org/10.1007/s00382-016-3327-9

Lohou, F., Patton, E.G., 2014. Surface Energy Balance and Buoyancy Response to Shallow Cumulus Shading. Journal of the Atmospheric Sciences 71, 665–682. https://doi.org/10.1175/JAS-D-13-0145.1

Lozowski, E.P., Stallabrass, J.R., Hearty, P.F., 1983. The Icing of an Unheated, Nonrotating Cylinder. Part I: A Simulation Model. J. Climate Appl. Meteor. 22, 2053–2062. https://doi.org/10.1175/1520-0450(1983)022%253C2053:TIOAUN%253E2.0.CO;2

Mahedi, M., Rajewski, D., Ceylan, H., Kim, S., Takle, E.S., Cho, I.-H., 2024. Have climate change and warmer winters altered freeze-thaw patterns? Transportation Geotechnics 46, 101250. https://doi.org/10.1016/j.trgeo.2024.101250

Mallet, J., Fortin, G., Germain, D., 2018. Extreme weather events in northeastern New Brunswick (Canada) for the period 1950–2012: Comparison of newspaper archive and weather station data. The Canadian Geographer / Le Géographe canadien 62, 130–143. https://doi.org/10.1111/cag.12411

Marinier, S., Thériault, J.M., Ikeda, K., 2023. Changes in freezing rain occurrence over eastern Canada using convection-permitting climate simulations. Clim Dyn 60, 1369–1384. https://doi.org/10.1007/s00382-022-06370-6

Marquis, B., Bergeron, Y., Houle, D., Leduc, M., Rossi, S., 2022. Variability in frost occurrence under climate change and consequent risk of damage to trees of western Quebec, Canada. Sci Rep 12, 7220. https://doi.org/10.1038/s41598-022-11105-y

Marshall, J.S., Palmer, W.M.K., 1948. The Distribution of Raindrops with Size. J. Meteor.51. https://doi.org/10.1175/1520-0469(1948)005%253C0165:TDORWS%253E2.0.CO;2

Martner, B.E., Rauber, R.M., Rasmussen, R.M., Prater, E.T., Ramamurthy, M.K., 1992. Impacts of a Destructive and Well-Observed Cross-Country Winter Storm. Bulletin of the American Meteorological Society 73, 169–172. https://doi.org/10.1175/1520-0477(1992)073%253C0169:IOADAW%253E2.0.CO;2

Martner, B.E., Snider, J.B., Zamora, R.J., Byrd, G.P., Niziol, T.A., Joe, P.I., 1993. A remote-sensing view of a freezing-rain storm. Monthly weather review 121, 2562–2577.

McCray, C.D., Atallah, E.H., Gyakum, J.R., 2019. Long-Duration Freezing Rain Events over North America: Regional Climatology and Thermodynamic Evolution. Weather and Forecasting 34, 665–681. https://doi.org/10.1175/WAF-D-18-0154.1

McCray, C.D., Gyakum, J.R., Atallah, E.H., 2020. Regional Thermodynamic Characteristics Distinguishing Long- and Short-Duration Freezing Rain Events over North America. Weather and Forecasting 35, 657–671. https://doi.org/10.1175/WAF-D-19-0179.1

McGinn, s, 2010. Weather and Climate Patterns in Canada's Prairie Grasslands. Arthropods of Canadian Grasslands (Volume 1): Ecology and Interactions in Grassland Habitats. https://doi.org/10.3752/9780968932148.ch5

McTaggart-Cowan, R., Vaillancourt, P.A., Zadra, A., Chamberland, S., Charron, M., Corvec, S., Milbrandt, J.A., Paquin-Ricard, D., Patoine, A., Roch, M., Separovic, L., Yang, J., 2019. Modernization of Atmospheric Physics Parameterization in Canadian NWP. Journal of Advances in Modeling Earth Systems 11, 3593–3635. https://doi.org/10.1029/2019MS001781

Mekis, E., Stewart, R.E., Theriault, J.M., Kochtubajda, B., Bonsal, B.R., Liu, Z., 2020. Near-0°C surface temperature and precipitation type patterns across Canada. Hydrology and Earth System Sciences 24, 1741–1761. https://doi.org/10.5194/hess-24-1741-2020

Meyers, M.P., Walko, R.L., Harrington, J.Y., Cotton, W.R., 1997. New RAMS cloud microphysics parameterization. Part II: The two-moment scheme. Atmospheric Research 45, 3–39.

Milbrandt, J.A., Bélair, S., Faucher, M., Vallée, M., Carrera, M.L., Glazer, A., 2016. The Pan-Canadian High Resolution (2.5 km) Deterministic Prediction System. Weather and Forecasting 31, 1791–1816. https://doi.org/10.1175/WAF-D-16-0035.1

Milbrandt, J.A., Yau, M.K., 2005. A multimoment bulk microphysics parameterization. Part I: Analysis of the role of the spectral shape parameter. Journal of the atmospheric sciences 62, 3051–3064.

Milton, J., 1999. A Climatological Account of the January 1998 Ice Storm in Quebec: Scientific Report. Environment Canada, Quebec Region, Atmospheric Sciences & Environmental Issues Division.

Mohammadlou, M., Bahremand, A., Princz, D., Kinar, N., Haghnegahdar, A., Razavi, S., 2022. Objective evaluation of the Global Environmental Multiscale Model (GEM) with precipitation and temperature for Iran. Natural Resource Modeling 35, e12343. https://doi.org/10.1111/nrm.12343

Morrison, H., Milbrandt, J.A., 2015. Parameterization of Cloud Microphysics Based on the Prediction of Bulk Ice Particle Properties. Part I: Scheme Description and Idealized Tests. https://doi.org/10.1175/JAS-D-14-0065.1

Morrison, H., Milbrandt, J.A., Bryan, G.H., Ikeda, K., Tessendorf, S.A., Thompson, G., 2015. Parameterization of Cloud Microphysics Based on the Prediction of Bulk Ice Particle Properties.

Part II: Case Study Comparisons with Observations and Other Schemes. https://doi.org/10.1175/JAS-D-14-0066.1

Moumouni, S., Gosset, M., Houngninou, E., 2008. Main features of rain drop size distributions observed in Benin, West Africa, with optical disdrometers. Geophysical Research Letters 35.

Mulherin, N.D., 1998. Atmospheric icing and communication tower failure in the United States. Cold Regions Science and Technology 27, 91–104. https://doi.org/10.1016/S0165-232X(97)00025-6

Namias, J., 1963. Large-scale air-sea interactions over the North Pacific from summer 1962 through the subsequent winter. Journal of Geophysical Research (1896-1977) 68, 6171–6186. https://doi.org/10.1029/JZ068i022p06171

Nie, D., Demetriades-Shah, T., Kanemasu, T, E., 1992. Surface energy fluxes on four slope sites during FIFE 1988. Journal of Geophysical Research: Atmospheres 97, 18641–18649. https://doi.org/10.1029/91JD03043

Notaro, M., Zhong, Y., Xue, P., Peters-Lidard, C., Cruz, C., Kemp, E., Kristovich, D., Kulie, M., Wang, J., Huang, C., Vavrus, S.J., 2021. Cold Season Performance of the NU-WRF Regional Climate Model in the Great Lakes Region. Journal of Hydrometeorology 22, 2423–2454. https://doi.org/10.1175/JHM-D-21-0025.1

Ohtake, T., 1969. Observations of Size Distributions of Hydrometeors Through the Melting Layer. Journal of the Atmospheric Sciences 26, 545–557. https://doi.org/10.1175/1520-0469(1969)026%253C0545:OOSDOH%253E2.0.CO;2

Phillips, D., 1990. The Climates of Canada, 1st Edition. ed. Minister of Supply and Services., Ottawa, Ontario.

Pielke Sr., R.A., 2001. Influence of the spatial distribution of vegetation and soils on the prediction of cumulus Convective rainfall. Reviews of Geophysics 39, 151–177. https://doi.org/10.1029/1999RG000072

Prein, A.F., Heymsfield, A.J., 2020. Increased melting level height impacts surface precipitation phase and intensity. Nature Climate Change 10, 771–776.

Pruppacher, H.R., Klett, J.D., Wang, P.K., 1998. Microphysics of clouds and precipitation.

Quéno, L., Vionnet, V., Cabot, F., Vrécourt, D., Dombrowski-Etchevers, I., 2018. Forecasting and modelling ice layer formation on the snowpack due to freezing precipitation in the Pyrenees. Cold Regions Science and Technology 146, 19–31. https://doi.org/10.1016/j.coldregions.2017.11.007

Raga, G.B., Stewart, R.E., Donaldson, N.R., 1991. Microphysical characteristics through the melting region of a midlatitude winter storm. Journal of Atmospheric Sciences 48, 843–855.

Ralph, F.M., Rauber, R.M., Jewett, B.F., Kingsmill, D.E., Pisano, P., Pugner, P., Rasmussen, R.M., Reynolds, D.W., Schlatter, T.W., Stewart, R.E., Tracton, S., Waldstreicher, J.S., 2005. Improving Short-Term (0–48 h) Cool-Season Quantitative Precipitation Forecasting: Recommendations from a USWRP Workshop. Bulletin of the American Meteorological Society 86, 1619–1632.

Rauber, R.M., Olthoff, L.S., Ramamurthy, M.K., Miller, D., Kunkel, K.E., 2001. A Synoptic Weather Pattern and Sounding-Based Climatology of Freezing Precipitation in the United States East of the Rocky Mountains. Journal of Applied Meteorology and Climatology 40, 1724–1747. https://doi.org/10.1175/1520-0450(2001)040%253C1724:ASWPAS%253E2.0.CO;2

Rawlins, M.A., Bradley, R.S., Diaz, H.F., Kimball, J.S., Robinson, D.A., 2016. Future Decreases in Freezing Days across North America. https://doi.org/10.1175/JCLI-D-15-0802.1

Reeves, H.D., Ryzhkov, A.V., Krause, J., 2016. Discrimination between winter precipitation types based on spectral-bin microphysical modeling. Journal of Applied Meteorology and Climatology 55, 1747–1761.

Ressler, G.M., Milrad, S.M., Atallah, E.H., Gyakum, J.R., 2012. Synoptic-Scale Analysis of Freezing Rain Events in Montreal, Quebec, Canada. https://doi.org/10.1175/WAF-D-11-00071.1

Riahi, K., Rao, S., Krey, V., Cho, C., Chirkov, V., Fischer, G., Kindermann, G., Nakicenovic, N., Rafaj, P., 2011. RCP 8.5—A scenario of comparatively high greenhouse gas emissions. Climatic Change 109, 33–57. https://doi.org/10.1007/s10584-011-0149-y

Robbins, C.C., Cortinas, J.V., 2002. Local and Synoptic Environments Associated with Freezing Rain in the Contiguous United States.

Roberge, F., Di Luca, A., Laprise, R., Lucas-Picher, P., Thériault, J., 2024. Spatial spin-up of precipitation in limited-area convection-permitting simulations over North America using the CRCM6-GEM5.0 model. Geoscientific Model Development 17, 1497–1510. https://doi.org/10.5194/gmd-17-1497-2024

Roe, G.H., 2005. Orographic Precipitation. Annu. Rev. Earth Planet. Sci. 33, 645–671. https://doi.org/10.1146/annurev.earth.33.092203.122541

Sanders, K., Gravelle, C., Gagan, J., Graves, C., 2013. Characteristics of major ice storms in the central United States. J. Operational Meteor. 1, 100–113. https://doi.org/10.15191/nwajom.2013.0110

Sankaré, H., Thériault, J.M., 2016. On the relationship between the snowflake type aloft and the surface precipitation types at temperatures near 0°C. Atmospheric Research 180, 287–296. https://doi.org/10.1016/j.atmosres.2016.06.003

Schär, C., Frei, C., Lüthi, D., Davies, H.C., 1996. Surrogate climate-change scenarios for regional climate models. Geophysical Research Letters 23, 669–672. https://doi.org/10.1029/96GL00265

Shi, Q., Xue, P., 2019. Impact of Lake Surface Temperature Variations on Lake Effect Snow Over the Great Lakes Region. Journal of Geophysical Research: Atmospheres 124, 12553–12567. https://doi.org/10.1029/2019JD031261

Smith, A., Lott, N., Vose, R., 2011. The Integrated Surface Database: Recent Developments and Partnerships. Bulletin of the American Meteorological Society 92, 704–708.

Sospedra-Alfonso, R., Melton, J.R., Merryfield, W.J., 2015. Effects of temperature and precipitation on snowpack variability in the Central Rocky Mountains as a function of elevation. Geophysical Research Letters 42, 4429–4438. https://doi.org/10.1002/2015GL063898

Spiridonov, V., Ćurić, M., 2021. Air Masses and Fronts, in: Spiridonov, V., Ćurić, M. (Eds.), Fundamentals of Meteorology. Springer International Publishing, Cham, pp. 253–261. https://doi.org/10.1007/978-3-030-52655-9_16

Splawinski, S., 2014. An assessment of freezing rain processes in the Saint- Lawrence River Valley: synoptic-dynamic analysis and operational model verification.

Stallabrass, J.R., 1983. Aspects of freezing rain simulation and testing, in: Proc First International Workshop on Atmospheric Icing of Structures. pp. 67–74.

Stewart, R.E., 1985. Precipitation types in winter storms. PAGEOPH 123, 597–609. https://doi.org/10.1007/BF00877456

Stewart, R.E., King, P., 1987. Freezing Precipitation in Winter Storms. Monthly Weather Review 115,1270–1280. https://doi.org/10.1175/15200493(1987)115%253C1270:FPIWS%253E2.0.CO;2

Stewart, R.E., Liu, Z., Thériault, J.M., Ruman, C.J., 2023. The Occurrence of Near-0°C Surface Air Temperatures in the Current and Pseudo-Global Warming Future Over Southern Canada. Journal of Geophysical Research: Atmospheres 128, e2022JD037981. https://doi.org/10.1029/2022JD037981

Stewart, R.E., Szeto, K.K., Bonsal, B.R., Hanesiak, J.M., Kochtubajda, B., Li, Y., Thériault, J.M., DeBeer, C.M., Tam, B.Y., Li, Z., Liu, Z., Bruneau, J.A., Duplessis, P., Marinier, S., Matte, D., 2019. Summary and synthesis of Changing Cold Regions Network (CCRN) research in the interior of western Canada – Part 1: Projected climate and meteorology. Hydrology and Earth System Sciences 23, 3437–3455. https://doi.org/10.5194/hess-23-3437-2019

Strack, J.E., Pielke, R.A., Adegoke, J., 2003. Sensitivity of Model-Generated Daytime Surface Heat Fluxes over Snow to Land-Cover Changes. Journal of Hydrometeorology 4, 24–42. https://doi.org/10.1175/1525-7541(2003)004%253C0024:SOMGDS%253E2.0.CO;2

Stuart, R.A., Isaac, G.A., 1999. Freezing precipitation in Canada. Atmosphere-Ocean 37, 87–102.

Sutton, C., Hamill, T.M., Warner, T.T., 2006. Will Perturbing Soil Moisture Improve Warm-Season Ensemble Forecasts? A Proof of Concept. Monthly Weather Review 134, 3174–3189. https://doi.org/10.1175/MWR3248.1

Takeuchi, Y., Kodama, Y., Ishikawa, N., 2002. The Thermal Effect of Melting Snow/Ice Surface on Lower Atmospheric Temperature. Arctic, Antarctic, and Alpine Research 34, 20–25. https://doi.org/10.1080/15230430.2002.12003464

Tapiador, F.J., Checa, R., De Castro, M., 2010. An experiment to measure the spatial variability of rain drop size distribution using sixteen laser disdrometers. Geophysical Research Letters 37.

Thériault, J.M., McFadden, V., Thompson, H.D., Cholette, M., 2022. Meteorological Factors Responsible for Major Power Outages during a Severe Freezing Rain Storm over Eastern Canada. https://doi.org/10.1175/JAMC-D-21-0217.1

Thériault, J.M., Stewart, R.E., 2010. A Parameterization of the Microphysical Processes Forming Many Types of Winter Precipitation. Journal of the Atmospheric Sciences 67, 1492–1508. https://doi.org/10.1175/2009JAS3224.1

Thériault, J.M., Stewart, R.E., 2007. On the effects of vertical air velocity on winter precipitation types. Natural Hazards and Earth System Sciences 7, 231–242. https://doi.org/10.5194/nhess-7-231-2007

Thériault, J.M., Stewart, R.E., Henson, W., 2012. Impacts of terminal velocity on the trajectory of winter precipitation types. Atmospheric Research, Remote Sensing of Clouds and Aerosols: Techniques and Applications - Atmospheric Research 116, 116–129. https://doi.org/10.1016/j.atmosres.2012.03.008

Thériault, J.M., Stewart, R.E., Henson, W., 2010. On the Dependence of Winter Precipitation Types on Temperature, Precipitation Rate, and Associated Features. Journal of Applied Meteorology and Climatology 49, 1429–1442. https://doi.org/10.1175/2010JAMC2321.1

Thériault, J.M., Stewart, R.E., Milbrandt, J.A., Yau, M.K., 2006. On the simulation of winter precipitation types. Journal of Geophysical Research: Atmospheres 111. https://doi.org/10.1029/2005JD006665

Trapp, R.J., Schultz, D.M., Ryzhkov, A.V., Holle, R.L., 2001. Multiscale structure and evolution of an Oklahoma winter precipitation event. Monthly weather review 129, 486–501.

Trenouth, W.R., Gharabaghi, B., 2015. Soil amendments for heavy metals removal from stormwater runoff discharging to environmentally sensitive areas. Journal of Hydrology 529, 1478–1487. https://doi.org/10.1016/j.jhydrol.2015.08.034

Tropea, B., Stewart, R., 2021. Assessing past and future hazardous freezing rain and wet snow events in Manitoba, Canada using a pseudo-global warming approach. Atmospheric Research 259, 105656. https://doi.org/10.1016/j.atmosres.2021.105656

Turunen, M.T., Rasmus, S., Bavay, M., Ruosteenoja, K., Heiskanen, J., 2016. Coping with difficult weather and snow conditions: Reindeer herders' views on climate change impacts and coping strategies. Climate Risk Management 11, 15–36. https://doi.org/10.1016/j.crm.2016.01.002

Verseghy, D.L., 2000. The Canadian land surface scheme (CLASS): Its history and future. Atmosphere-Ocean 38, 1–13. https://doi.org/10.1080/07055900.2000.9649637

Verseghy, D.L., McFarlane, N.A., Lazare, M., 1993. Class—A Canadian land surface scheme for GCMS, II. Vegetation model and coupled runs. International Journal of Climatology 13, 347–370. https://doi.org/10.1002/joc.3370130402

Wexler, A., Hasegawa, S., 1954. Relative humidity-temperature relationships of some saturated salt solutions in the temperature range 0 degree to 50 degrees C. J. RES. NATL. BUR. STAN. 53, 19. https://doi.org/10.6028/jres.053.003

Wexler, R., Reed, R.J., Honig, J., 1954. Atmospheric Cooling by Melting Snow. Bulletin of the American Meteorological Society 35, 48–51.

Xu, H., Wu, Z., Luo, L., He, H., 2018. Verification of High-Resolution Medium-Range Precipitation Forecasts from Global Environmental Multiscale Model over China during 2009–2013. Atmosphere 9, 104. https://doi.org/10.3390/atmos9030104

Yuter, S.E., Kingsmill, D.E., Nance, L.B., Löffler-Mang, M., 2006. Observations of precipitation size and fall speed characteristics within coexisting rain and wet snow. Journal of Applied Meteorology and Climatology 45, 1450–1464.

Zarnani, A., Musilek, P., Shi, X., Ke, X., He, H., Greiner, R., 2012. Learning to predict ice accretion on electric power lines. Engineering Applications of Artificial Intelligence 25, 609–617. https://doi.org/10.1016/j.engappai.2011.11.004

Zerr, R.J., 1997. Freezing Rain: An Observational and Theoretical Study.

Zhang, G., Luchs, S., Ryzhkov, A., Xue, M., Ryzhkova, L., Cao, Q., 2011. Winter Precipitation Microphysics Characterized by Polarimetric Radar and Video Disdrometer Observations in Central Oklahoma. Journal of Applied Meteorology and Climatology 50, 1558–1570. https://doi.org/10.1175/2011JAMC2343.1

Zhang, T., Stamnes, K., Bowling, S.A., 1996. Impact of Clouds on Surface Radiative Fluxes and Snowmelt in the Arctic and Subarctic. Journal of Climate 9, 2110–2123. https://doi.org/10.1175/1520-0442(1996)009%253C2110:IOCOSR%253E2.0.CO;2